Nonequilibrium Dynamics in Some Phase Transitions: From finite to infinite length

A Thesis
Submitted for the Degree of
DOCTOR OF PHILOSOPHY
in the Faculty of Science

by

Suman Majumder

THEORETICAL SCIENCES UNIT
JAWAHARLAL NEHRU CENTRE FOR ADVANCED SCIENTIFIC RESEARCH
Bangalore – 560 064

DECEMBER 2012

To my family

DECLARATION

I hereby declare that the matter embodied in the thesis entitled “ **Nonequilibrium Dynamics in Some Phase Transitions: From finite to infinite length** ” is the result of investigations carried out by me at the Theoretical Sciences Unit, Jawaharlal Nehru Centre for Advanced Scientific Research, Bangalore, India under the supervision of Dr. Subir K. Das and that it has not been submitted elsewhere for the award of any degree or diploma.

In keeping with the general practice in reporting scientific observations, due acknowledgement has been made whenever the work described is based on the findings of other investigators.

Suman Majumder

CERTIFICATE

I hereby certify that the matter embodied in this thesis entitled " **Nonequilibrium Dynamics in Some Phase Transitions: From finite to infinite length** " has been carried out by Mr. Suman Majumder at the Theoretical Sciences Unit, Jawaharlal Nehru Centre for Advanced Scientific Research, Bangalore, India under my supervision and that it has not been submitted elsewhere for the award of any degree or diploma.

Dr. Subir K. Das
(Research Supervisor)

Acknowledgements

I am grateful to my supervisor Dr. Subir K. Das for his constant help, guidance and encouragement throughout my entire Ph.D life.

I would like to acknowledge all the faculty members of TSU - Prof. Shobhana Narasimhan, Prof. Srikanth Sastry, Prof. Umesh V. Waghmare, Prof. Swapan K. Pati, Dr. Kavita Jain and Dr. N.S. Vidhyadhiraja - for the interesting courses they offered.

Thanks are due to all the past and present complab members - Vikas, Vishnu, Ashish, Ravi, Nishaj, Dharma and others for their generous help, whenever needed.

I acknowledge all my labmates Sutapa, Shaista, Prabhat, Saugata, Subhajit, Jiarul and Saikat, for all the scientific and nonscientific discussions. Apart from them I would also like to thank my other friends in JNCASR, especially Sarada, Gayatri, Sona, Priyanka and Pralok, for making my stay in JNCASR enjoyable. A BIG THANK to my longtime friend Arun for being helpful in difficult times.

I thank CSIR, DST and JNCASR for fellowship and funding.

Finally, I express my deep gratitude towards Sonali for being with me and my family for their constant support.

SYNOPSIS

Non-equilibrium dynamics in phase transitions, due to variation in temperature (T), pressure (P), etc., is of fundamental research interest both theoretically and experimentally. Often, during such transitions, systems move towards the equilibrium via the formation and usually non-linear growth of "particle" rich and "particle" depleted domains. Such kinetics for various transitions have been studied extensively over several decades. Nevertheless, it appears that the understanding of the phenomena is significantly incomplete. In this thesis, we try to answer some of the longstanding questions in this area via computer simulations.

In computer simulations, often the finite sizes of systems create difficulty, particularly in situations when there is a diverging length scale, in drawing conclusions with respect to thermodynamic limit. In the modern day of advanced and high-power computers, it has been possible to consider very large system sizes. Inspite of that many basic questions remain unsolved. In this thesis we intend to appropriately address some of these important basic facts which were either overlooked or misunderstood in the past. These include the effect of system sizes in computer simulations of different systems undergoing phase transitions, e.g., solid-solid, vapor-liquid, etc.; the composition and temperature dependence of growth kinetics; correction to the growth law at small length scale limit; hydrodynamic effects in the kinetics of phase separation; aging dynamics in such non-equilibrium processes including paramagnetic to ferromagnetic transition; etc. In addition, we have also studied the kinetics of phase separation in more realistic and technologically relevant systems, viz., in systems under confinement. In our studies we have used the state of the art Monte Carlo and molecular dynamics simulations and applied finite-size scaling theory for the purpose of extracting accurate information from the results thus obtained. Number of our results have been justified via simple analytical arguments. The thesis consists of six chapters as briefly discussed below.

First chapter is the Introduction where we discuss all the basic information needed for carrying out the work presented in the subsequent chapters as well as for their understanding. It covers the theoretical foundation of phase ordering dynamics. Different scaling laws related to the conservation of order parameter, effect of hydrodynamics, etc., are discussed. It also introduces the aging phenomena in nonequilibrium systems. Further, a brief account of the "expected" effects of surface on growth kinetics during phase separation is presented. On the technical side, it describes different simulation techniques, viz., Monte Carlo and molecular dynamics methods. Various functions, useful for characterizing pattern formation, have been defined. Finally, methodologies for analysis, in particular the finite-size scaling theory, have been discussed in reasonable depth. At the end of the chapter a brief overview of the thesis is also given.

The **second chapter** discusses the diffusive dynamics of phase separation in a symmetric solid binary (A+B) mixture with critical composition of A and B particles, following a quench below the demixing critical temperature, both in spatial dimensions $d = 2$ and $d = 3$. Note that this is the only mechanism in solids. In this work, in addition to studying pattern formation and gaining accurate knowledge about the asymptotic growth law, other important objectives are to obtain information about effects of system size and early-time correction to the growth law. These questions have been appropriately addressed via successful application of the finite-size scaling technique to the results obtained from Kawasaki exchange Monte Carlo simulation, that conserves the order parameter, of the Ising model. The Lifshitz-Slyozov law for the diffusive phase separation has been confirmed. Our observation of only weak size effects in such non-equilibrium processes, which defies the traditional belief, is a significant and welcome message for the computer simulation community. It has also been shown that the correction to scaling in the growth law, at small length scale, is negligibly small. We also provide detailed discussion on the standard methods of understanding simulation results which may lead to inappropriate conclusions.

In the **third chapter**, we demonstrate the effects of temperature and composition on the kinetics of diffusive phase separation. For compositions close to the co-existence curve one has droplet-like domains of the minority component. We investigate the curvature dependent correction to the Lifshitz-Slyozov law during growth of these droplets. In the temperature dependent study, we observe, at low temperature, a crossover from interface diffusion to bulk diffusion mediated growth. Amplitude of domain growth as a function of temperatures is also studied. Furthermore, from finite-size scaling analysis it has been convincingly shown that the extent of finite-size effect is independent of the composition and temperature.

In the fourth chapter, we deal with kinetics of vapor-liquid transition. We have obtained the equilibrium phase diagram for the Lennard

Jones model considered for this study. Domain growth, in this case, is studied for critical quench. Here our objective is to investigate the influence of hydrodynamics and establish the universality in kinetics of phase separation involving liquid-liquid and vapor-liquid phase transitions. A brief period of slow diffusive growth is observed which is followed by a linear viscous hydrodynamic growth that lasts for an extended period of time. This result is in contradiction with earlier inconclusive reports of late time growth exponent 1/2 that questions the uniqueness of the above mentioned nonequilibrium universality. We have studied the finite-size effects in this case also and our observation is found to be consistent with similar studies in solid-solid phase separation. Our finding of apparently universal finite-size effect in coarsening phenomena with conserved order parameter is certainly interesting.

The **fifth chapter** consists of the results for aging in domain coarsening phenomena with particular emphasis on the vapor-liquid phase transitions presented in Chapter 4. Other systems considered are solid binary mixtures and ferromagnetic system. The two-time order-parameter correlation function is used as a probe to study the aging dynamics. For phase separation with diffusive kinetics, these correlations are observed to decay in a power-law manner for which we have estimated the exponent. In the phase separating vapor-liquid systems, an exponential decay of the auto-correlation function at the late time was observed which is a striking observation. The latter fact is related to the hydrodynamic effects dominant at long length scales in fluids and we have provided analytical justification for that via simple dimensional argument. We have also estimated the aging exponent for non-conserved dynamics.

In the **last chapter**, results from the kinetics of phase separation in thin films are reported. In thin film basically one of the spatial dimensions is restricted. This chapter discusses how the domain growth occurs in presence of such geometric restriction that imposes surface effects. In this case, our interest has been to study phase separation in solid binary mixtures as well as in vapor-liquid phase separation using Monte Carlo and molecular dynamics simulations, respectively.

List of Publications

- "Domain coarsening in two dimensions: Conserved dynamics and finite-size scaling", **Suman Majumder** and Subir K. Das, Rapid Communication in Phys. Rev. E **81** 050102, (2010).
- "Diffusive Domain Coarsening : Early-Time Dynamics and Finite-Size Effects", **Suman Majumder** and Subir K. Das, Phys. Rev. E **84** 021110, (2011).
- "Universality in Fluid Domain Coarsening: The case of vapor-liquid transition", **Suman Majumder** and Subir K. Das, Europhys. Lett. **95** 46002, (2011).
- "Finite-size effects in dynamics: Critical vs coarsening phenomena", Subir K. Das, Sutapa Roy, **Suman Majumder** and Shaista Ahmad, Europhys. Lett. **97** 66006, (2012).
- "Kinetics of Phase Separation in Solid Binary Mixture: Temperature and composition dependence", **Suman Majumder** and Subir K. Das, to be published.
- "Aging in Domain Coarsening", **Suman Majumder** and Subir K.

Das, to be published.

- “Atomistic Studies of Kinetics of Phase Separation in Thin Films”, **Suman Majumder** and Subir K. Das, to be published.

List of Figures

Contents

Chapter 1

Introduction

1.1 Phase Transitions

In nature many substances are commonly seen in solid, liquid and gas phases. Existence of a substance in a particular phase is dependent on certain thermodynamic conditions defined by temperature, pressure, density or composition [1,2]. Thus one encounters transition from one phase to the other by varying such parameters. Fig. 1.1 shows the basic schematic phase diagram of a simple chemical substance in the pressure (P) vs temperature (T) plane. Different phases are marked in the figure. There along various solid lines, referred to as the coexistence curves, two phases coexist with each other, in equilibrium. The point at which all the three coexistence lines meet is known as the triple point where all three phases coexist. Unlike the solid-liquid coexistence line which extends indefinitely, the vapor-liquid coexistence line ends at a point called the critical point (P_c, T_c). In the region beyond the critical point the system exists in a homogeneous one phase state where the

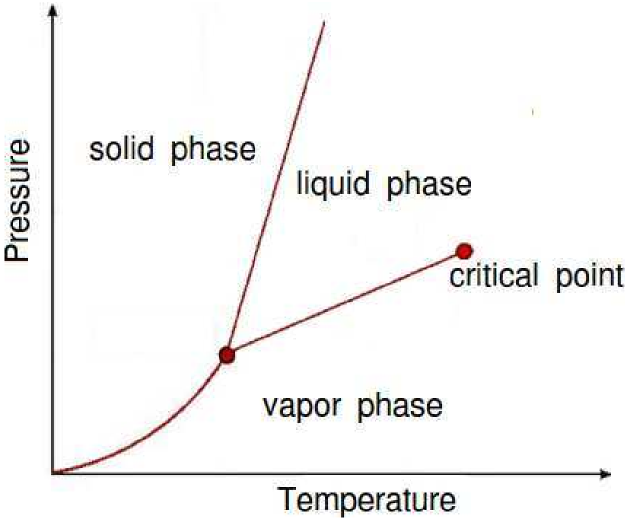

Figure 1.1: Phase diagram of a simple substance in the P vs T plane. Different phases are marked. The solid lines correspond to different coexisting lines (see text for details).

density difference between the liquid and vapor phase is zero. Around the vicinity of the critical point, number of interesting physical processes occur, referred to as the *critical phenomena* [1].

Fig. 1.2 shows the phase diagram (coexistence curve) of the same system in the temperature vs density (ρ) plane in the vicinity of the critical point. Above T_c the system is in a single phase with "uniform" density. Inside the coexistence curve, the system is in a two-phase region of different densities. The left branch of the curve corresponds to the density of the coexisting vapor phase and the right branch to the high density liquid phase. From the diagram it is quite evident that with the increase of T the two branches are approaching each other implying a decrease of the density difference between the liquid and vapor phases which finally vanishes at T_c. In this context, it is worth mentioning that for the study of a phase transition one needs

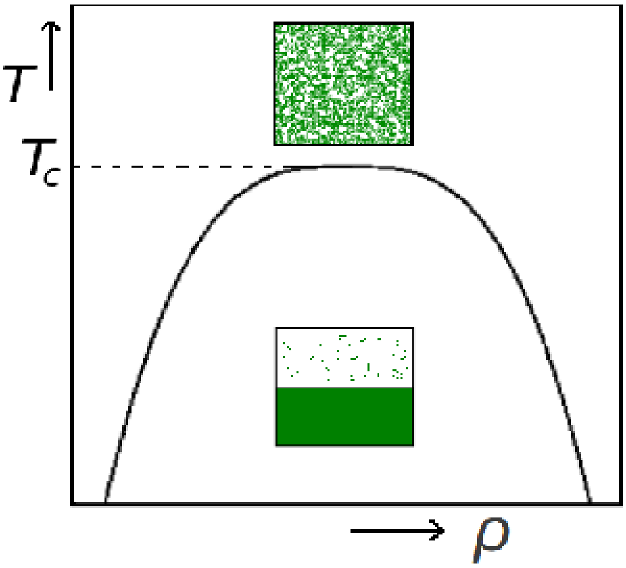

Figure 1.2: Schematic phase diagram of the substance of Fig. 1.1 in the temperature vs density plane. The solid line represents the coexistence line. The box outside the coexistence curve represents a homogeneous system while the one inside depicts a phase separated state.

to define the so called *order parameter*. In the context of an order-disorder transition, e.g., paramagnetic to ferromagnetic transition, above T_c (in the disordered state), the value of this order parameter is zero and below T_C (in the ordered state) it has a non-zero value. Such definitions can be constructed in other transitions also. For example, in the gas-liquid transition the density difference between the liquid and vapor phase ($\rho_l - \rho_g$) is the relevant order parameter which is zero above T_c and has nonzero value below T_c. With the increase of T, the order parameter vanishes as $(T - T_c)^\beta$, where β is a critical exponent [1, 2]. Throughout this thesis we will be dealing only with scalar order parameter.

The diagram in Fig. 1.2 can also be used to describe the phase diagram of a binary mixture (A+B). In this case, the density is replaced by the concentration of one of the components (say $x_A = N_A/N$, where N_A and N are respectively the number of A particles and total number of particles). Above T_c the system is a homogeneous mixture of A and B particles and below T_c (demixing critical temperature) it separates into A- and B-rich phases which are represented by the right and left branches of the coexisting curve. One can explain paramagnet to ferromagnetic transition from a similar diagram as well. Then the critical temperature corresponds to the Curie temperature above which all the magnetic spins are randomly oriented giving rise to zero net magnetization. In this case the x-axis should be the magnetization (m) which is the relevant order parameter for a ferromagnetic transition. Below the critical temperature, the spins are aligned with each other giving rise to net non-zero magnetization.

1.2 Domain Coarsening in Bulk Systems

Many of the equilibrium aspects of these phase transitions are well studied [1,2] and of fundamental importance. Understanding the nonequilibrium evolution of a system having been quenched from a high temperature homogeneous phase to inside the coexistence curve is another interesting and fascinating scientific topic [2–8]. As stated, at high temperature, the system is in a homogeneous state. If the temperature of the system is suddenly quenched to a lower temperature, the system falls out of equilibrium and it starts evolving towards its new equilibrium state which is the phase separated state or ordered state, if the state point lies inside the coexistence curve. This transformation to the new equilibrium takes time and occurs via the formation and growth of domains of different phases. This is referred to as the *phase ordering dynamics* or *domain coarsening.* In this section we discuss it for bulk systems. Here we note that for the purpose of studying bulk properties in computer simulations one applies periodic boundary conditions to get rid of the surface effects.

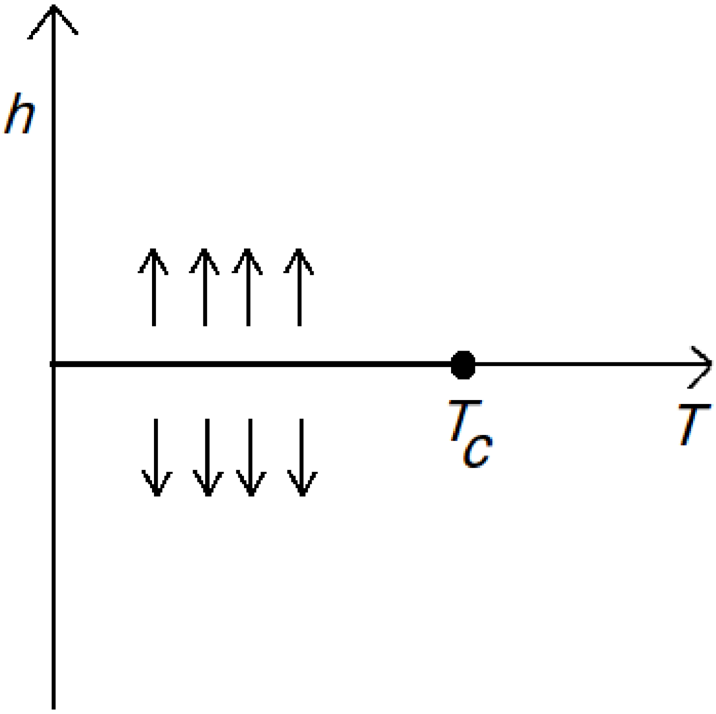

Figure 1.3: Schematic phase diagram of a ferromagnetic substance in $h-T$ plane. T_c is the Curie temperature. Above T_c is the paramagnetic state with zero spontaneous magnetization and below T_c is ferromagnetic state, where the system exhibits spontaneous magnetization.

Let us consider a ferromagnetic substance at a temperature above the Curie temperature (See Fig 1.3 for a phase diagram of a ferromagnet). It says that in absence of any external field ($h = 0$), at high temperature $T > T_c$, the system is in disordered state having a zero net magnetization. Below the critical temperature, however, the system exhibits magnetization even for $h = 0$. Now if the system is quenched from high temperature ($T > T_C$) to a temperature $T < T_c$, the system will evolve via the formation and growth of domains of like spins. Similarly when a binary mixture (A+B) is quenched from the high temperature homogeneous phase to a temperature below the demixing critical temperature the system falls out of equilibrium and it approaches the phase-separated state via the formation and growth of A- and B- rich domains. The dynamics of evolution of these systems is rich in interesting mechanisms that usually gives rise to a power law growth of domains [3]:

$$\ell(t) \sim t^{\alpha}. \tag{1.1}$$

Here $\ell(t)$ is the average domain-size at a particular time t and α is the corresponding growth exponent which is dependent on the dominant transport mechanism, system dimensionality, number of order parameter components and the order parameter conservation law. The scaling laws for some situations are discussed below.

1.2.1 Growth Laws

In this section we discuss about different growth laws for bulk phase ordering in $d = 3$, for scalar order parameters. The evolution of a system following a quench from homogeneous state to a temperature below the coexistence curve can be classified into different classes based on the growth mechanism. The growth laws are different depending upon whether the order parameter remains conserved or not. In addition, effect of hydrodynamics can significantly alter the growth exponent in case of conserved order parameter dynamics. Below we discuss different scenarios along with some models typically used to study coarsening phenomena in corresponding situations.

(a) NonConserved Order-Parameter Kinetics

The paramagnetic to ferromagnetic transition is an example of a coarsening phenomena with non-conserved kinetics. Here the magnetization (m), the order parameter, is zero for the paramagnetic state and in the final equilibrium state, after the quench, it acquires a spontaneous magnetization ($m \neq 0$) with majority of the spins pointing either up or down. At the microscopic level this non-conserved evolution can be well described by implementing the spin flip Glauber kinetics [9] in the nearest neighbor Ising model given by the Hamiltonian

$$H = -J \sum_{<ij>} S_i S_j;\ S_i = \pm 1,\ J > 0, \tag{1.2}$$

where S_i corresponds to up or down spins and J is the interaction strength. One can study the evolution via Monte Carlo (MC) simulation [10] of this model. The evolution snapshots from such a simulation is presented in Fig. 1.4 which shows the growth of domains of like spins with the increase of time.

At the coarse-grained level such non-conserved dynamics is studied via

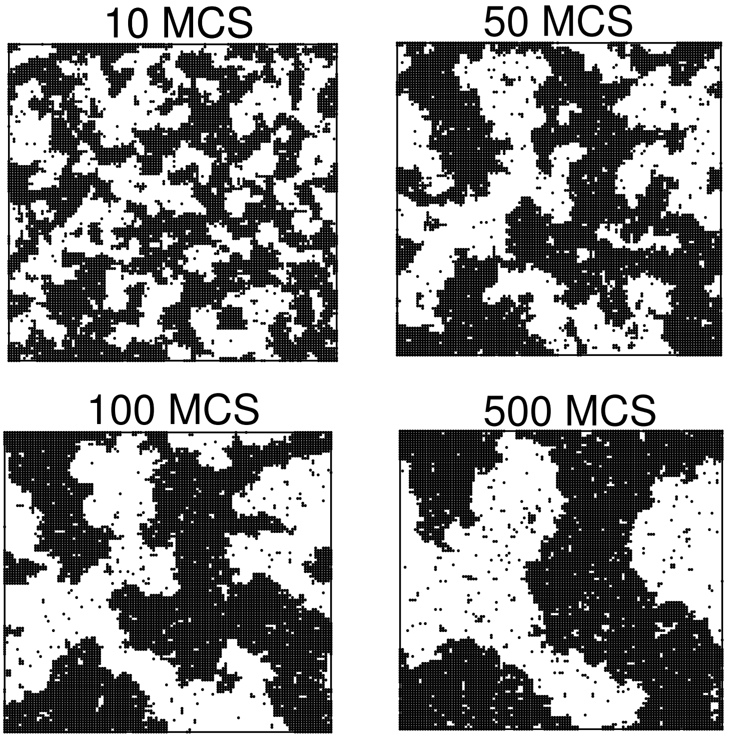

Figure 1.4: Evolution snapshots of domain growth in an Ising ferromagnet upon quenching to a temperature $T \simeq 0.7T_c$, obtained from Monte Carlo simulation. Black dots in the snapshots mark the location of the up spins. The times are in units of Monte Carlo Steps (MCS).

solving the time-dependent Ginzburg-Landau (TDGL) equation [3, 5]

$$\frac{d\psi(\vec{r},t)}{dt} = \psi(\vec{r},t) + \nabla^2\psi(\vec{r},t) - \psi^3(\vec{r},t), \tag{1.3}$$

where $\psi(\vec{r},t)$ is a coarse-grained space ($\vec{r}$) and time dependent order parameter. This equation can be obtained in a phenomenological manner [3, 5, 6] using the Ginzburg-Landau(GL) free energy functional

$$F[\psi(\vec{r}) = \int d\vec{r}[-\psi^2(\vec{r}) + \psi^4(\vec{r}) + (\nabla\psi(\vec{r}))^2], \tag{1.4}$$

in

$$\frac{\partial \psi}{\partial t} = -\frac{\delta F}{\delta t}, \tag{1.5}$$

in slow dynamics approximation. Eq. (1.3) is referred to as Model A according to the Hohenberg and Halperin [11] nomenclature.

For nonconserved evolution, considering the domain growth as a curvature driven phenomena, one writes down the interface velocity as

$$v_\ell = \frac{d\ell}{dt} \propto \frac{1}{\ell}. \tag{1.6}$$

This gives

$$\ell(t) \sim t^{1/2}, \tag{1.7}$$

known as the Cahn-Allen (CA) [12] growth law.

(b) Conserved Order-Parameter Kinetics

For a conserved order parameter dynamics, during the entire evolution, the sum of the order parameter remains constant. Example of conserved dynamics is the coarsening in a binary mixture (A+B) after quenching it from a high temperature homogeneously mixed phase to a temperature below the demixing critical temperature or a similar exercise in case of a vapor-liquid transition. Here we discuss the case of a solid binary mixture only.

The kinetics of phase separation in a solid binary mixture is studied via the Kawasaki-exchange [13] Monte Carlo simulation of the Ising model given

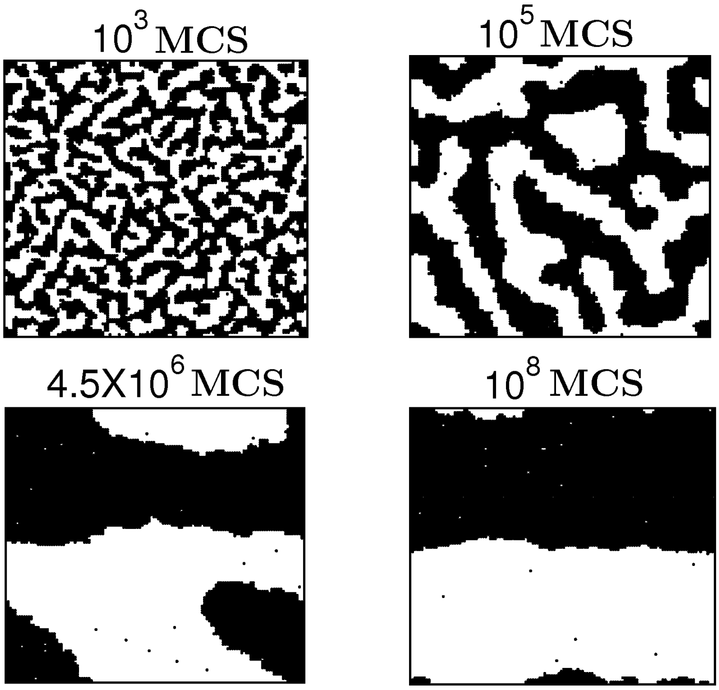

Figure 1.5: Snapshots showing the evolution of a conserved system obtained via Monte Carlo simulation of Kawasaki exchange Ising model, upon quenching from a high temperature ($T > T_c$) state to a temperature $T \simeq 0.5T_c$. The black dots mark the location of the up spins and the down spins are left unmarked.

by Eq. (1.2). Here the up spins correspond to one of the species (say A) and down spins to the other one. Evolution snapshots from this model are shown in Fig. 1.5. One can also use continuum dynamical equations, similar to the TDGL model, to study the phase separation in binary alloys. In this case one needs to incorporate the condition of conservation of order parameter which is done via the order parameter continuity equation

$$\frac{d\psi(\vec{r},t)}{dt} = -\nabla.\vec{j}. \tag{1.8}$$

In Eq.(1.8), the current $\vec{j}$ is defined as $\vec{j} = -\nabla\mu$, μ being the chemical potential that can be obtained from the derivative of GL free energy with respect to the order parameter. This leads to the Cahn Hilliard (CH) equation [14]

$$\frac{d\psi(\vec{r},t)}{dt} = -\nabla^2[\psi(\vec{r},t) + \nabla^2\psi(\vec{r},t) - \psi^3(\vec{r},t)], \tag{1.9}$$

which is also referred to as model B.

For solids the domain growth occurs via the diffusive transport of materials. In that case one associates the rate of domain growth with the gradient of chemical potential and writes [3]

$$\frac{d\ell(t)}{dt} \sim |\vec{\nabla}\mu| \sim \frac{\gamma}{\ell(t)^2}, \tag{1.10}$$

where γ is the A-B interfacial tension. Solving Eq.(1.10) one gets

$$\ell(t) \sim t^{1/3}. \tag{1.11}$$

This is known as the Lifshitz-Slyozov (LS) [15] growth law. This is the only expected growth law in solids.

(c) Conserved Domain Growth influenced by Hydrodynamics

In case of solid, hydrodynamics does not play any role. In contrast, for fluids and polymers, hydrodynamics does play an important role leading to an advective transport of material, due to which the growth is much faster [16–20]. The lattice gas (LG) Ising model has been extensively used to study the gas-liquid phase behavior and static critical phenomena. In the

LG model one considers a lattice system where a site is either occupied (by at most one particle) or empty. The kinetic energy of the particles is not considered and it is assumed that only the nearest neighbors interact which is given by the Hamiltonian

$$H = -\epsilon \sum_{<ij>} \delta(n_i, n_j);\ \epsilon > 0. \tag{1.12}$$

In Eq. (1.12), n_i is the occupation number which is 1 if a particle is present at the ith site and 0 if it is empty. This model is very well studied in the literature and as already stated above, this is reliable to study the phase behavior of gas-liquid phase separation. But, in order to study the fluid dynamics it is not appropriate since it does not account for hydrodynamics. For the latter purpose, a straight forward method is the Molecular Dynamics (MD) simulation [21] of a continuous potential model. In MD simulation hydrodynamics is automatically inbuilt.

Analogous to the coarse-grained continuum dynamical models in the solid case, there exists a model H [11] for the study of kinetics of fluid phase separation, where the CH equation is coupled with the Navier-Stokes equation, the later being introduced to take care of the velocity ($\vec{v}$) field. The equations for model H are written as [2,3,5,11]

$$\frac{\partial \psi(\vec{r},t)}{\partial t} + \vec{v}.\vec{\nabla}\psi(\vec{r},t) = D\nabla^2\mu, \tag{1.13}$$

$$\rho\frac{\partial \vec{v}(\vec{r},t)}{\partial t} = \eta\nabla^2 v - [\psi(\vec{r},t)\vec{\nabla}\mu + \rho(\vec{v}.\vec{\nabla})\vec{v}]_{\perp}, \tag{1.14}$$

where ρ is the density of the fluid, η is the viscosity, D is a diffusion constant and $\perp$ stands for the transverse component.

Now let us discuss the growth kinetics in a fluid. For fluid, initially the growth occurs via diffusive mechanism as in solids. But when the domain size becomes considerably large, the system enters the hydrodynamic regime. In $d = 3$, for a critical quench where one expects interconnected domain structures, to obtain the growth law, the surface energy density (γ/ℓ) is balanced by the viscous stress[$(6\pi\eta v_\ell/\ell)$, v_ℓ being the interface velocity and η is the shear viscosity]. This gives [2, 16]

$$v_\ell = \frac{d\ell(t)}{dt} = \frac{\gamma}{6\pi\eta}, \tag{1.15}$$

from which one obtains

$$\ell(t) \sim t. \tag{1.16}$$

This is referred to as the *viscous hydrodynamic* growth. The crossover from the initial diffusive growth to this linear regime occurs when $\ell(t) \gg \ell_{vis} \sim (D\eta)^{1/2}$. At late time, when $\ell(t) \gg \ell_{in}(= \eta^2/(\rho\gamma))$, one needs to balance the surface energy density with kinetic energy density (ρv_ℓ^2) to obtain

$$\frac{d\ell(t)}{dt} = \left(\frac{\gamma}{\rho\ell}\right)^{1/2}, \tag{1.17}$$

the solution of which gives

$$\ell(t) \sim t^{2/3}. \tag{1.18}$$

This is referred to as the inertial hydrodynamic growth [2,16]. Thus, domain growth in fluids with conserved order parameter can be summarized in the following sequence:

$$\ell(t) = \begin{cases} t^{1/3} & \text{(Diffusive Growth)}, \\ t & \text{(Viscous Hydrodynamic Growth)}, \\ t^{2/3} & \text{(Inertial Hydrodynamic Growth)}. \end{cases} \tag{1.19}$$

However, in case of off-critical quenches, where the droplet-like domain morphology is expected, the growth occurs via motion and collision [22,23] of the droplets of minority phase in the background of the majority phase. Here also the growth exponent α has a value $1/3$, but the mechanism of growth is entirely different from LS diffusive growth.

1.2.2 Calculation of average domain size in Computer Simulation

The coarsening phenomena in general is a self similar process, i.e, structures at two different times differ from each other only by a change in length scale, $\ell(t)$. One investigates this scaling property in the evolution pattern by looking at certain functions that characterize the morphology of the system. Examples are the two-point equal time-correlation function, structure factor, domain size distribution function, etc. All these functions exhibit dynamic scaling relation [3–5,22,24], arising from the self-similar property, that will be discussed subsequently.

The two point equal-time correlation function, $C(r,t)$, is calculated as

$$C(r,t) = \langle \psi(\vec{R},t)\psi(\vec{R}+\vec{r},t)\rangle - \langle \psi(\vec{R},t)\rangle\langle \psi(\vec{R}+\vec{r},t)\rangle, \tag{1.20}$$

where the angular brackets denote statistical averaging. The correlation functions obtained at different times show a scaling of the following form

$$C(r,t) = \tilde{C}(r/\ell(t)), \tag{1.21}$$

where $\tilde{C}$ is a time independent master function and $\ell(t)$, as already defined, is the characteristic time dependent length which is proportional to the average domain size at the time t. We have used this property as one of the measures for $\ell(t)$, in addition to others, as discussed below. The quantity which is directly measurable in experiments is the structure factor $S(\vec{k},t)$, Fourier transform of $C(r,t)$:

$$S(\vec{k},t) = \int d\vec{r} e^{i.\vec{k}.\vec{r}} C(\vec{r},t), \tag{1.22}$$

where $\vec{k}$ is the wave vector. $S(\vec{k},t)$ has the scaling form

$$S(k,t) = \ell(t)^d \tilde{S}(k\ell(t)), \tag{1.23}$$

where $\tilde{S}$ is the corresponding master function. In Eqs (1.21) and (1.23) we have assumed that the patterns are isotropic so that the vectors $\vec{r}$ and $\vec{k}$ can be replaced by their scalar counterparts. In addition, there has been significant interest in the domain-size distribution function $P(\ell_d,t)$. This quantity has a scaling behavior

$$P(\ell_d, t) = \ell(t)^{-1}\tilde{P}[\ell_d/\ell(t)]. \tag{1.24}$$

All the above scaling properties can be used to calculate $\ell(t)$. In addition, it is of much interest to learn the functional form of the master functions. In this context, significant understanding has been obtained for nonconserved dynamics. But it remains a major challenge for conserved order-parameter dynamics.

1.2.3 Aging in Domain Growth

Another important aspect to study in nonequilibrium systems is aging [25–28]. It is related to the phenomena of increase of relaxation time with the increase of age of the system, i.e., a younger system relaxes faster than the older ones. Unlike the standard studies in kinetics of phase separation, where the main focus is on calculation of different equal-time quantities, here the probes which are used are two-time quantities, e.g., the two-time correlation function or the auto-correlation function, $C(t, t_w)$, and the auto-response function, $R(t, t_w)$, which are defined as

$$C(t, tw) = \langle \psi(t)\psi(t_w)\rangle \tag{1.25}$$

$$R(t, t_w) = \delta\langle \psi(t)\rangle/\delta\langle h(t_w)\rangle, \tag{1.26}$$

where t_w is the *waiting time* or *age* of the system and t is the *observation time.* In the rest of this section, we will focus only on $C(t, t_w)$. Fig. 1.6 shows

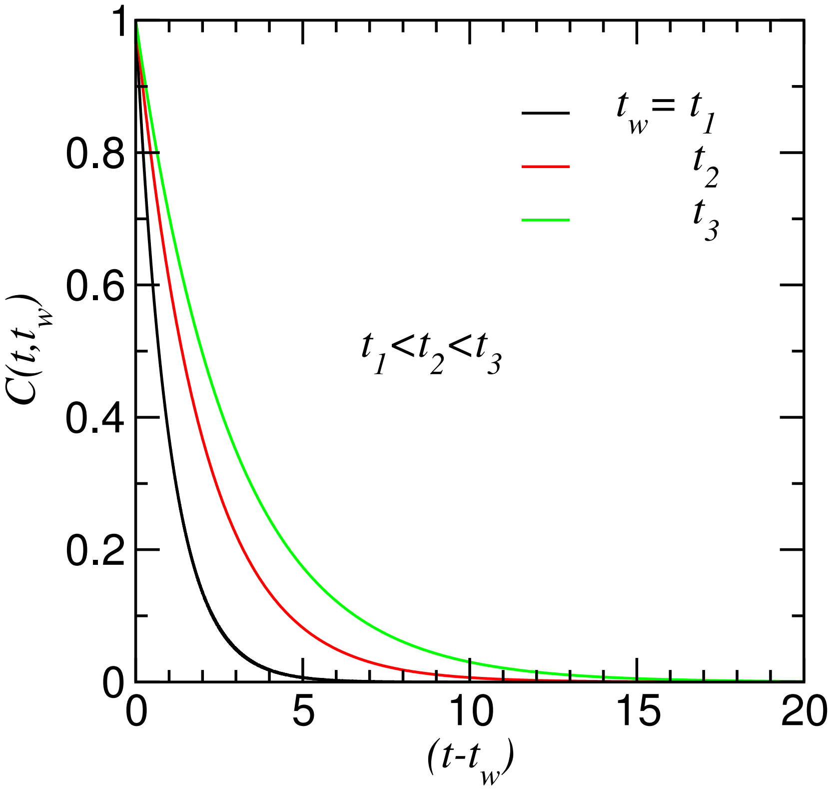

Figure 1.6: Schematic representation of behavior of auto-correlation function $C(t, t_w)$ as a function of $(t - t_w)$ for different t_ws. The diagram shows that $C(t, t_w)$ for lower t_w values are decaying faster than the ones with higher t_w values.

a schematic diagram of the behavior of $C(t, t_w)$ as a function of $(t - t_w)$ for different values of t_w. The picture depicts that as t_w increases $C(t, t_w)$ decays slower and slower.

Aging properties are of importance for slowly relaxing systems [26, 27] which includes a wide class of problems starting from structural and spin glasses to ferromagnetic ordering. A particular focus of the aging study in nonequilibrium scenario is to find out and understand the scaling behavior, if any, of the auto-correlation function $C(t, t_w)$. In this regard the works by Fisher and Huse [29, 30] are worth mentioning. From the studies of spin glass systems they predict a power law behavior of $C(t, t_w)$ as a function of characteristic length. They also provide bounds for the exponents. It is thought that their works are of relevance to the aging phenomena in broad varieties of nonequilibrium systems. Following them one can write down the scaling form for the auto-correlation function in terms of $\ell(t)$ and $\ell(t_w)$ as

$$C(t, t_w) \sim \left(\frac{\ell(t)}{\ell(t_w)}\right)^{-\lambda}, \tag{1.27}$$

where λ is an aging exponent.

In this thesis we would have a look on the aging behavior of the phase ordering systems in general. Of particular interest is the nonequilibrium evolution during the vapor-liquid transition. The interesting point in the fluid domain coarsening is the presence of different growth regimes. The crossovers from one regime to the other are expected to show up in the aging properties of the system as well.

1.3 Domain Coarsening in Confined Geometry

In this section we will discuss about phase separation in confined geometry with surface effects. Bulk phase separation in fluids and solids are relatively better understood. Recent developments in nano-structured materials and thin films have led to consider the effects of geometry or surface in the kinetics of phase separation, both theoretically and experimentally [31–38]. Particular interest is in the case when there is preferable attraction from the surfaces. For a binary fluid or solid, the surface may attract one of the components giving rise to the surface enrichment which causes the *surface directed spinodal decomposition* (SDSD). In case of vapor-liquid phase separation one needs to introduce attraction for all the particles. Before discussing the nonequilibrium phenomena, let us discuss some simple equilibrium aspects when a droplet, because of such interaction, has formed on a surface.

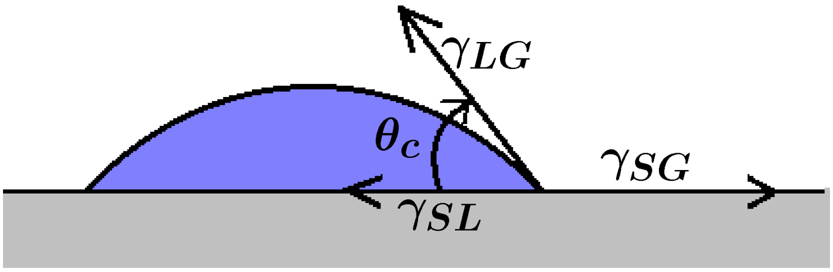

Figure 1.7: Schematic diagram showing a liquid droplet sitting on a surface. Different forces acting along the interfaces are marked by arrows in the figure and θ_c is the contact angle.

Fig.1.7 shows a liquid droplet placed on solid surface. This is related to vapor-liquid transition but has relevance to other types of transitions also e.g., solid-solid, liquid-liquid, solid-liquid. The arrows in the figure show the surface tensions γ_{SL}, γ_{SG} and γ_{LG}, acting along the solid-liquid (SL), solid-vapor (SG) and liquid-vapor (LG) interfaces, respectively. Here θ_c is the contact angle that is defined as the angle between solid-liquid interface and the liquid-gas interface. Now from the force balance equation one can easily write down the following equation:

$$\gamma_{LG}\ cos\theta_c = \gamma_{SG} - \gamma_{SL}. \tag{1.28}$$

This is the celebrated Young's equation [39]. The value of this angle θ_c decides the morphology. For $0° < \theta_c < 90°$ the surface is said to be in a wetting condition, while for $90° < \theta_c < 180°$ it is in a non-wet condition. The values $\theta_c = 0°$ and $\theta_c = 180°$ denote the perfectly wet and perfectly non-wet situations respectively. Fig. 1.7 shows a wet condition, the non-wet condition is shown in Fig. 1.8.

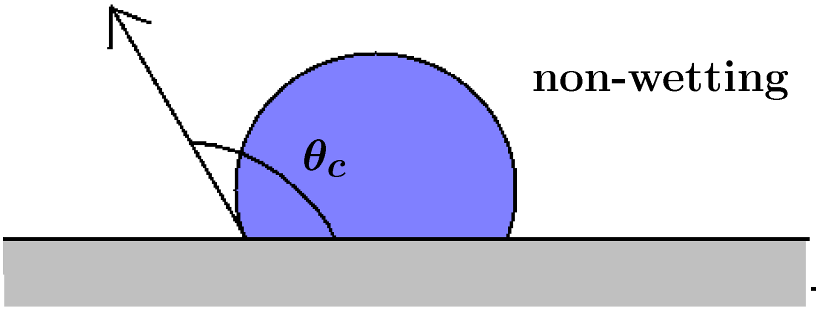

Figure 1.8: Schematic diagram showing the non-wet condition of a liquid droplet sitting on a surface. The corresponding wet condition is shown in Fig. 1.7.

The analogous Young's equation for a binary mixture (A+B) can be written as

$$\gamma_{AB}\ cos\theta_c = \gamma_{BS} - \gamma_{AS}, \tag{1.29}$$

where γ_{AB} denotes the surface tension between A and B phases, γ_{BS} between B phase and the substrate, while γ_{AS} is for A phase and substrate. For

$\gamma_{BS} - \gamma_{AS} > \gamma_{AB}$ A-rich phase covers the surface completely, i.e., forms a completely wet (CW) morphology whereas for $\gamma_{BS} - \gamma_{AS} < \gamma_{AB}$, both the phases are in contact with the surface, giving rise to a partially wet (PW) morphology.

In the nonequilibrium context, a popular coarse-grained continuum dynamical model for studying kinetics of phase separation in thin films is due to Puri and Binder (PB) [40]. Let us consider a binary mixture confined between two walls (S_1 and S_2) at $z = 0$ and D. One writes down the GL free energy functional in this case as

$$\begin{aligned} F[\psi] &= \int d\vec{r}\left[-\frac{\psi^2}{2} + \frac{\psi^4}{4} + \frac{1}{4}(\vec{\nabla}\psi)^2 + V(z)\psi\right] \\ &+ \int_{S_1} d\vec{\rho}\left\{-\frac{g}{2}[\psi(\vec{\rho},0)]^2 - h_1\psi(\vec{\rho},0) - \gamma\psi(\vec{\rho},0)\frac{\partial\psi}{\partial z}|_{z=0}\right\} \\ &+ \int_{S_2} d\vec{\rho}\left\{-\frac{g}{2}[\psi(\vec{\rho},D)]^2 - h_2\psi(\vec{\rho},D) + \gamma\psi(\vec{\rho},D)\frac{\partial\psi}{\partial z}|_{z=D}\right\} \\ &\equiv F_b + F_{S_1} + F_{S_2}, \end{aligned} \tag{1.30}$$

where F_b is the bulk contribution, whereas F_{S_1} and F_{S_2} are surface contributions. There, $V(z)$ is potential due to the surfaces whose values at the surfaces are h_1 and h_2. The parameters g and γ depend upon temperature and exchange coupling strengths in the bulk as well as in the surfaces. They characterize the equilibrium phase diagram of the film. For elaborate expressions of these quantities, we refer the readers to Ref. [40] . PB obtained dynamical equations using this functional for both bulk and surfaces. In the bulk, the order parameter evolves via the CH equation

$$\frac{\partial\psi(\vec{r},t)}{\partial t} = \vec{\nabla}.\left\{\vec{\nabla}\left[-\psi+\psi^3-\nabla^2\psi+V(z)\right]\right\};0<z<D. \tag{1.31}$$

The evolution of the order parameter at the surfaces is not conserved and is given as

$$\frac{\partial\psi(\vec{\rho},0,t)}{\partial t} = h_1 + g\psi(\vec{\rho},0,t)+\gamma\frac{\partial\psi}{\partial z}|_{z=0}; \tag{1.32}$$

$$\frac{\partial\psi(\vec{\rho},D,t)}{\partial t} = h_2 + g\psi(\vec{\rho},D,t)-\gamma\frac{\partial\psi}{\partial z}|_{z=D}. \tag{1.33}$$

In the above equations $\vec{\rho}$ is the coordinate in directions parallel to the surfaces (i.e. perpendicular to the z-axis). These equations are supplemented by the no-flux conditions at the surfaces:

$$J_z(\vec{\rho},0,t) = \left\{\frac{\partial}{\partial z}\left[-\psi+\psi^3-\nabla^2\psi+V(z)\right]\right\}_{z=0} = 0, \tag{1.34}$$

$$J_z(\vec{\rho},D,t) = \left\{\frac{\partial}{\partial z}\left[-\psi+\psi^3-\nabla^2\psi+V(z)\right]\right\}_{z=D} = 0. \tag{1.35}$$

One can also use the “full” molecular field description, using the Kawasaki-exchange kinetic Ising model [41], to study such phase separation in thin films. This kind of model is favorable over the Ginzburg-Landau kind of description as it works well even at temperatures far below the criticality. In fact, for more accurate study, MC simulations of Ising models with Kawasaki exchange kinetics can be used with additional terms in the Ising model due to surface effects. The corresponding Ising Hamiltonian for phase separation in confined geometry is given as

$$H = -J \sum_{<ij>} S_i S_j - J_s \sum_{<ij>} S_i S_j - H_{S_1} \sum_{i \in S_1} S_i - H_{S_2} \sum_{i \in S_2} S_i, \qquad (1.36)$$

where J and J_s are the interaction strength in bulk and surfaces respectively, while H_{S_1} and H_{S_2} are the surface fields. This gives a microscopic description of phase separation of solid binary mixtures in a thin film geometry.

So far we have discussed phase separation with diffusive dynamics in thin films which holds for solid binary mixture. However, for fluid mixtures, as already pointed out, hydrodynamics plays a major role. In this case, molecular dynamics simulations will prove to be useful with appropriate surface conditions. Of course, one can also use Model H by devising reasonable boundary conditions. It will be interesting to check if the growth laws and aging properties discussed in the bulk context are also valid in the present scenario.

1.4 Methodologies

This thesis deals with computer simulations of different microscopic models. We have studied three different phase transitions, viz., the solid binary mixture phase separation, the vapor-liquid phase transition and the paramagnetic to ferromagnetic transition. As mentioned earlier, in solids hydrodynamics is not important and growth occurs via diffusive transport of materials which could be mimicked very well by the MC simulations. In this case, one starts with a lattice containing randomly placed up and down spins in the Ising model context. This corresponds to a binary mixture at high temperature random phase where the A and B species are homogeneously mixed. Then the system is updated according to the standard Metropolis algorithm [10]. Note that MC simulations apply also for paramagnetic to ferromagnetic transition as well. In Metropolis algorithm configurations are generated by the non-deterministic time evolution using a transition probability which depends on the energy difference between the final and initial state. Let us discuss it in general context.

The time dependent behavior of a system can be described by the master equation

$$\frac{\partial P_n(t)}{\partial t} = -\sum_{n \neq m} [P_n(t) W_{n\to m} - P_m(t) W_{m\to n}], \tag{1.37}$$

where $P_n(t)$ is the probability of finding the system at state n at time t and $W_{n\to m}$ is the transition rate from $n \to m$. At equilibrium, left hand side of Eq. (1.37) is zero. Hence one gets

$$P_n(t) W_{n\to m} = P_m(t) W_{m\to n}. \tag{1.38}$$

This is referred to as the detailed balance. Any transition rate which satisfies the detailed balance is acceptable. For Metropolis algorithm these are as follows:

$$W_{n\to m} = \exp(-\Delta E/k_B T); \qquad \Delta E > 0 \tag{1.39}$$

$$= 1; \qquad \Delta E < 0, \tag{1.40}$$

where $\Delta E = E_m - E_n$. The presence of the argument ΔE in the exponential is justified considering that the relative probability between two states depends upon it. Note that we have set the time required to make a trial move to unity. This algorithm is implemented in computer simulations via the following steps.

(1) A particle i is randomly chosen.

(2) Particle i is given a random displacement or exchanged with one of its neighbors or its identity is changed (equivalent to flipping of a spin) depending upon the type of dynamics one is interested in.

(3) Difference in energy ΔE between the trial state and old state is calculated.

(4) A random number r is generated within the range $0 < r < 1$.

(5) If $r < \exp(-\Delta E/k_B T)$, then the new state is retained.

One Monte Carlo time step (MCS) means N such attempts, where N is the total number of spins or particles in the system.

For fluids, as mentioned earlier, hydrodynamics plays a major role. Hence in this thesis, for fluids, we have used molecular dynamics (MD) simulations to study the kinetics of vapor-liquid phase transition. In MD simulations, typically one incorporates the interaction between the particles via a smooth potential and calculates the forces on each particle. After computing the forces, one needs to solve the Newton's equations of motion for which several algorithms have been designed. In this thesis we have used the Verlet velocity algorithm [21]. The position update for the ith particle in this algorithm is given by

$$\vec{r_i}(t+\Delta t) = \vec{r_i}(t) + \vec{v_i}(t)\Delta t + \frac{\vec{f_i}(t)}{2m_i}\Delta t^2, \tag{1.41}$$

where $\vec{r_i}$ is the position, $\vec{v_i}$ is the velocity, $\vec{f_i}$ is the force on the particle and m_i is the mass of the particle. The corresponding velocity update is given as

$$\vec{v_i}(t+\Delta t) = \vec{v_i}(t) + \frac{\vec{f_i}(t+\Delta t) + \vec{f_i}(t)}{2m_i}\Delta t. \tag{1.42}$$

It can be shown that these equations are time reversal in nature which preserves the features of the Newton's Equations of motion.

In our study, we mainly have studied systems in the NVT or canonical ensemble, due to the need to keep the temperature constant. The above algorithm in the microcanonical ensemble, however, cannot keep the temperature constant. For that we need to use a thermostat. There are several thermostats available. In this thesis we have used the Nosé-Hoover thermostat for the purpose of preserving hydrodynamics. Here essentially one solves the equations

$$\frac{d^2\vec{r_i}}{dt^2} = \frac{f_i}{m_i} - \zeta(t)\vec{p_i}; \ \frac{d\zeta(t)}{dt} = \frac{1}{Q}\left(\sum_i {p_i}^2/m_i - 3N/k_BT\right), \tag{1.43}$$

where Q is a fictitious mass of the thermostat and p_i is the momentum. One can appreciate here that due to the introduction of the time dependent "viscosity" $\zeta(t)$, whenever the temperature (defined by the kinetic energy) tries to deviate from the assigned value, this quantity adjusts itself in such a way that the temperature starts coming back towards the desired value. For more on this algorithm and others, we refer the readers to Ref. [21].

1.5 Finite-Size Effects in Simulations and Corresponding Scaling

In computer simulations we always deal with systems of finite size. Such systems play a negative role in characterizing the behavior of observables in thermodynamic limit. Often the results which are expected to follow certain trend, deviate strongly due to finiteness of the system and because of this one might end up making wrong conclusions. This is referred to as the finite-size effect. The effect is very destructive in situations when there is a diverging length scale in a system. A crude way of eliminating this effect is to use larger and larger system sizes and wait for a situation when results for two different but large enough systems do overlap. But this method is not "elegant" and

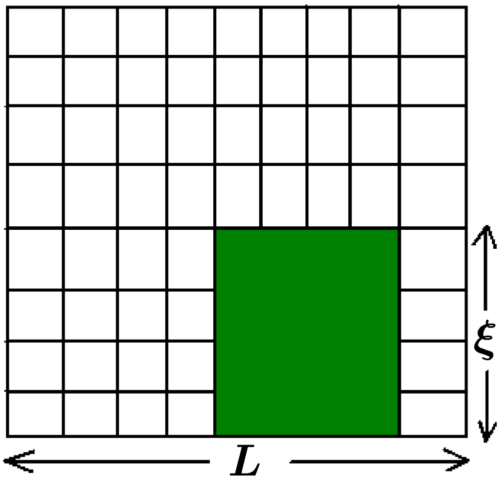

Figure 1.9: Schematic diagram showing the definition of equilibrium correlation length ξ. The maximum value of the correlation length is always limited by size of the system during the simulation.

is not safe to apply to systems with diverging lengths. A popular example for the latter is critical phenomena where the equilibrium correlation length

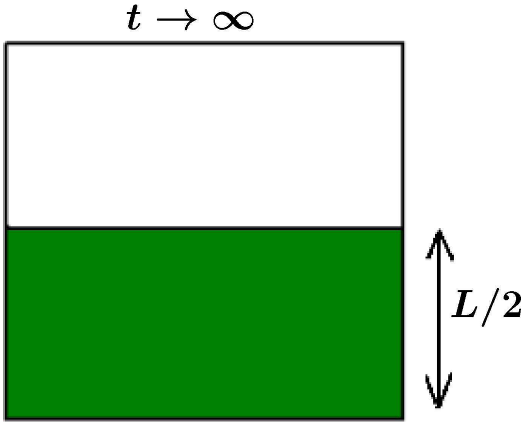

Figure 1.10: Schematic diagram showing that the maximum domain size $\ell_{\rm max}$ is limited by the length of the simulation box. The diagram shows that for 50 : 50 $2-d$ binary mixture (A+B) the maximum domain area that can be attained at $t \to \infty$ is $L^2/2$, where L is the system size.

(ξ) diverges as

$$\xi \approx \xi_0 \epsilon^{-\nu}, \tag{1.44}$$

where ν is the corresponding critical exponent and $\epsilon = |T-T_c|/T_c$, such that ξ is infinite at T_c. In Fig. 1.9, we schematically demonstrate the correlation length which measures the length over which the particles or spins in a system are correlated. It is quite easy to understand that ξ cannot grow beyond the system size. Thus for a finite system we cannot achieve the infinite length correlation. Here we must mention that the finite size effects are reasonably understood in the context of static critical phenomena.

Analogous to the correlation length in critical phenomena, in nonequilibrium domain coarsening the domain size diverges in the asymptotic limit

$t \rightarrow \infty$. In Fig. 1.10, we show that for $50 : 50$ $2-d$ binary mixture the maximum domain area that the system can attain is $L^2/2$, where L is the system size. In this nonequilibrium context, the traditional belief regarding the onset of the finite-size effect was that it appears when the average domain size $\ell(t)$ is an order of magnitude smaller than the system size. With this anticipation in mind, general trend has been to use larger and larger system sizes in order to achieve the asymptotic growth law. But we did not come across any rigorous study that truly quantified the size effects in such nonequilibrium systems. One of the major goals of this thesis is to point out the extent of finite size effects in domain coarsening problems. For this purpose, we have used the finite-size scaling analysis technique [42] which we discuss below.

This method can elegantly overcome the difficulties of finite-size effects. This technique has been extensively used in understanding of equilibrium critical phenomena. There, combining the expected behavior of a quantity in the thermodynamic limit with the system size, one arrives at certain scaling relations that contain the size L of the system. Then performing simulations for different values of L, one can confirm various theoretical predictions in thermodynamic limit. Despite its popularity in critical phenomena, this useful method is only rarely used in nonequilibrium problems. Here we briefly introduce it in the critical phenomena context following which we will provide hints of how to construct it for domain coarsening problems. In subsequent chapters it will be further discussed.

In critical phenomena, the divergence of a quantity Z, in the thermodynamic limit, is quantified in terms of the reduced temperature $\epsilon = |T - T_c|/T_c$

as

$$Z \sim \epsilon^{-z}. \tag{1.45}$$

Now, for a finite system, to account for the size effect, one introduces a scaling function Y, to write

$$Z \approx Y(y)\epsilon^{-z}, \tag{1.46}$$

where $y = L/\xi$ is a dimensionless scaling variable. Note that in the limit $y \to \infty$ ($L \to \infty$ or $\epsilon > 0$) one should recover Eq. (1.45). Hence Y should approach unity in that limit. Another important thing is that Y should be independent of system size. Thus, data coming from different system sizes should exhibit nice collapse, if, of course, the exponent is chosen correctly. So, it is advisable that one acquires data for different values of L and use the exponent as adjustable parameter to obtain data collapse and the value that accomplishes this purpose describes the behavior of the quantity correctly, in the thermodynamic limit. Here we note that this type of analysis is applicable in situations with nice scaling behavior of the observables. We end this section by mentioning that similar scaling can be constructed for coarsening problems also, by identifying ξ with ℓ and ϵ with $1/t$ [43, 44].

1.6 Overview of the Thesis

In this thesis we have studied domain coarsening phenomena, related to different phase transitions, via computer simulations. Based on the need we have used either Monte Carlo or molecular dynamics methods. For the analysis of the results, in addition to other techniques, we have used finite-size scaling theory. We have addressed questions related to pattern formation, domain growth laws and aging phenomena. Systems both in bulk and confined geometries were considered. Below we provide brief summary of results presented in different chapters.

In the second chapter, we have studied the kinetics of phase separation in a solid binary mixture with critical composition via Monte Carlo simulations of the kinetic Ising model in both $d = 2$ and $d = 3$. In this work we have successfully demonstrated the usefulness of finite-size scaling theory to understand simulation results for domain growth. We present results for morphology and time dependence of domain length. We have confirmed the Lifshitz-Slyozov (LS) diffusive growth law for conserved order-parameter kinetics. Our elegant finite-size scaling analysis showed that the correction to this growth law, at small length scales, is negligible for this composition. We have provided analytical argument for that. Finally, we have quite convincingly demonstrated that the finite-size effects is negligible for such coarsening problem. All our results have general validity in $d = 2$ and 3.

The results of Chapter 2 are for fixed composition and temperature. In Chapter 3, we took up detailed study on the temperature and composition dependence of kinetics of phase separation in $2 - d$ Ising model. In the temperature dependent case, a crucial issue is the difference between growth laws dominated by bulk diffusion and interface diffusion. In the latter case it is expected that the growth exponent is smaller than the LS value. Our finite-size scaling analysis shows that there is signature of small exponent at low enough temperature. A contrasting fact between the critical composition and off-critical composition is that, as opposed to the former, in the off-critical case one obtains droplet morphology with finite radius of curvature. So, composition dependent study is more useful to probe any correction to the growth law at early time. We note here that, for a long time it was thought that there was strong curvature dependent correction to the growth laws. Our studies show that at moderate temperature at least, such corrections are weak even for off-critical compositions. The results are linked with findings in equilibrium context for an understanding. Thirdly, our observation on finite-size effects appears to be composition and temperature independent. In addition, we presented comparative results on morphology also, involving critical and off-critical mixtures.

The fourth chapter deals with kinetics of vapor-liquid phase separation in a single component Lennard-Jones fluid. For this study we have used molecular dynamics simulations. Before getting into the nonequilibrium studies, we have estimated the phase diagram and critical point for this system. We also have made preliminary confirmation that this model belongs to the Ising universality class of equilibrium critical phenomena, as expected. On the nonequilibrium front, our objective was to find out the effect of hydrodynamics in domain growth as well as to address the question of the general validity of the weak finite-size effects in bulk phase separation. For the first time we show the presence of viscous hydrodynamic growth via MD simulation of vapor-liquid transitions. This confirms that the nonequilibrium universality of liquid-liquid and vapor-liquid transitions are unique. Our claim about the observation of hydrodynamic effect is confirmed via various different method of analysis. Finally, we find that the observation of weak size effect in case of solid binary mixture is true in the present case also.

In the fifth chapter we have studied the aging dynamics in various domain coarsening problems with particular focus on vapor-liquid transition of Chapter 4. For the latter system we have seen that at early time the autocorrelation function obeys the power-law decay. We have estimated the exponent of this power law which falls within the bound predicted by Fisher and Huse. At a later time we observed that the above power law decay crosses over to an exponential behavior. This crossover, we have clarified, is related to the diffusive to hydrodynamic crossover in domain growth laws. Further, we have provided analytical understanding of this exponential decay. Finally, we made interesting comparisons for the aging dynamics involving vapor-liquid, solid-solid and paramagnetic-ferromagnetic transitions.

In the last chapter, we have studied the kinetics of phase separation in thin films. We have studied the phase separation in solid binary mixture in confined geometry via Monte Carlo simulations by modeling the system with the atomistic Ising model. Our results show that the growth law is consistent with Lifshitz-Slyozov law. We have also reported preliminary results for off-critical compositions in solid-solid as well as vapor-liquid systems in contact with surfaces. The latter systems are of significant relevance in the context of surface induced heterogeneous nucleation.

Bibliography

[1] H.E. Stanley, *Introduction to Phase Transitions and Critical Phenomena* (Oxford University Press, Oxford, 1971).

[2] A. Onuki, *Phase Transition Dynamics* (Cambridge University Press, Cambridge, 2002).

[3] A.J. Bray, Adv. Phys. **51**, 481 (2002).

[4] K. Binder, in *Phase Transformation of Materials*, ed. R.W. Cahn, P. Haasen and E.J. Kramer, Material Science and Technology, Vol **5** (VCH, Weinheim, 1991), p.405.

[5] S. Puri and V. Wadhawan (eds.), *Kinetics of Phase transitions* (CRC Press, Boca Raton, 2009).

[6] R.A.L. Jones, *Soft Condensed Matter* (Oxford University Press, Oxford, 2008).

[7] K. Binder, Rep. Prog. Phys. **50**, 783 (1987).

[8] H. Furukawa, Adv. Phys. **34**, 703 (1985).

[9] R.J. Galuber, J. Math. Phys. **4**, 294 (1963).

[10] D.P. Landau and K. Binder, *A Guide to Monte Carlo Simulations in Statistical Physics* (Cambridge University Press, Cambridge, 2009).

[11] P.C. Hohenberg and B.I. Halperin, Rev. Mod. Phys. **49**, 435 (1977).

[12] S.E. Allen and J.W. Cahn, Acta. Metall. **27**, 1085 (1979).

[13] K. Kawasaki, in *Phase Transition and Critical Phenomena*, edited by C. Domd and M.S. Green (Academic, New York, 1972), Vol. 2, p.443.

[14] J.W. Cahn and J.I. Hilliard, J. Chem. Phys. **28**, 258 (1958).

[15] I.M. Lifshitz and V.V. Slyozov, J. Phys. Chem. Solids **19**, 35 (1961).

[16] E.D. Siggia, Phys. Rev. A **20**, 595 (1979).

[17] H. Furukawa, Phys. Rev. A **31**, 1103 (1985).

[18] H. Furukawa, Phys. Rev. A **36**, 2228 (1987).

[19] S. Ahmad, S.K. Das and S. Puri, Phys. Rev. E **82**, 040107 (2010).

[20] S. Majumder and S.K. Das, Europhys. Lett. **95**, 46002 (2011).

[21] D. Frankel and B. Smit, *Understanding Molecular Simulations: From Algorithms to Applications* (Academic Press, San Diego, 2002).

[22] K. Binder and D. Stauffer, Phys. Rev. Lett. **33**,1006 (1974).

[23] K. Binder, Phys. Rev. B **15**, 4425 (1977).

[24] A. Sicilia, Y. Sarrazin, J.J. Arenzon, A.J. Bray, L.F. Cugliandolo, Phys. Rev. E **80**, 031121 (2009).

[25] M. Zannetti in *Kinetics of Phase Transitions*, edited by S. Puri and V. Wadhawan (2009).

[26] J.-P. Bouchaud, L.F. Cugaliandolo, J. Kurchan and M. Mezard in *Spin Glasses and Random Fields*, edited by A.P. Young (World Scientific, Singapore, 1997), Chap. 6.

[27] L.F. Cugaliabdolo, Dynamics of glassy systems, in *Slow Relaxation and Non-equilibrium Dynamics in Condensed Matter* edited by J.-L. Barrat, J. Dalibard, J. Kurchan and M.V. Fiegel'man (Springer -Verlag, Heidelberg, 2002).

[28] L.C.E. Struick, *Physical Aging in Amorphous Polymer and Other Materials* (Elsevier, Houston, 1976).

[29] D.A. Huse, Phys. Rev. B, **40**, 304 (1989).

[30] D.S. Fisher and D.A. Huse, Phys. Rev. B, **38**, 373 (1989).

[31] R. A. L. Jones, L. J. Norton, E. J. Kramer, F. S. Bates, and P. Wiltzius, Phys. Rev. Lett. **66**, 1326 (1991).

[32] G. Krausch, Mater. Sci. Eng. R. **14**, 1 (1995).

[33] S. Puri and K. Binder, Phys. Rev. A **46**, R4487 (1992); Phys. Rev. E **49**, 5359 (1994).

[34] G. Brown and A. Chakrabarti, Phys. Rev. A **46**, 4829 (1992).

[35] S. Puri and H. L. Frisch, J. Phys.: Condens. Matter **9**, 2109 (1997).

[36] S. Puri and K. Binder, Phys. Rev. Lett. **86**, 1797 (2001); Phys. Rev. E **66**, 061602 (2002).

[37] S. K. Das, S. Puri, J. Horbach, and K. Binder, Phys. Rev. E **72**, 061603 (2005).

[38] S. K. Das, S. Puri, J. Horbach, and K. Binder, Phys. Rev. Lett. **96**, 016107 (2006); Phys. Rev. E **73**, 031604 (2006).

[39] T. Young, Philos. Trans.R. Soc. London **95**, 65 (1805).

[40] S. Puri and K. Binder, J. Stat. Phys. **77**, 145 (1994).

[41] S.K.Das, J. Horbach and K.Binder Phys. Rev. E. **79**, 021602 (2009).

[42] M.E. Fisher, in *Critical Phenomena*, edited by M.S. Green (Academic, London, 1971) p1.

[43] D.W. Heermann, L. Yixue and K. Binder, Physica A **230**, 132 (1996).

[44] S. Majumder and S.K. Das, Phys. Rev. E **81**, 050102 (R) 2010.

Chapter 2

Kinetics of Phase Separation in Ising Model with Symmetric Composition in d=2 and 3

2.1 Introduction

Despite the fact that kinetics of phase separation is introduced in Chapter 1, for the sake of completeness, we discuss some of the basic facts here again. Also note that the results presented here are almost entirely reproduced (including text) from References [1, 2] for which American Physical Society has the copyright.

When a homogeneous binary mixture (A+B) is quenched inside the miscibility gap, the system falls out of equilibrium and moves towards its new equilibrium state via formation and growth of domains rich in A- or B- particles [3–5]. This coarsening of domains is a scaling phenomenon, e.g., two-point equal-time correlation function $C(r,t)$, the structure factor $S(k,t)$ and the domain size distribution function $P(\ell_d,t)$ obey the scaling relations

$$\begin{aligned} C(r,t) &\equiv \tilde{C}(r/\ell(t)), && (2.1)\\ S(k,t) &\equiv \ell(t)^d \tilde{S}(k\ell(t)), && (2.2)\\ P(\ell_d,t) &\equiv \ell(t)^{-1}\tilde{P}[\ell_d/\ell(t)], && (2.3) \end{aligned}$$

where the average domain size $\ell(t)$ increases with time (t) in a power-law fashion

$$\ell(t) \sim t^{\alpha}, \tag{2.4}$$

and $\tilde{C}(x)$, $\tilde{S}(y)$ and $\tilde{P}(z)$ are scaling functions independent of $\ell(t)$. In Eq. (2.4), the growth exponent α depends upon the transport mechanism.

For diffusive growth, associating the rate of increase of $\ell(t)$ with the chemical potential (μ) gradient, one can write [3]

$$\frac{d\ell(t)}{dt} \sim |\vec{\nabla}\mu| \sim \frac{\sigma}{\ell(t)^2}, \tag{2.5}$$

σ being the A-B interfacial tension. Solution of Eq. (2.5) gives $\alpha = 1/3$, known as Lifshitz-Slyozov (LS) law [6]. The LS behavior is the only asymptotic growth law expected for phase-separating solid mixtures. However, for fluids and polymers, one expects faster growth at large length scales where hydrodynamic effects are dominant. For the latter, in $d = 3$, convective transport yields additional growth regimes [7,8] with

$$\begin{aligned}\alpha &= 1, \quad \ell(t) \ll \ell_{in}, \\ &= 2/3, \quad \ell(t) \gg \ell_{in}. \end{aligned} \tag{2.6}$$

In Eq. (2.6), the inertial length $\ell_{in}[\simeq \eta^2/(\rho\sigma), \eta$ and ρ being the shear viscosity and mass density] marks the crossover from a low-Reynold-number viscous hydrodynamic regime to an inertial regime.

In this work we have undertaken a comprehensive study to learn about the finite-size effects in domain coarsening in Ising model with conserved order parameter dynamics and understand the behavior of growth exponent as a function of time, via application of finite-size scaling method [9,10], both in space dimensions $d = 2$ and $d = 3$. While originally developed to understand simulations in equilibrium critical phenomena, finite-size scaling method has found interesting applications [2,11,12] in nonequilibrium processes as well. In this chapter, we exploit this method appropriately in the context of diffusive phase separation kinetics to show that for critical quench the LS value of α sets in very early and the effect of size is very small.

Diffusive domain coarsening in solid binary mixtures has been extensively studied via Ising model

$$H = -J \sum_{<ij>} S_i S_j; \; S_i = \pm 1, \; J > 0, \tag{2.7}$$

prototype for a large class of critical phase transitions. Here one can identify the spin $S_i = +1(-1)$ at lattice site i with an A-particle (B-particle). Note that $< ij >$ in Eq. (2.7) stands for summation over only the nearest neighbors. One can also study the kinetics of phase separation via dynamical equations which can be obtained from Ising models in mean field approximation by using a master equation approach [13, 14] with Kawasaki exchange kinetics [15]. Upon coarse-graining, such equations lead to the Cahn-Hilliard (CH) equation

$$\frac{d\psi(\vec{r},t)}{dt} = -\nabla^2[\psi(\vec{r},t) + \nabla^2\psi(\vec{r},t) - \psi^3(\vec{r},t)], \tag{2.8}$$

where $\psi(\vec{r},t)$ is a coarse-grained time-dependent local order parameter. Note that such continuum description could also be obtained in a phenomenological manner [3, 16] using a coarse-grained Ginzburg-Landau(GL) free energy functional with the requirement of conservation of material. The CH equation with an added thermal noise is expected to be equivalent to Monte Carlo (MC) simulations [17, 18] of kinetic Ising models.

In Eq. (2.8), typical distance over which the order parameter is coarse-grained is of the size of equilibrium correlation length, ξ. In situations when one is interested in studying the kinetics in the close vicinity of the critical point, without focusing on the dynamics at microscopic level, Eq. (2.8) is computationally very useful in achieving the asymptotic [19] behavior. However, for deep quenches one needs to incorporate higher order terms than are usually used in the GL Hamiltonian. Also at very low temperature, where ξ is of the order of a lattice constant, CH equation would not provide information of a large effective system size compared to the atomistic Ising model. Particular focus of this work is to learn finite-size effects and dynamics at the early stage both of which have received much less attention as opposed to the identification of domain growth law in long-time limit, despite their obvious importance both fundamentally as well as technologically, e.g, in nano-science and technology. In view of that, we choose to revisit kinetics of phase separation in Ising model via MC simulations.

While MC simulations have been used immensely in the understanding of nonequilibrium domain growth phenomena both with conserved [11, 12, 20–25] and non-conserved [12, 26, 27] order parameter, earlier studies of phase ordering in conserved Ising model with critical (50:50) composition reported [28, 29] estimates of $\alpha \epsilon [0.17, 0.25]$, deviating drastically from the expected LS law. Even arguments in favor of logarithmic growth were proposed [30]. Note that these earlier reports were based on MC simulations for very short period of time where contamination of domain structures due to thermal noise might not have been taken care of, which could act as a source of significant error in the measurement of average domain size.

Later, the discrepancy of the previous results with the expected LS behavior was understood to be due to strong corrections to scaling at early time. To account for this [21] higher order terms in Eq. (2.5) were incorporated to write

$$\frac{d\ell(t)}{dt} = \frac{C_1}{\ell(t)^2} + \frac{C_2}{\ell(t)^3} + O(\ell(t)^{-4}), \tag{2.9}$$

which in the long time limit gives a solution $\propto t^{1/3}$, however, would give rise to leading order correction linear in $1/\ell(t)$ to the instantaneous exponent. Thus LS behavior will be observed only in the limit $\ell(t \to \infty) \to \infty$. Indeed, consistency with a linear correction was observed for 50:50 binary mixture [21, 22] as well as for multicomponent mixtures [25]. Present work, however, convincingly demonstrates that the observation of LS value of the exponent only in the asymptotic limit was misleading and presence of a time independent bare length in $\ell(t)$ was responsible for the numerical data exhibiting such trend.

Most of the studies till date, stressed on using large systems, with the anticipation of strong finite-size effects [31] combined with the expectation that the LS law will be realized only in the large $\ell(t)$ limit. This strategy, of course, will prove to be useful when there is dynamical crossover as in domain coarsening in fluids [cf. Eq. (2.6)] where the system size should be significantly larger than smallest characteristic length scale in a particular regime. However, consideration of arbitrarily large system sizes restricts the access of large time scale, particularly for molecular dynamics simulation of fluid phase separation [32–34]. It is worth mentioning that the typical system sizes authors consider these days contain number of lattice sites or particles of the order of million, which is too large, even for present day computers, to access long time scale that often is a necessity. Such choice of large systems, in addition to the anticipation of strong finite-size effect, was often motivated by the expectation of better self-averaging [31], an issue [26] that needs further attention to be resolved. Thus a judicial choice of system sizes is very crucial for such problems [35] which in turn requires appropriate knowledge of finite-size effects [2]. While recent focus has been in more complicated systems [36–43] with realistic interactions and physical boundary conditions, many such basic information as discussed above are lacking even in a situation as simple as Ising systems.

This chapter is organized as follows. In Sec.2.2, we describe the details of simulation and finite-size scaling method. Results for both $d = 2$ and $d = 3$ are presented in Sec. 2.3, while Sec. 2.4 concludes the chapter along with a discussion of future possibilities in this direction.

2.2 Methods

2.2.1 Details of Simulation and Calculation of observables

In the MC simulation of Ising model, the conserved order-parameter dynamics, where composition of up (A particle) and down (B particle) spins remains fixed during the entire evolution, is implemented via standard Kawasaki exchange mechanism [15] where interchange of positions between a randomly chosen pair of nearest neighbor (nn) spins consists a trial move. A move is accepted or rejected according to standard Metropolis algorithm [17]. One MC step (MCS) consists of exchange trials over L^d pairs of spins, L being the linear dimension of a square (cubic) system. Periodic boundary conditions were applied in all directions.

Note that with the increase of temperature, accurate measurement of average domain size becomes difficult due to the presence of noisy clusters of the size of $\xi(T)$. On the other hand, at very low temperature growth is

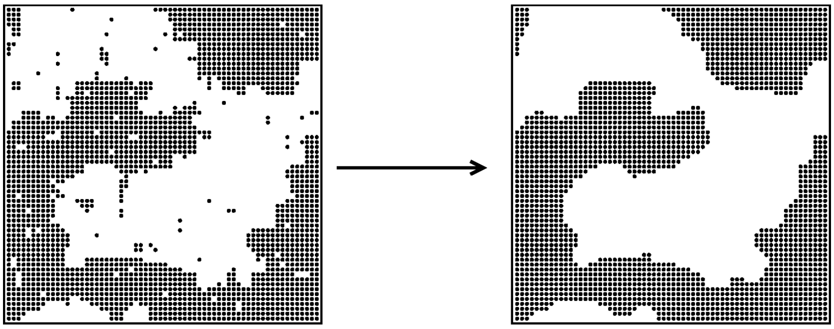

Figure 2.1: Left panel: Snapshot of a $2-d$ Ising model at $T = 0.85T_c$ obtained from the Monte Carlo simulation via Kawasaki exchange kinetics, for $L = 64$ at $t = 5 \times 10^3$ MCS. Right panel: Same snapshot after removing the noise via the exercise described in the text. A-particles are marked by black dots whereas B-particles are unmarked.

hampered by metastability. To avoid the latter problem, we have set the temperature towards the higher side and calculated all the physical quantities from pure domain morphology after eliminating the thermal noise via a majority spin rule. There a spin at a lattice site i was replaced by the sign of the majority of the spins sitting at i and nn of i (depending upon the noise level i.e., average size of noise clusters, extension to distant neighbors may also become necessary). In Fig. 2.1 we demonstrate such filtering process for a rather high temperature. The left panel corresponds to the original snapshot from the MC simulation on $2-d$ square lattice at $T = 0.85T_c$ with $L = 64$ at $t = 5 \times 10^3$ MCS. One can appreciate that presence of substantial noise elements here would give rise to smaller value of $\ell(t)$ than the actual. The right panel of the figure shows the snapshot with pure domain morphology obtained after implementing the noise removal exercise described above. Of course, one should be careful that too many such iterations or consideration of very distant neighbors may alter the basic structure. However, in the present case, no such deformation has taken place. All the quantities in our simulation were calculated by using snapshots with such pure domain structure. In brief, the advantage of the above procedure could be understood in the following way. In most aging processes fast, quasi-equilibrium degrees of freedom co-exist with slow nonequilibrium degrees, leading to an additive separation of the thermodynamic observables. Our method gets rid of the faster, equilibrium degrees of freedom.

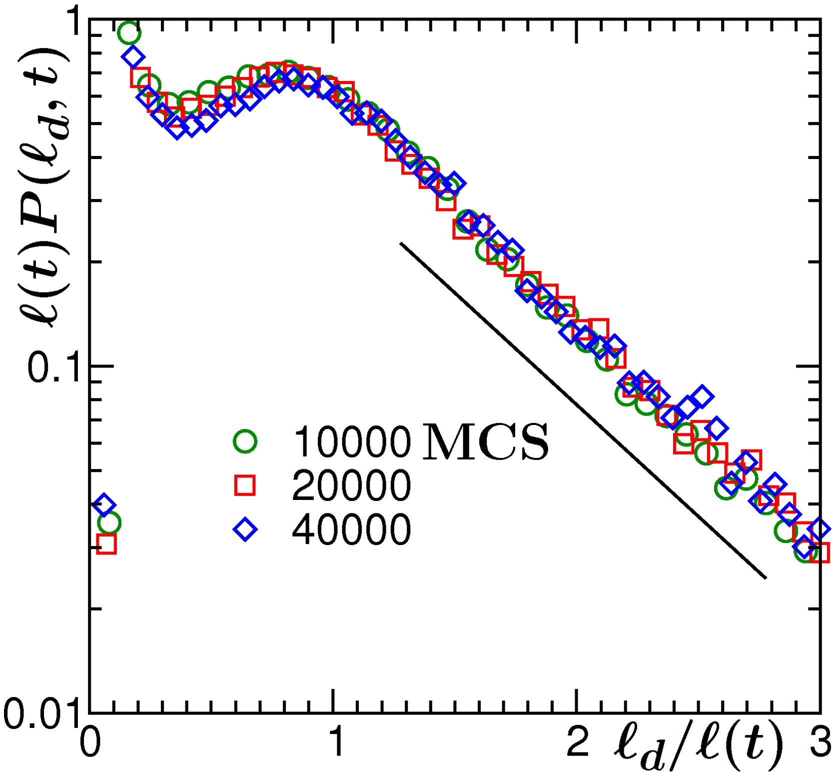

Figure 2.2: Scaling plot of domain size distribution $P(\ell_d, t)$, from different times, as indicated, for the system in Fig. 2.1. The data were averaged over 50 independent initial configurations. The solid line verifies exponential decay of the tail.

In Fig. 2.2 we present the scaling plots of domain size distribution function, viz., plots of $\ell(t)P(\ell_d, t)$ vs $\ell_d/\ell(t)$ where $\ell(t)$ was calculated from the first moment of the normalized distribution $P(\ell_d, t)$ as

$$\ell(t) = \int d\ell_d \; \ell_d P(\ell_d, t), \tag{2.10}$$

with length ℓ_d being obtained from the separation between two successive interfaces (between A and B domains) in x-, y- or z- directions. Figs. 2.3 and 2.4 show the scaling plots of correlation function $C(r, t)$ and its Fourier transform $S(k, t)$, in accordance with Eqs. (2.1) and (2.2), where $C(r, t)$ was calculated as

$$C(r, t) = \langle S_i S_j \rangle; \quad r = |\vec{i} - \vec{j}|. \tag{2.11}$$

Note that these scaling plots for all the quantities were obtained by using the values of $\ell(t)$ obtained from Eq. (2.10). Of course, independently $\ell(t)$ could be calculated from the decay of $C(r, t)$ as well the first moment of normalized $S(k, t)$ as

$$C(r = \ell(t), t) = h, \tag{2.12}$$

and

$$\ell(t) = \frac{1}{\int dk \; kS(k)}. \tag{2.13}$$

When calculated from a completely noise-free morphology, all the above mentioned methods for the calculation of $\ell(t)$ must give results proportional to each other. When h is set to a rather small value, particularly when the

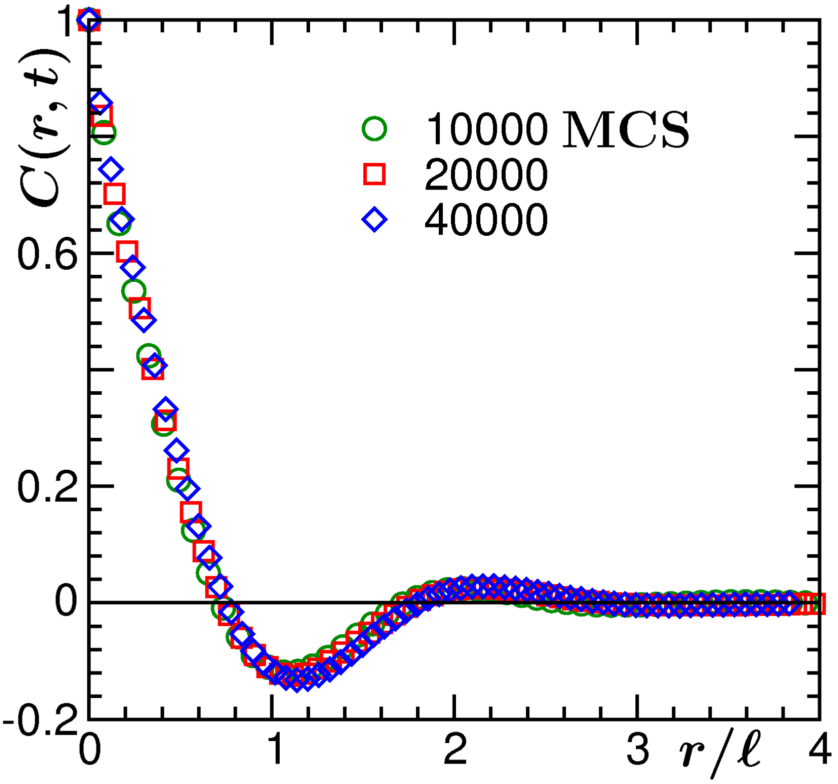

Figure 2.3: Scaling plot of correlation function $C(r,t)$ at different times, as indicated, for the system in Fig. 2.1.

decay length is larger than the average size of the noisy clusters, calculation of $\ell(t)$ from Eq. (2.12) is not expected to be affected much by the presence of noise. The same applies for Eq. (2.13). However, when calculated via Eq. (2.10), either the distribution up-to the length of average noise size should be appropriately modified or noise should be completely eliminated. The latter strategy is more appropriate since it gives better shape to all the form functions. In our calculation, in Eq. (2.12), h will correspond to first zero of $C(r,t)$.

All the results presented in Figs. 2.2, 2.3, and 2.4 are obtained from pure domain morphology and the nice data collapse obtained in each case

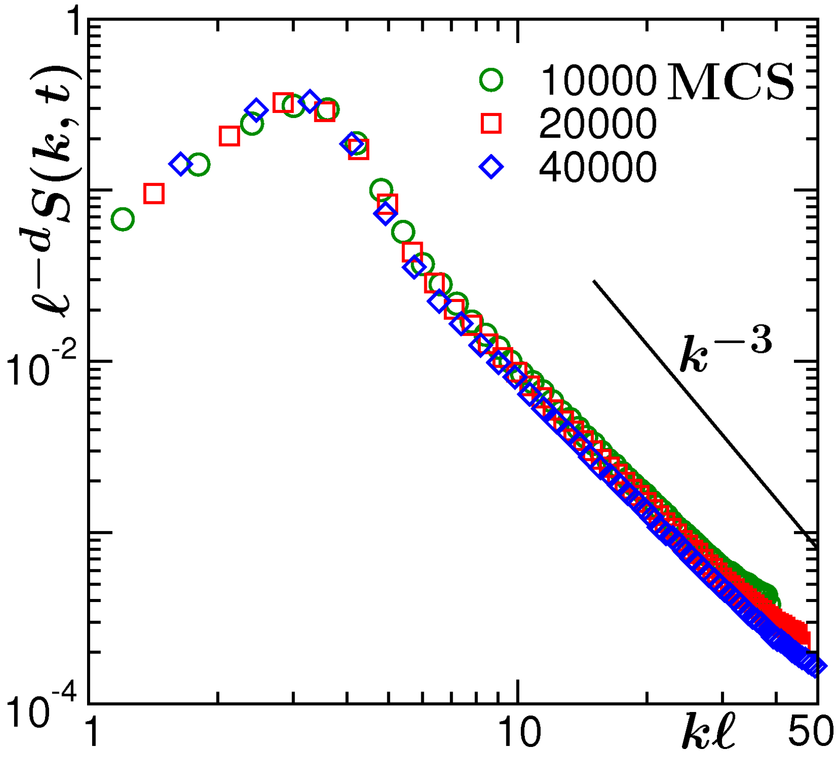

Figure 2.4: Scaling plot of structure factor $S(k,t)$, from different times, as indicated, for the system in Fig. 2.1. The solid line there corresponds to the Porod tail.

using the measure of $\ell(t)$ from Eq. (2.10) speaks for the equivalence of all the definitions, Eqs. (2.10), (2.12) and (2.13). The linear behavior of the tail region in (a) on a semi-log plot is consistent with an exponential decay of $P(\ell_d,t)$. Here the noisy look (oscillatory behavior) at late time or large domain size limit (which was also observed in other recent studies [44,45]) is due to lack of statistics when $\ell(t)$ becomes of the order of the system size. On the other hand, the linear look of large wave vector (k) data in (c) confirms the generalized Porod law [3,46,47]

$$S(k,t) \sim k^{-(d+n)}. \tag{2.14}$$

Note that in the present case $d = 2$ and $n = 1$ (number of components of the order parameter). It is worth mentioning that one would have observed a slower decay of the structure factor had the noise not been removed.

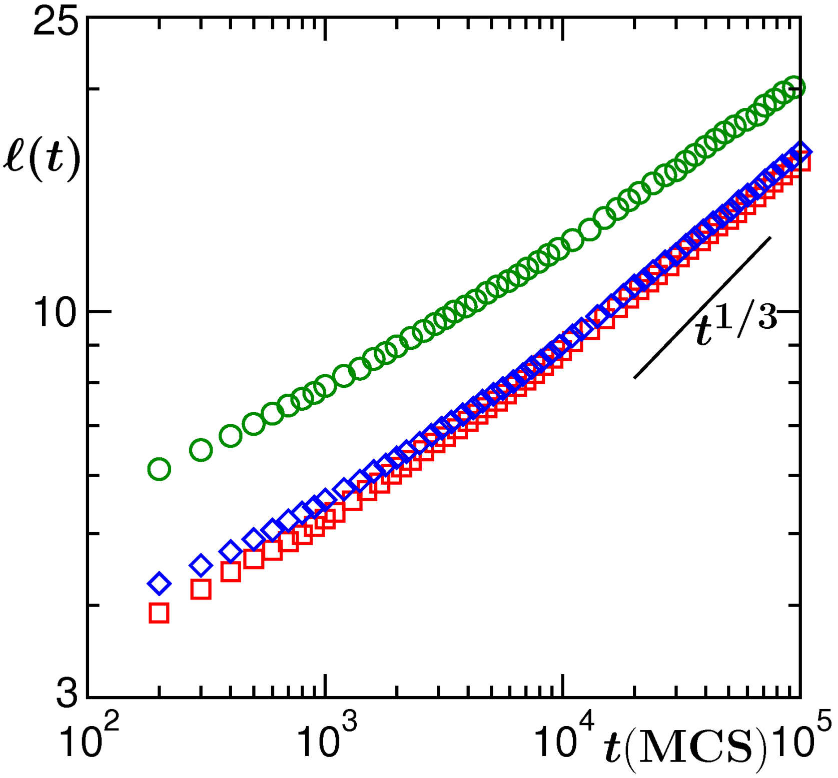

Figure 2.5: Average domain size is plotted on a log-scale as a function of time t. Different symbols correspond to calculation of $\ell(t)$ from different quantities : circles from $P(\ell_d, t)$, squares from first zero-crossing of $C(r, t)$, diamonds from the first moment of $S(k, t)$. Results presented were obtained from pure domain structure as demonstrated in the right panel of Fig. 2.1, with $L^2 = 128^2$ and $T = 0.85T_c$. The solid line corresponds to the theoretically expected $t^{1/3}$ behavior.

In Fig. 2.5 we present the length scale results obtained from all the above mentioned methods on log scale, all of which look proportional to each other as was also clear from the exercise of Figs. 2.2, 2.3 and 2.4. The data at late times look consistent with the expected exponent $\alpha = 1/3$. Note that if the temperature is sufficiently close to T_c, for long enough time the noise might not have equilibrated to the equilibrium value inside the true domains. In such a situation, presence of two length scales in the problem may give rise to misleading value of the exponent if the noise (equilibrium degree of freedom) is not eliminated and range of fitting is small. Indeed a fitting of the data, obtained from original snapshots (not shown), at temperature $0.85T_c$, to the form

$$\ell(t) = C + At^{\alpha}, \tag{2.15}$$

in the range $[0, 20000]$ MCS gives $\alpha = [0.15, 0.25]$ (the value being larger when $\ell(t)$ is calculated from (2.12) or (2.13)) which is consistent with earlier reports [28,29]. On the other hand a similar fitting to the data obtained after removing the noise gives $\alpha = [0.3, 0.34]$ and within statistical deviation, does not depend upon the range of fitting. This latter result is already suggestive of absence of strong correction to the scaling. However, since data fitting is always not a very reliable exercise as will be discussed later, to further substantiate the claim about small correction to scaling, we take the route of finite-size scaling analysis that will also be useful in quantifying the finite-size effect.

Before describing the finite-size scaling technique we put some more words about the appropriateness and caveats of the noise elimination exercise. In Fig. 2.6, we show the plots of $\ell(t)$ vs t, on a double log scale, for two different temperatures. For both the temperatures we have included results from noisy as well as noise-free environment. For the lower temperature,

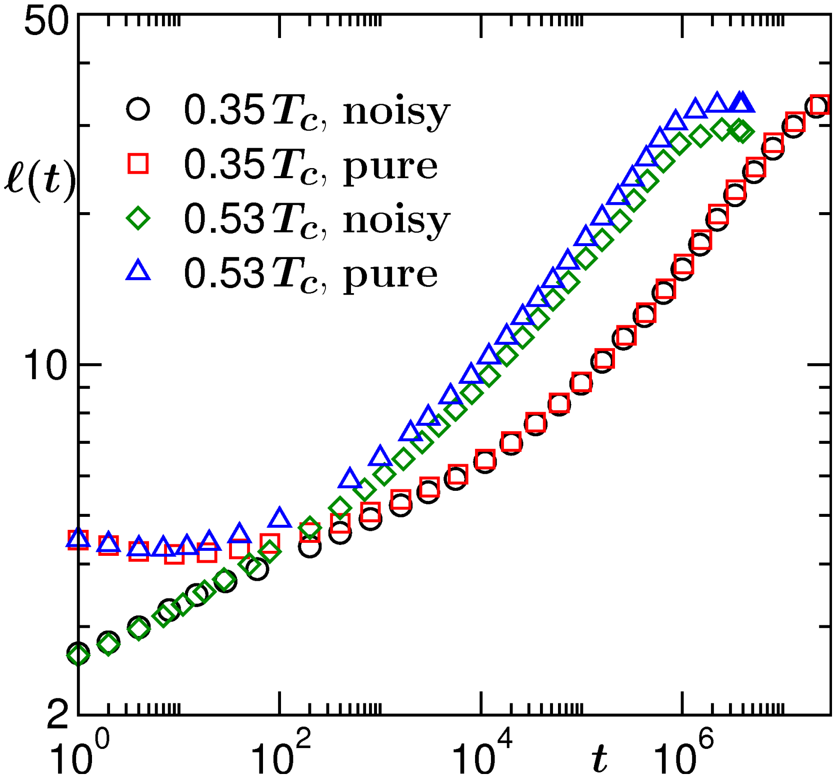

Figure 2.6: Log-log plot of average domain size, $\ell(t)$, as function of time for $50:50$ composition. Results from two different temperatures are shown. For each of the temperatures we have included results obtained from noisy and noise-free environments as indicated. All results are obtained from the domain size distribution functions.

of course, both the curves almost overlap with each other. This is due to very low level of noise. In addition to the discussion already provided, the appropriateness of the method can be further appreciated from the following fact. The equilibrium value of $\ell(t)$ (where the plot flattens) is different for the two temperatures for the calculation with noise though the system size L is same for both the cases. Note that since the results are presented for the same system size, the equilibrium length, henceforth referred to as ℓ_{max}, should be same for both the temperatures. Indeed, this is the case when the calculation is done from configurations without noise. However, at very early time, when the domains are very small, the noise removal exercise comes with some problem. In this regime, along with noise, many domains also get removed. But it could be seen that during very early time, $\ell(t)$ for both the temperatures match with each other which is expected if, of course, the growth amplitude is not significantly different from each other. (This latter scenario may be true when the presented temperatures are very close to T_c). In view of that, for the purpose of finite-size scaling analysis, we will combine the $\ell(t)$ data with noise upto $t = 10^2$ Monte Carlo steps (MCS) and the noise-free data from the rest of the period.

2.2.2 Formulation of Finite-Size Scaling

In equilibrium critical phenomena, the singularity of a quantity Z is characterized in terms of $\epsilon = |T - T_c|$, temperature deviation from the critical point, as

$$Z \approx Z_0 \epsilon^z \approx Z_0' \xi^{-z/\nu};\ Z_0' = Z_0 \xi_0^{z/\nu} \tag{2.16}$$

where the correlation length ξ grows as

$$\xi \approx \xi_0 \epsilon^{-\nu}, \tag{2.17}$$

with z and ν being the critical exponents. However, for finite values of L any critical enhancement is restricted and Z is smooth and analytic. Such finite-size effects may appear as a difficulty in understanding results from computer simulations. However, this problem can be tackled by writing down finite-size scaling ansatz, thus accounting for the size effect, as

$$Z \approx Y(x)\epsilon^z = Y'(x)\xi^{-z/\nu}. \tag{2.18}$$

In Eq. (2.18), $Y(x)$ is the finite-size scaling function that depends upon the scaled variable $x = L/\xi$ and is independent of system size. Note that Y and Y' differ by a factor originating from different amplitudes Z_0 and Z_0' used in Eq. (2.16). In further discussion, however, we will remove primes from both Z_0 and Y and distinction can be derived from whether the scaling forms are written in terms of ϵ or ξ.

At this stage, it is important to ask about the behavior of Y as a function of x. While for static quantities, such question is already addressed, for dynamics, where the finite-size effects are found [48] to be much stronger, there is no appropriate understanding of the variation of $Y(x)$. Nevertheless, one can write down the following limiting behaviors:

$$\text{for } x \to 0 \ (\xi \to \infty; L < \infty), \quad Y(x) \sim x^{-z/\nu}, \tag{2.19}$$

such that Z is finite at criticality :

$$Z \sim L^{-z/\nu}. \tag{2.20}$$

Eq. (2.20), when compared with Eq. (2.16), is consistent with the fact that at criticality ξ is the only important length in the problem and it must scale with varying system size L. Keeping this important fact in mind, in fact,

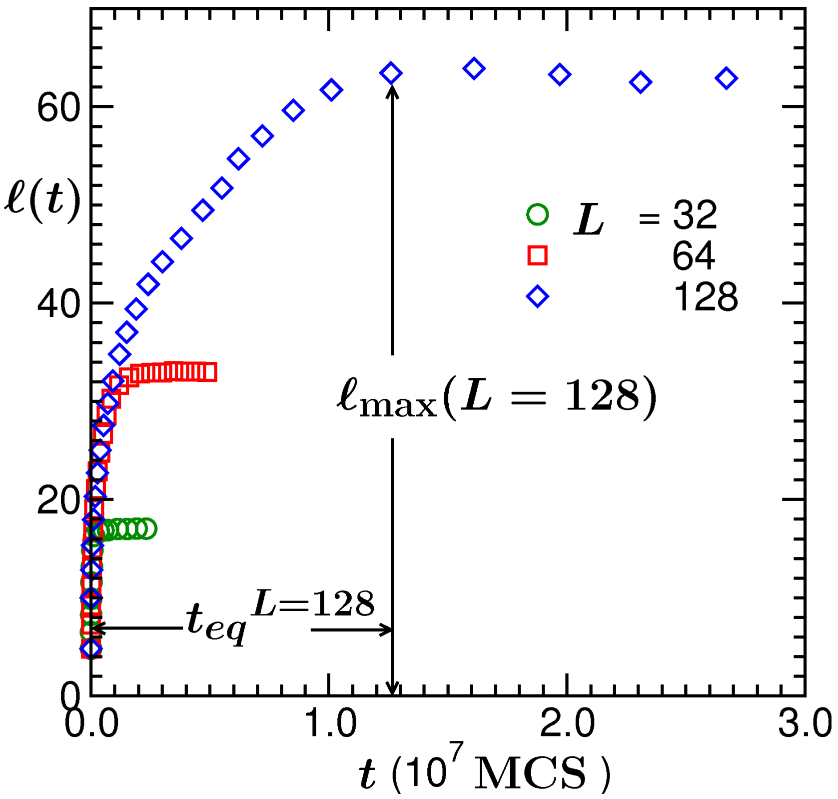

Figure 2.7: Plot of average domain size $\ell(t)$, obtained from Eq. (2.10), for the $2-d$ Ising model, for different system sizes (indicated on the figure) at $T = 0.6T_c$. Definitions of $\ell_{\max}$ and t_{eq}^{L} are demonstrated. Data for $L = 32$ and $L = 64$ were averaged over 1000 independent initial configurations whereas only 40 different initial realizations were used for $L = 128$. Note that all subsequent results in this chapter are obtained at the same temperature as this.

one can write (2.18) as

$$Z \approx Y(x)L^{-z/\nu}. \tag{2.21}$$

On the other hand,

$$\text{for } x \to \infty \ (L \to \infty, \epsilon > 0), \quad Y(x) = Z_0, \tag{2.22}$$

so that Eq. (2.16) is recovered in the thermodynamic limit.

With the knowledge of ν, Eq. (2.20) can be used to estimate z by calculating Z at T_c for various system sizes. A better strategy however is to study Z at finite-size critical points T_c^L, such that

$$Z|_{T_c^L} \sim L^{-z/\nu}; \quad T_c^L - T_c \sim L^{-1/\nu}, \tag{2.23}$$

though true meaning of a critical point can be assigned to T_c^L only in the limit $L \to \infty$.

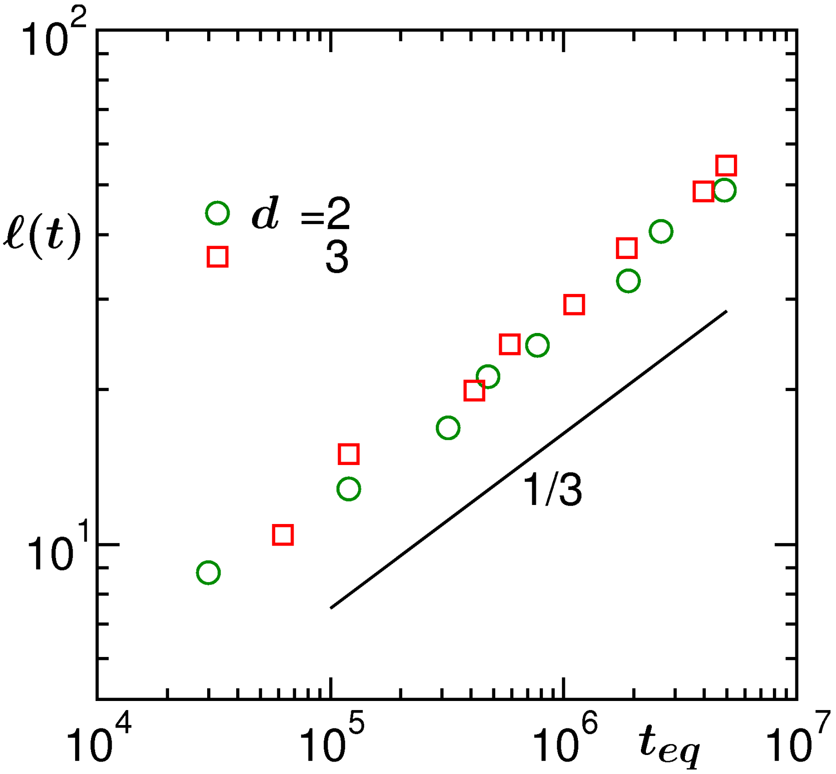

Figure 2.8: Demonstration of the scaling behavior (2.29) in $d = 2$ and 3.

This general discussion about finite-size scaling method could be used to construct the similar formalism for nonequilibrium domain coarsening problem where $\ell(t)$ is the variable analogous to ξ and $1/t$ to ϵ. In the present problem, $\ell(t)$ should scale with L, more precisely $\ell_{\max} \sim \ell(t)$, where, as already stated, $\ell_{\max}(L)$ is the equilibrium domain size and proportional to the system size L. In Fig. 2.7 we show plots of $\ell(t)$ vs t for various different values of L, in $d = 2$. The flat regions in the plots at late times correspond to $\ell_{\max}$.

At this stage, we would like to quantify the domain growth in an infinite system as

$$\ell(t') = \ell_0 + At'^{\alpha}, \tag{2.24}$$

where ℓ_0 is temperature dependent (so is the amplitude A) and could possibly be interpreted as the average cluster size when the system becomes unstable to fluctuations at time t_0 since the quench or the domain length at t_0 when the system enters the scaling regime. Of course our measurement of time starts from there, i.e. $t' = t - t_0$. Note that we do not assign a meaning of domain size to this quantity and this should be treated in a manner similar to a background quantity in critical phenomena that appears from small length fluctuations whose temperature variation is usually neglected. Having said that, scaling part in Eq. (2.24) is only At'^{α}. Of course, when $\ell(t')$ is significantly large, subtraction of the microscopic length ℓ_0 does not bring in noticeable difference. However, in computer simulations, where one deals with small systems, presence of ℓ_0 can bring in completely different conclusions.

Eq. (2.24) is valid only in absence of any finite-size effect. For a finite $\ell_{\max}(L)$, analogous to (2.18), one can write down the scaling ansatz as

$$\ell(t') - \ell_0 = Y(x)t'^{\alpha} \tag{2.25}$$

where now

$$x = \frac{\ell_{\max} - \ell_0}{t'^{\alpha}} \tag{2.26}$$

is the scaling variable. Both in Eqs. (2.25) and (2.26), ℓ_0 is subtracted to deal with the scaling parts only. By observing (2.16), (2.19) and (2.22) as well as (2.24), (2.25) and (2.26), one can arrive at the limiting forms of $Y(x)$ as

$$Y(x) \approx x, \text{ for } x \to 0(t' \to \infty, \ell_{\max} < \infty) \tag{2.27}$$

and

$$Y(x) = A, \text{ for } x \to \infty(t' < \infty, \ \ell_{\max} \to \infty). \tag{2.28}$$

Of course, it would again be interesting to learn about the full form of $Y(x)$.

Also, analogous to T_c^L in critical phenomena, one can define a finite size equilibration time t_{eq}^L that is needed to reach $\ell_{\max}$, as demonstrated in Fig 2.7. Then one can write down a scaling equation analogous to (2.23) as

$$[\ell_{\max} - \ell_0] \sim {t_{eq}^L}^{1/3}. \tag{2.29}$$

This scaling behavior is demonstrated in Fig. 2.8, where we show plots of $\ell_{\max}$ vs t_{eq}^{L} on a log scale, in both $d = 2$ and $d = 3$. Consistency of the simulation data with the solid line of the form (2.29) confirms the validity of this approach. Note that in this figure, we did not subtract ℓ_0 and the corresponding microscopic time from the abscissa. As will be seen later, $\ell_{\max}$ for the systems considered here are significantly larger than ℓ_0, so one does not expect a big difference after subtracting. Eq. (2.29) is analogous to the one used to obtain the equilibrium dynamic critical exponent from simulations done at criticality [17], viz., the relaxation time $\tau \sim L^z$.

2.3 Simulation Results and Analysis

Having set the methodology in place, in this section we present results from MC simulation of Kawasaki-Ising model in $d = 2$ and 3, combined with the finite-size scaling analysis.

2.3.1 Results in d=2

In Fig. 2.9 we present snapshots during the evolution of an Ising system, starting from a 50 : 50 random mixture of up and down spins, obtained via MC simulation at temperature $T = 0.6T_c$. The times at which the shots were taken are mentioned on the figure. While the last snapshot corresponds to a situation when A and B phases are completely separated, the one at $t = 3.5 \times 10^5$ MCS represents the situation when finite-size effect began to enter, which will be clear from subsequent discussion.

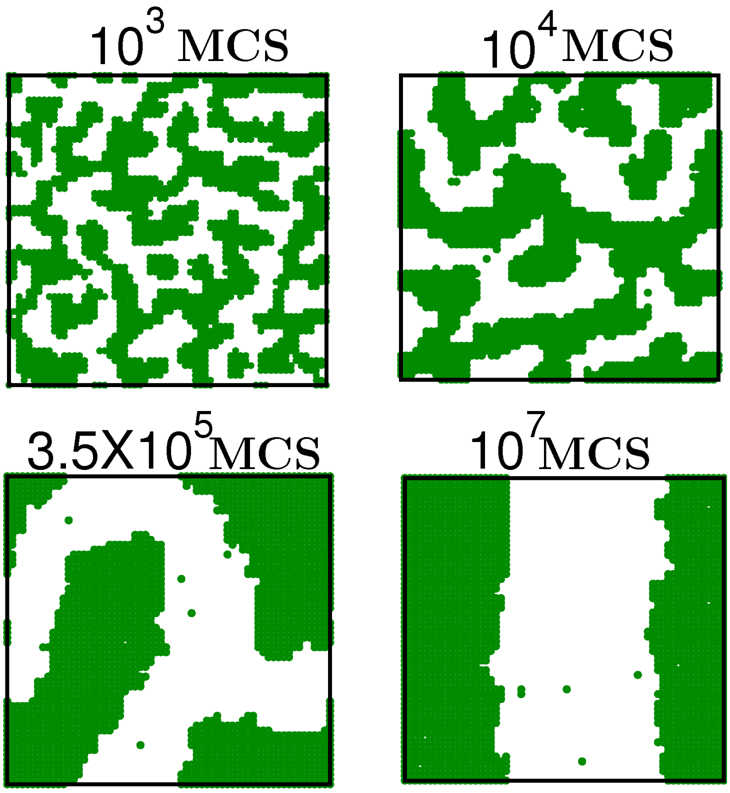

Figure 2.9: Evolution snapshots from different times, as indicated, for the Kawasaki-Ising model in $d = 2$ at $T = 0.6T_c$. The last snapshot corresponds to a completely equilibrated configuration.

From Fig. 2.7, by observing that the data for smaller systems are following the ones for larger systems almost all the way upto the saturation value, it is already evident that finite-size effect is rather weak. However, for a quantitative statement and to gain detail information about the growth exponent, more sophisticated analysis is called for. Following the discussion in the previous section, in Figs. 2.10 and 2.11 we plot $Y = [\ell(t') - \ell_0]/t'^{\alpha}$ as a function of $x/(x + x_0)$. Note that x_0 was introduced to see behavior of Y properly both for small and large x. For convenience we set it to 5.

In this exercise we have varied α and ℓ_0 (or the microscopic time t_0 associated with this length) to get optimum collapse of data from different system sizes. In Fig. 2.10, where $\ell(t)$ is being used from Eq. (2.10), the optimum data collapse is obtained for $\ell_0 \simeq 4a$ (average cluster size after 20 MCS since quench), a being the lattice spacing and $\alpha \simeq 0.33$. Similar exercise when $\ell(t)$ is being obtained from Eq. (2.12), as shown in Fig. 2.11), gives $\alpha \simeq 0.35$ and ℓ_0 there corresponds to the same number of MCS after quench. Note that ℓ_0 in our analysis is a bare length independent of time and the scaling behavior (2.25) will be obtained when this is chosen appropriately. These numbers, as expected, provided a constant value of $Y(x)$ in the region unaffected due to finite system size, which should be identified with the growth amplitude A for which we quote 0.29 ± 0.01 (cf. Fig. 2.10).The arrows in Figs. 2.10 and 2.11 marks the location where $Y(x)$ starts deviating from its constant value. The sharp nature of the crossover is indicative of only small size effect which we quantify from the location of the arrow marks as

$$\ell(t) = (0.75 \pm 0.05)\ell_{\max}. \tag{2.30}$$

Of course, this value is significantly large compared to earlier understanding and expectation. Note that the snapshot at $t = 3.5 \times 10^5$ MCS in Fig. 2.9 corresponds to this length.

Here we mention that for very small values of t' (upto $\sim 10^2$, data upto this time are not shown) we had difficulty in getting good quality collapse. This is due to minor ambiguity about the actual value of ℓ in this time range. If "noise free" configurations are used the trend of the data is to

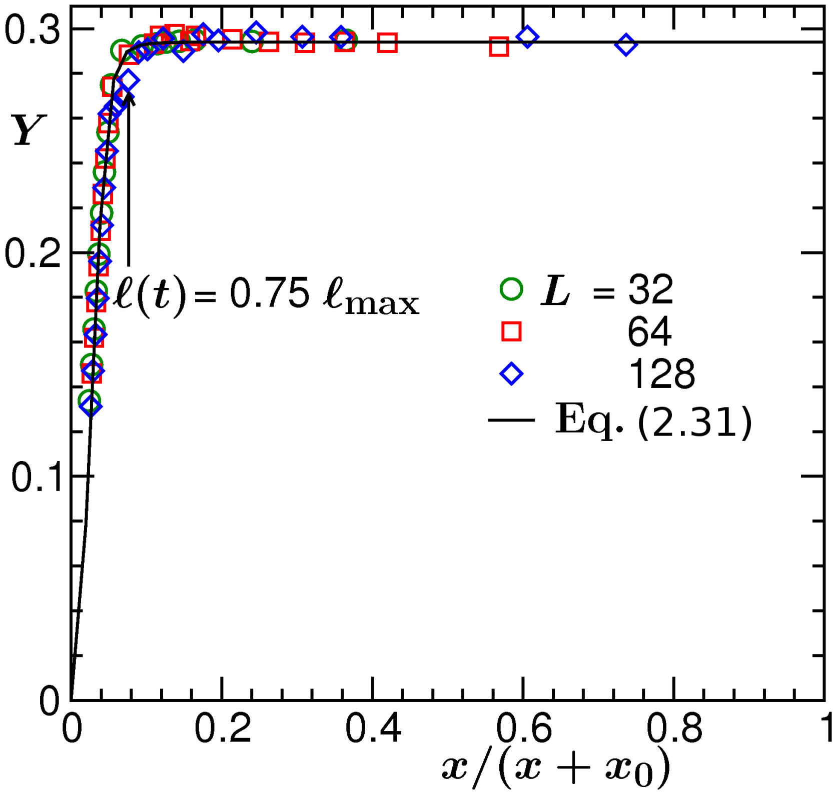

Figure 2.10: Finite-size scaling plot of Y, with $\ell_0 = 3.6$ lattice constants (after 20 MCS from the quench time) and $\alpha \simeq 0.33$, as a function of $x/(x+x_0)$; $x_0 = 5$. This redefinition of the abscissa variable helps seeing the whole range of $x \in [0, \infty]$. The continuous curve is a fit to Eq. (2.31) with the best fit parameters mentioned in the text. The arrow roughly marks the appearance of finite-size effect.

move upwards with the increase of x. On the other hand there is a downward trend when results are obtained from noisy configurations. Assuming that the latter choice is appropriate, this downward trend could be due to correction to scaling or dominant interface diffusion at early time. Note that in the next Chapter we will address the problem of interface diffusion in detail. Further, we mention that the ambiguity about the calculation of $\ell(t)$ at early time, which is minor in the present case, can become significant at temperatures very close to T_c.

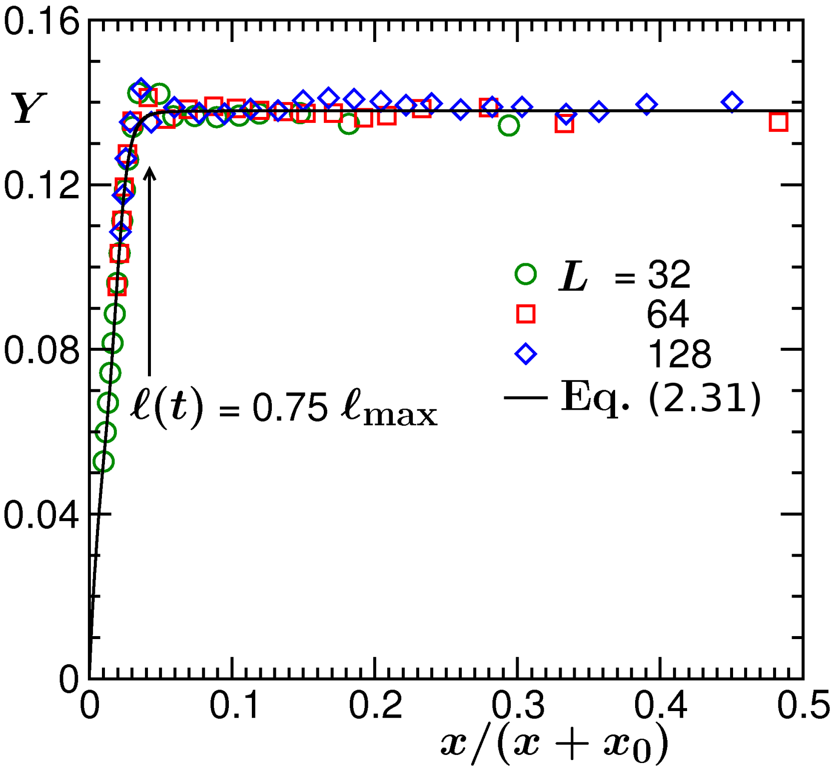

Figure 2.11: Same as Fig. 2.10 but $\ell(t)$ obtained from the first zero-crossing of $C(r,t)$ [cf. Eq. (2.12)]. In this case $\ell_0 \simeq 2.7$ lattice constants (at 20 MCS from quench) and $\alpha \simeq 0.35$.

In an attempt to learn the full form of $Y(x)$, we construct the following functional form

$$Y(x) = \frac{Ax}{x + 1/(p + qx^{\beta})}, \tag{2.31}$$

that has limiting behaviors consistent with (2.27) and (2.28). The continuous lines in Figs. 2.10 and 2.11 are fits to the form (2.31) with

$$A \simeq 0.29,\ \ p \simeq 3,\ \ q \simeq 6400,\ \ \beta = 4 \tag{2.32}$$

and

$$A \simeq 0.14,\ p \simeq 7,\ q \simeq 13700,\ \beta = 4, \tag{2.33}$$

thus have the convergence

$$(x \to \infty)\ Y(x) \approx A[1 - fx^{-n}]; n = 5. \tag{2.34}$$

Of course, possibility of an exponential correction cannot be ruled out. This may be compared with much slower convergence of such function in dynamic critical phenomena [48]. Note that the understanding of finite-size effect in both equilibrium and nonequilibrium dynamics is a non-trivial task and significant attention is called for.

To take a direct view of what happens after the corrective measure, in terms of subtraction of ℓ_0, has been taken, in Fig. 2.12 we plot $[\ell(t') - \ell_0]^{-3}$ vs $1/t'$ and $\ell(t)^{-3}$ vs $1/t$ for $L = 64$. A log-scale was used to bring visibility to a wide range of data. The linear behavior of the data after subtracting ℓ_0, starting from very early time justifies the introduction of ℓ_0 again. The continuous line there is a plot of the form $\tilde{A}x$ with $\tilde{A} \simeq 39 = 1/A^3$. On the other hand, notice the strong curvature when ℓ_0 is not subtracted. The dashed lines marked by $1/t$ and $(\frac{1}{t})^{3/5}$ on this figure corresponds to $\ell(t) \sim t^{1/3}$ and $t^{1/5}$ respectively. Thus, when ℓ_0 is not appropriately subtracted, only observing the trend on a log-log plot one may be misled to conclude that there is gradual crossover from one regime to the other. Even though a surface-diffusion dominated regime leading to $t^{1/4}$ growth appears to be missing (at

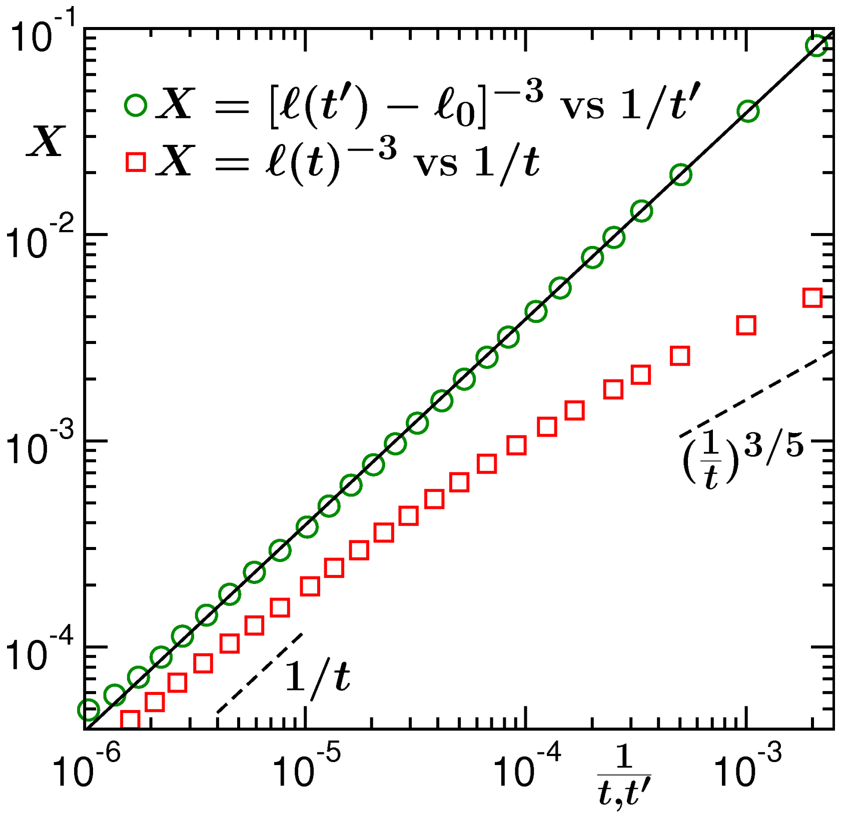

Figure 2.12: Plot of $[\ell(t') - \ell_0]^{-3}$ vs $1/t'$ and $\ell(t)^{-3}$ vs $1/t$ for $L^2 = 64^2$, with $\ell(t)$ being calculated from Eq. (2.10). The continuous line has slope $39 = 1/A^3$.

least we could not catch) at this temperature, may become prominent at lower temperature. See Ref [49] for a discussion on crossover from $t^{1/4}$ to $t^{1/3}$. Note that the exercise here as well as one in Figs. 2.10 and 2.11 , where Y is very flat from very early time all the way to the moment when finite-size effect enters, are already indicative of absence of any strong corrections to scaling.

Before moving ahead for another elegant proof of the evidence for the absence of negligible corrections to scaling, we pass by showing the scaling plot of $C(r,t)$ in Fig. 2.13 where good quality data collapse is obtained

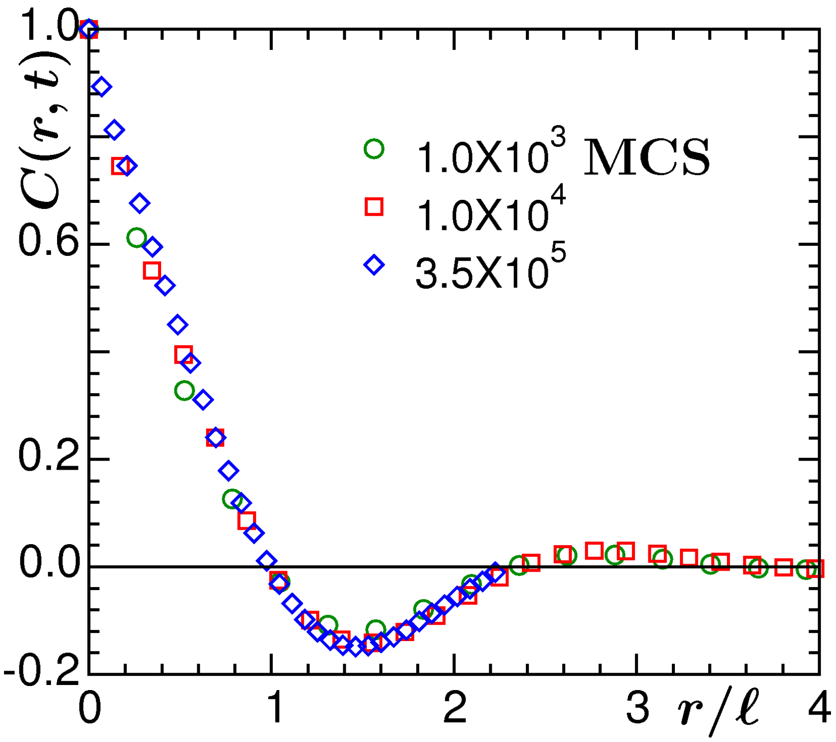

Figure 2.13: Scaling plot of $C(r,t)$ at $T = 0.6T_c$. Note that $\ell(t)$ was obtained using Eq. (2.10).

starting from very beginning till $t = 3 \times 10^5$ MCS when the finite-size effect begins. Next we introduce a length ℓ_s to write

$$\ell'(t') = \ell(t') - \ell_s = [\ell_0 - \ell_s] + At'^{\alpha}, \tag{2.35}$$

and calculate the instantaneous exponent [21]

$$\alpha_i = \frac{d[\ln \ell'(t')]}{d[\ln t']}, \tag{2.36}$$

to obtain

$$\alpha_i = \alpha \left[1 - \frac{\ell_0 - \ell_s}{\ell'(t')} \right]. \tag{2.37}$$

According to Eq. (2.37), when α_i is plotted as a function of $1/\ell'(t')$, for $\ell'(t') > 0$, one expects linear behavior with a y-intercept equal to α. Fig. 2.14 shows such plots for $\ell_s = 0.0, 3.6$, and 5.0, as indicated. The dashed lines have y-intercept $\alpha = 1/3$ and slopes

$$m = -\frac{\ell_0 - \ell_s}{3}. \tag{2.38}$$

In this exercise essentially we have, by force, invoked different initial lengths into the average domain size because of which one obtains different slopes in the instantaneous exponent when plotted vs inverse length. The consistency of the slopes with (2.38) (represented by dashed lines) is interesting. Particularly the behavior of α_i for $\ell_s = 3.6$, again speaks for the choice of ℓ_0 and indicates that the LS scaling regime is realized very early. In Fig. 2.15 we present results with $\ell_s = 3.6$ for various system sizes $L^2 = 16^2, 32^2$ and 64^2. In all the cases, α_i oscillates around 1/3. This observation, using a system size as small as $L^2 = 16^2$, stresses against unnecessary attempt to simulate larger systems.

This result is in strong disagreement with the earlier [21] understanding of domain coarsening in $2-d$ conserved Ising model for critical quench that α is strongly time dependent and the LS value is recovered only asymptotically as $\ell(t) \to \infty$. The route to this finite-time correction was thought to be an

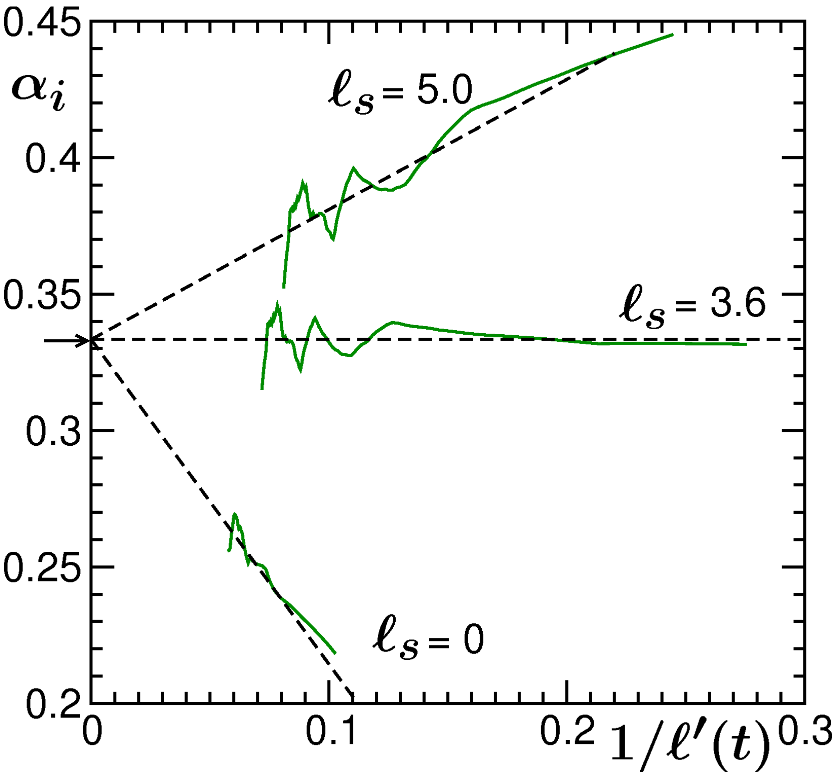

Figure 2.14: Plot of instantaneous exponent α_i as a function of $1/\ell'(t')$ for three different choices of ℓ_s as indicated, with $L^2 = 64^2$. The dashed straight lines have slopes $-1.19, 0$ and 0.49, respectively. The arrow on the ordinate marks the value $\alpha = 1/3$. Note that $\ell(t)$ was calculated from Eq. (2.10).

additional term $\propto 1/\ell(t)^3$ in Eq. (2.5) [cf. Eq. (2.9)], accounting for an enhanced interface conductivity. Note that a term $\propto 1/\ell(t)^3$ could also be motivated by introducing a curvature dependence in σ as

$$\sigma[\ell(t)] = \frac{\sigma(\infty)}{1 + \frac{2\delta}{\ell(t)}}, \tag{2.39}$$

δ being the Tolman length [50]. However, our observation of negligible correction to the exponent, starting from the very early time, is consistent with

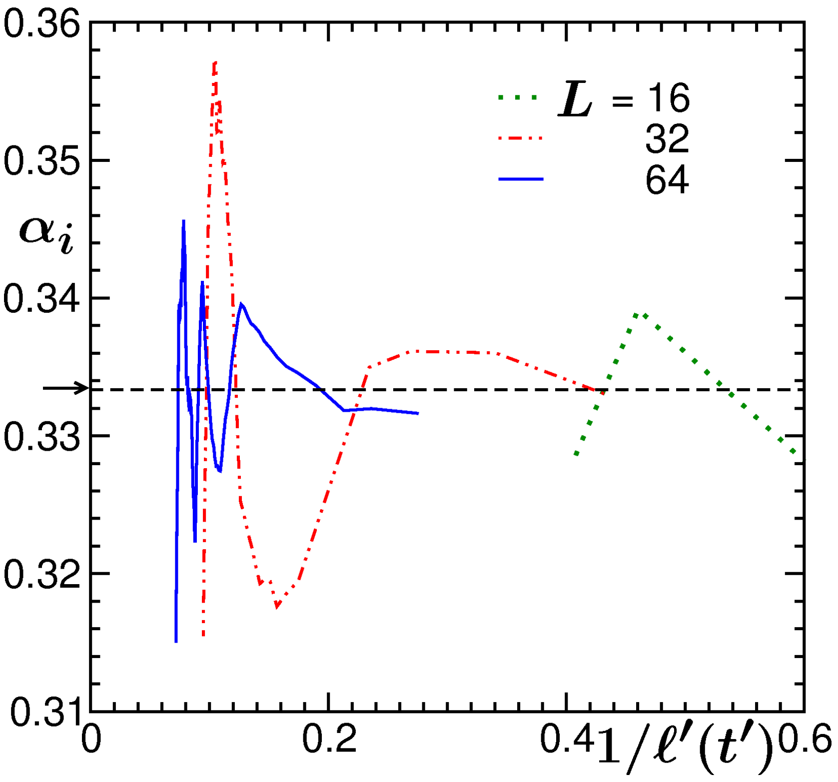

Figure 2.15: Plot of α_i vs $1/\ell'(t')$ for $\ell_s = 3.6$ and $L^2 = 16^2, 32^2$ and 64^2. Here also the arrow on the ordinate marks the value $\alpha = 1/3$. All data sets correspond to averaging over 1000 independent initial conditions.

the growing evidence [51, 52] that Tolman length is absent in a symmetrical model [53] where the leading correction is of higher order. Also, small corrections that may be present, coming from the curvature dependence of the kinetic pre-factor in Eq. (2.5) is beyond the accuracy of data in the present work. On the other hand, for 50 : 50 composition, since the domain boundaries are essentially flat starting from very early time, any curvature dependence is expected to be absent. Thus, we conclude that this misunderstanding about the strong time dependence in α was due to the presence of a time independent length ℓ_0 in $\ell(t)$ which our analysis subtracts out in appropriate way.

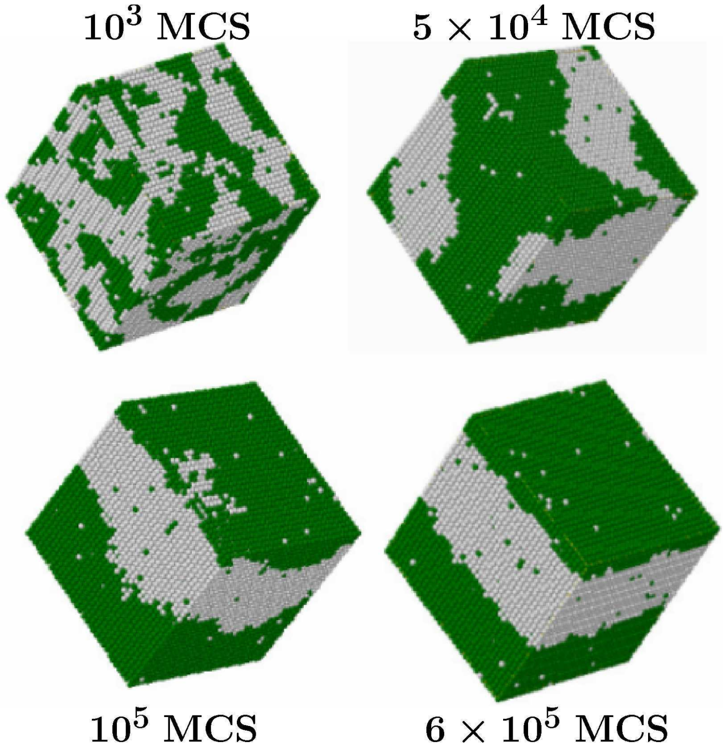

Figure 2.16: Evolution snapshots from different times for $3-d$ Ising model with $L^3 = 32^3$ and $T = 0.6T_c$. A and B particles are marked black and grey respectively.

2.3.2 Results in d=3

In this subsection we turn our attention to the kinetics of phase separation in $d = 3$. Fig. 2.16 shows $3-d$ snapshots of the time evolution of Kawasaki-Ising model at four different times as indicated on the figure where the last snapshot is clearly seen to have been equilibrated. Analogous to $d = 2$, all results presented here were obtained at $T = 0.6T_c$, with $T_c = 4.51k_BT/J$ in this case, and the composition was chosen to be 50 : 50 as well.

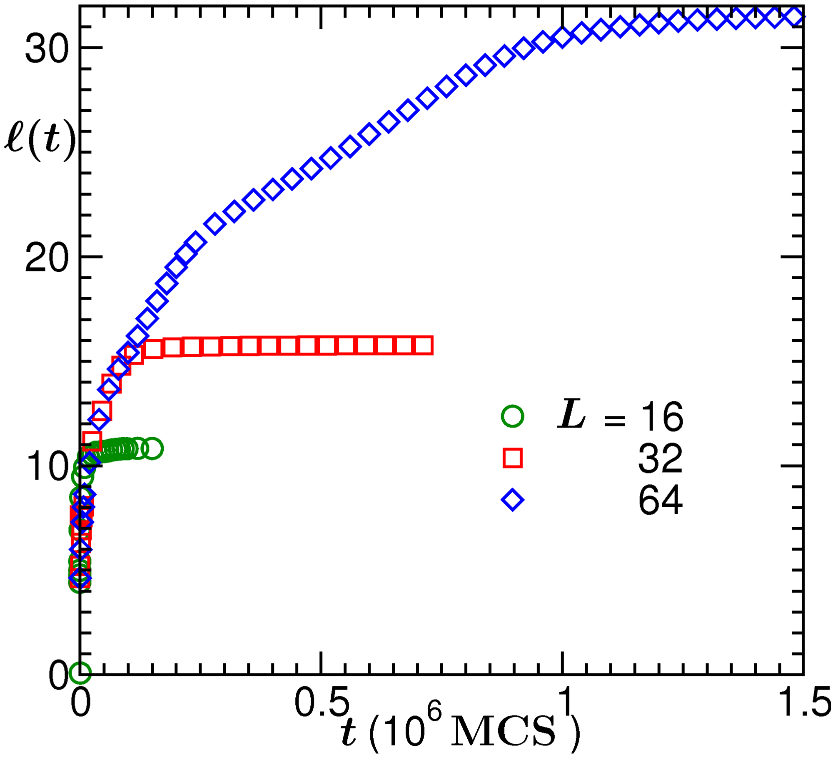

Figure 2.17: Plot of $\ell(t)$, obtained from the first zero crossing of $C(r,t)$, vs t, for the systems $L^3 = 16^3, 32^3$ and 64^3.

In Fig. 2.17 we present direct plots of $\ell(t)$ as a function of t, for $L^3 = 16^3, 32^3$ and 64^3 where $\ell(t)$ was calculated from Eq. (2.12). Again, the finite-size effects look to be small. In Fig. 2.18 we present a plot of $Y(x)$, using the data in Fig. 2.17, as a function of $x/(x+x_0); x_0 = 5$. Best data collapse in this case was obtained for $\ell_0 = 2.5$ (10 MCS after the quench, note that corresponding value of ℓ_0 from Eq. (2.10) is 3.0 and $\alpha \simeq 0.315$) and $\alpha \simeq 0.35$. Very flat behavior of $Y(x)$, starting from the beginning again speaks for absence of any strong correction to the growth law. However, compared to the $d = 2$ case, one may expect slightly stronger correction here because of the inherent curvature present in the cylinder like domain objects

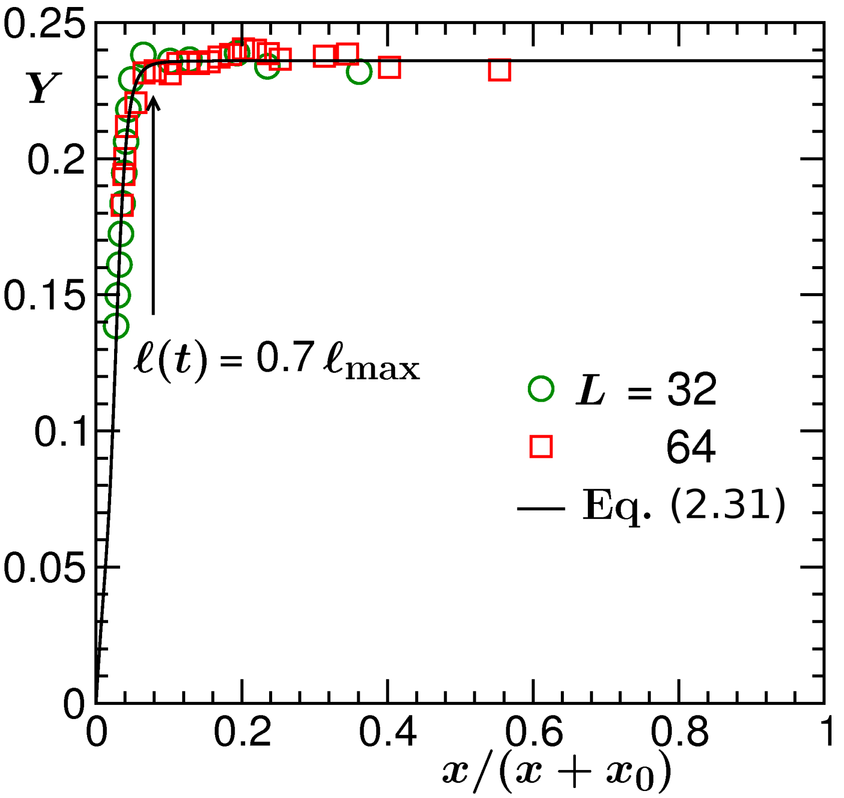

Figure 2.18: Finite-size scaling plot of Y, for the data presented in Fig. 2.17, vs $x/(x+x_0)$ with $x_0 = 5$. Here $t_0 = 10$ (10 MCS from the quench) and $\alpha = 0.35$. Appearance of finite size effect, obtained from the arrow mark, is estimated to be at $\ell(t) \simeq 0.7\ell_{\mathrm{max}}$, in close agreement with the one for $d = 2$.

as opposed to the stripe like structures in $d = 2$. Possibly because of that we could not obtain good collapse of data from $L^3 = 16^3$ on top of the ones presented, since the whole data set for $L^3 = 16^3$ is from very early time and suffers from corrections. Onset of finite size effect, as obtained from the arrow mark where $Y(x)$ deviates from the flat behavior, is in quantitative agreement with the 2-dimensional situation, as quoted in Eq. (2.30). Here also the third snapshot in Fig. 2.16 (at $t = 10^5$ MCS) is presented at this onset. A fitting, shown by the continuous line, to the form (2.31) [$A = 0.24$, $p \simeq 4$, $q \simeq 13050$ and $\beta = 4$], again is consistent with asymptotic convergence

(2.34).

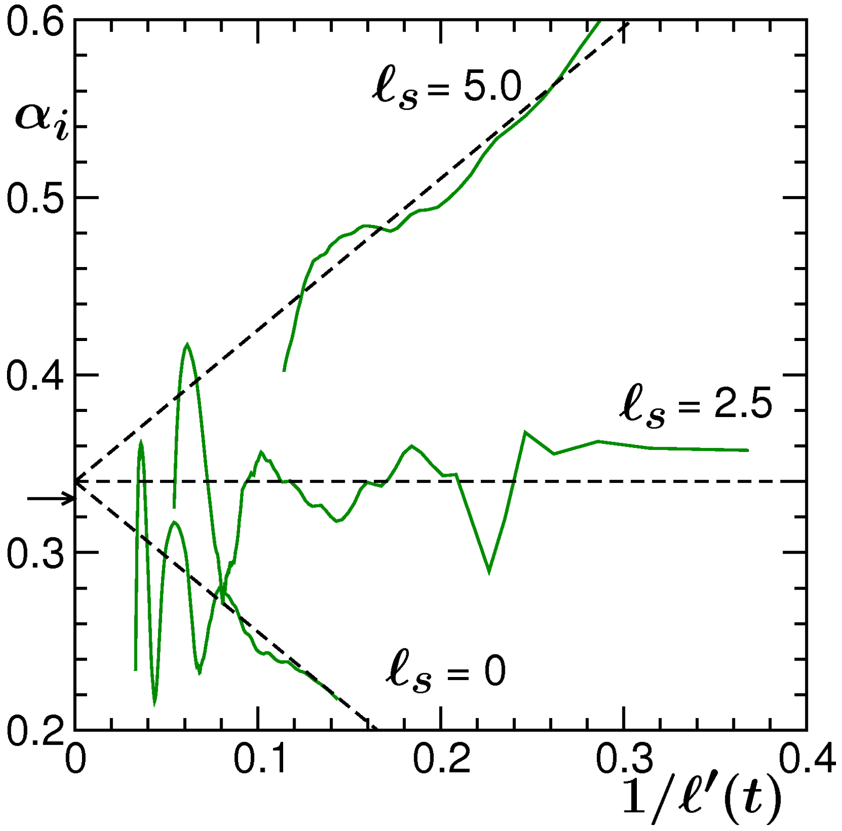

Figure 2.19: Plot of instantaneous exponent α_i vs $1/\ell'(t')$ with three different values of $\ell_s = 0, 2.5$ and 5. The dashed lines correspond to $\alpha = 0.34$. The arrow on the ordinate marks the value $\alpha = 1/3$. The data presented here correspond to $L = 64$ and were obtained from averaging over 150 initial configurations.

In Fig. 2.19, we present instantaneous exponent α_i as a function of $1/\ell'(t')$ for $L^3 = 64^3$ and three choices of ℓ_s as indicated. In all the cases, the exponent fluctuates around mean value 0.34. Note that α estimated from $S(k,t)$ and $P(\ell_d,t)$ are slightly higher and lower, respectively, compared to the one presented.

The appearance of growing oscillation in α_i, seen in Figs. 2.14, 2.15 and

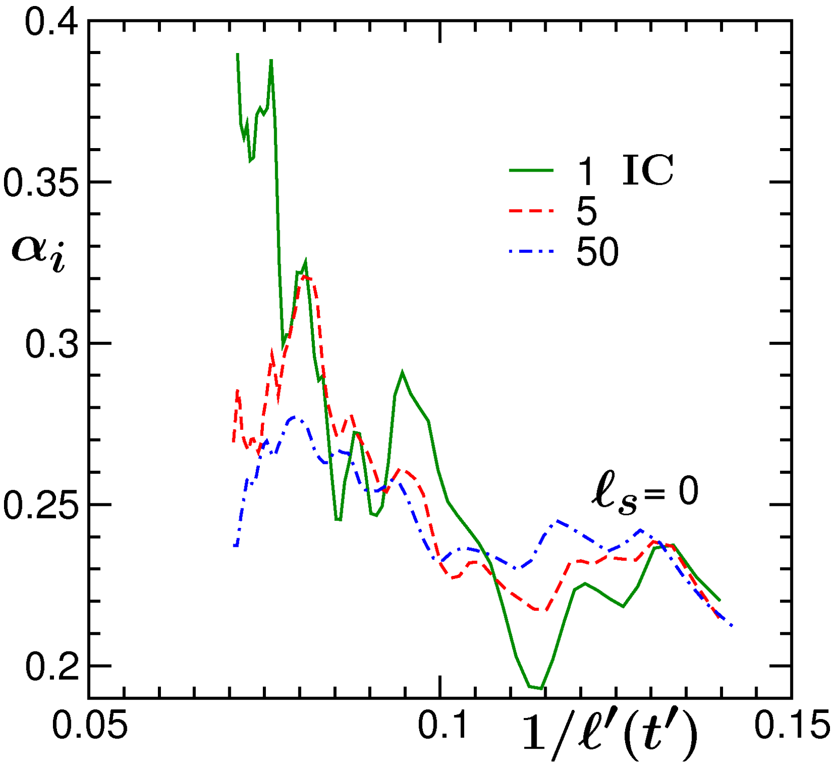

Figure 2.20: Plot of α_i vs $1/\ell'(t')$ for $\ell_s = 0$ showing reduction of noise when averaged over larger number of initial configurations (IC).

2.19, around the mean value is due to lack of statistics and was also pointed out by Shinozaki and Oono [31]. The results could be made smoother by considering a bigger system size [see Fig. 2.15] or averaging over a large number of systems [Fig. 2.20]. In a finite system, as time increases, for an extended period of time two large neighboring domains of same sign may not merge, thus lowering the value of α. After a long time when two large domains merge, brings in drastic enhancement. This character is in fact visible in the direct plot of $\ell(t)$ vs t at late times [cf. $L = 128$ in Fig. 2.7 and $L = 64$ in Fig. 2.17]. Note that this oscillation could be a route to an error if one obtains α from least square fitting without choosing the range appropriately.

Finally, it will be interesting to know the temperature dependence of ℓ_0 and amplitude A as well as of finite size effects. All these, however, we leave out for future work.

2.4 Conclusion

This chapter contains comprehensive study of domain coarsening in a phase separating system with diffusive dynamics in $d = 2$ and $d = 3$. Various different ways of analysis give results for growth law consistent with the expected LS exponent $\alpha = 1/3$. As opposed to the earlier understanding, correction appears to be very weak, thus LS scaling behavior being realized very early. Weak finite-size effect is a welcome message which is suggestive of avoiding large systems, rather focusing on accessing long time scale which often is necessary for systems exhibiting multiple scaling regimes.

Our observation should be contrasted with an earlier study of Heermann, Yixue and Binder [11] that reports very strong finite-size effect. However, this latter study was based on an extremely off-critical composition and should not be considered to have general validity. Note that due to the expected presence of correction in such off-critical composition, where droplet like structures form with finite radius of curvature at early time, the analysis is more difficult. Also, one should be prepared to encounter stronger size effect in more complicated situations, e.g., systems exhibiting anisotropic patterns [36–40, 42, 43].

One may of course ask if the small finite-size effect observed for diffusive dynamics is also valid for kinetics of phase separation in fluids. A comprehensive study in that direction, for both binary and single-component fluids, is in progress. In fact, preliminary findings from these latter studies are suggestive of more general validity of the results presented here. Such studies are important since brute force method of simulating very large systems, particularly for the study of fluid phase separation via MD simulation, is not often helpful to access long time scales even with the present day high speed computers and thus may not bring very conclusive understanding.

A deeper understanding of ℓ_0 requires further study, particularly, how the system is led to instability is a fundamental question to be asked. Studies with different initial configurations and quenching to different temperatures should be able to provide better understanding of this quantity. Even though scaling corrections appear to be negligible for critical quench due to the flat nature of the domain boundaries, one expects corrections for off-critical composition. This expected correction coming from surface tension should be of higher order than linear for a symmetric model. On the other hand, it would be interesting to learn about the leading order correction coming from the kinetic pre-factor.

Finally, we expect the observation, understanding and finite-size scaling technique used in this work to find relevance in other systems exhibiting growing length scales, e.g., ordering in ferromagnet, surface growth, clustering in cooling granular gas, dynamic heterogeneity in glasses, etc. In line of this work many earlier studies on domain coarsening may need to be revisited for better understanding which was not possible because of lack of reliable methods of analysis.

Bibliography

[1] S. Majumder and S.K. Das, Phys. Rev. E **84**, 021110 (2011).

[2] S. Majumder and S.K. Das, Phys. Rev. E **81**, 050102(R) (2010).

[3] A.J. Bray, Adv. Phys. **51**, 481 (2002).

[4] K. Binder, in *Phase Transformation of Materials*, ed. R.W. Cahn, P. Haasen and E.J. Kramer, Material Science and Technology, Vol **5** (VCH, Weinheim, 1991), p.405.

[5] S. Puri and V. Wadhawan (eds.), *Kinetics of Phase transitions* (CRC Press, Boca Raton, 2009).

[6] I.M. Lifshitz and V.V. Slyozov, J. Phys. Chem. Solids **19**, 35 (1961).

[7] E.D. Siggia, Phys. Rev. A **20**, 595 (1979).

[8] H. Furukawa, Phys. Rev. A **31**, 1103 (1985); *ibid* 36, 2288 (1987).

[9] M.E. Fisher in *Critical Phenomena*, ed. M.S. Green (Academic, London, 1971), p1.

[10] V. Privman (ed.), *Finite Size Scaling and the Numerical Simulations of Statistical Systems* (World Scientific, Singapore, 1990).

[11] D.W. Heermann, L. Yixue and K. Binder, Physica A **230**, 132 (1996).

[12] J. Viñals and D. Jasnow, Phys. Rev. B **37**, 9582 (1988).

[13] K. Binder, Phys. Rev. B **15**, 4425 (1977).

[14] K. Binder and H.L. Frisch, Z. Phys. B: Condens. Matter **84**, 403 (1991).

[15] K. Kawasaki, in *Phase Transition and Critical Phenomena*, ed. C. Domb and M.S. Green (Academic Press, New York, 1972), Vol **2**, p443.

[16] R.A.L. Jones, *Soft Condensed Matter*, (Oxford University Press, Oxford, 2008).

[17] D.P. Landau and K. Binder, *A Guide to Monte Carlo Simulations in Statistical Physics*, (Cambridge University Press, Cambridge, 2005).

[18] D. Frankel and B. Smit, *Understanding Molecular Simulations: From Algorithms to Applications*, (Academic Press, San Diego, 2002).

[19] T.M. Rogers and R.C. Desai, Phys. Rev. B **39**, 11956 (1989).

[20] J.F. Marko and G.T. Barkema, Phys. Rev. E **52**, 2522 (1995).

[21] D.A. Huse, Phys. Rev. B **34**, 7845 (1986).

[22] J.G. Amar, F.E. Sullivan and R.D. Mountain, Phys. Rev. B **37**, 196 (1988).

[23] C. Roland and M. Grant, Phys. Rev. Lett. **60**, 2657 (1988).

[24] C. Roland and M. Grant, Phys. Rev. B **39**,11971 (1989).

[25] S.K. Das and S. Puri, Phys. Rev. E **65**, 026141 (2002).

[26] A. Milchev, K. Binder and D.W. Heermann, Z. Phys. B-Cond. Mat. **63**, 521 (1986).

[27] C. Roland and M. Grant, Phys. Rev. Lett. **63**, 551 (1989).

[28] M. Rao, M.H. Kalos, J.L. Lebowitz and J. Marro Phys. Rev. B **13**, 4328 (1976).

[29] G.S. Grest and D.J. Srolovitz, Phys. Rev. B **30**, 5150 (1984).

[30] G.F. Mazenko, O.T. Valls and F.C. Zhang, Phys. Rev. B **31**, 4453 (1985); *ibid* **32**, 5807 (1985).

[31] A. Shinozaki and Y. Oono, Phys. Rev. E **48**, 2622 (1993).

[32] M. Laradji, S. Toxavaerd and O.G. Mousitsen, Phys. Rev. Lett **77**, 11 (1996).

[33] A.K. Thakre, W.K.den Oher and W.J. Briels, Phys. Rev. E **77**, 011503 (2008).

[34] H. Kabrede and R. Hentschke, Physica A **361**, 485 (2006).

[35] S. Ahmad, S.K. Das and S. Puri, Phys. Rev. E **82**, 040107 (R) (2010).

[36] S.K. Das, S. Puri, J. Horbach and K. Binder, Phys. Rev. E **72**, 061603 (2005); Phys. Rev. Lett. **96**, 016107 (2006); Phys. Rev. E **73**, 031604 (2006).

[37] S.J. Mitchell and D.P. Landau, Phys. Rev. Lett. **97**, 025701 (2006).

[38] K. Bucior, L. Yelash and K. Binder, Phys. Rev. E **77**, 051602 (2008).

[39] L. Yelash, P. Virnau, W. Paul, K. Binder and M. Müller, Phys. Rev. E **78**, 031801 (2008).

[40] K. Bucior, L. Yelash and K. Binder, Phys. Rev. E **79**, 031604 (2009).

[41] S.K. Das, J. Horbach and K. Binder, Phys. Rev. E **79**, 021602 (2009); Mod. Phys. Lett. B **23**, 549 (2009).

[42] M.J.A. Hore and M. Laradji, J. Chem. Phys. **132**, 024908 (2010).

[43] K. Binder, S. Puri, S.K. Das and J. Horbach, J. Stat. Phys. **138**, 51 (2010).

[44] A. Sicilia, Y. Sarrazin, J.J. Arenzon, A.J.Bray, and L.F. Cugliandolo, Phys. Rev. E **76**, 061116 (2007).

[45] A. Sicilia, Y. Sarrazin, J.J. Arenzon, A.J.Bray, and L.F. Cugliandolo, Phys. Rev. E **80**, 031121 (2009).

[46] A. J. Bray and S. Puri, Phys. Rev. Lett. **67**, 2670 (1991).

[47] Y. Oono and S. Puri, Mod. Phys. Lett. B **2**, 861 (1988).

[48] S.K. Das, M.E. Fisher, J.V. Sengers, J. Horbach and K. Binder Phys. Rev. Lett. **97**, 025702 (2006); S. Roy and S.K. Das, Europhys. Lett. **94**, 36001 (2011).

[49] S. Puri and Y. Oono, Phys. Rev. A **38**, 1542 (1988).

[50] R.C. Tolman, J. Chem. Phys. **17**, 333 (1949).

[51] D. Winter, P. Virnau and K. Binder, J. Phys. - Cond. Mat. **21**, 464118 (2009).

[52] B.J. Block, S.K. Das, M. Oettel, P. Virnau and K. Binder, J. Chem. Phys. **133**, 154702 (2010).

[53] M.P.A. Fisher and M. Wortis, Phys. Rev. B **29**, 6252 (1984).

Chapter 3

Kinetics of Phase Separation in Solid Binary Mixtures: Temperature and composition dependence

3.1 Introduction

In the theoretical literature of kinetics of phase separation, most of the studies deal with binary (A+B) solid mixtures quenched to a low temperature along the critical composition line. There one investigates the growth of average domain size, $\ell(t)$, of the interconnected A-rich and B-rich domains. Beyond that, it is also of significant importance to understand the effect of temperature (T) as well as composition on the growth law

$$\ell(t) \approx At^{\alpha}. \tag{3.1}$$

The Lifshitz-Slyozov (LS) law [1, 2] ($\alpha = 1/3$) for diffusive growth is expected to be valid for the situation when one has diffusion in the bulk (D_b). In that case, variation of temperature (quench depth) is expected to bring changes in the growth amplitude A only. On other hand, at very low temperature, diffusion along interfaces (D_s) plays the dominant role. In this case, one expects a change in the exponent [3–6] from $\alpha = 1/3$ to a lower value 1/4. This can be justified via the following arguments [6]. In fact, the Cahn-Hilliard (CH) equation (see Chapter 1) should be written down with concentration dependent mobility. A simple form for such mobility, due to Gemmert et. al. [6], is $M(\psi) = D_s\left(1 - \beta\frac{\psi^2}{{\psi_0}^2}\right)$, where $\beta = 1 - \frac{D_b}{D_s}$ and ψ_0 is the equilibrium magnetization. At moderate temperatures when D_b and D_s are comparable, one has nonzero mobility in the bulk. On the other hand, for very low T, $D_b \ll D_s$ and in the bulk $\psi = \psi_0$ everywhere. This gives rise to negligible bulk mobility. However, since $\psi = 0$ at the interfaces, one has nonzero mobility of particles there. From a dimensional analysis of the mobility dependent CH equation, Gemmert et. al. also worked out the crossover from $\alpha = 1/4$ to 1/3, as a function of β. We will provide further discussion on this later.

In case of composition variation, as one moves from the critical value, the domain structure no longer remains interconnected. Rather, one observes growth of droplets of the minority species in the background of the majority sea. In case of fluid phase separation, this difference in morphology brings in striking and important change in the mechanism and thus the exponent of the growth law [7–11]. In solid binary mixtures, however, one expects the mechanism to remain same. Here, an interesting objective could be to search for the correction to the scaling law [12–14], if any, due to the finite radius of curvature of well defined droplets. Recall that for $50 : 50$ composition, we failed to obtain such finite time correction. We have attributed this to the flat domain boundary for "all time". Another possible reason was pointed out to be the absence of any linear correction term in the curvature dependent interfacial tension in Ising-like symmetric models. If the former argument, due to flat interfaces for $50 : 50$ composition, is the only reason, then we expect visible corrections for composition closer to the co-existence curve.

In this work, we have undertaken a detailed study of kinetics of phase separation in solid binary mixtures via Monte Carlo (MC) [15] simulation of Kawasaki exchange [16] Ising model in two spatial dimensions ($d = 2$). We present results on the effect of variation of temperature as well as that of composition both on the morphology and growth dynamics. In addition, we present important results on the finite-size effects due to the variation of these parameters. To obtain information on the growth law, the corresponding correction at early time and the finite-size effects, we relied on finite-size scaling analysis [17, 18], among other techniques.

The rest of the chapter is organized as follows. In Section 3.2, we present the results for temperature dependence. The composition dependent results are discussed in Section 3.3. Finally, we conclude the chapter with a brief summary in Section 3.4.

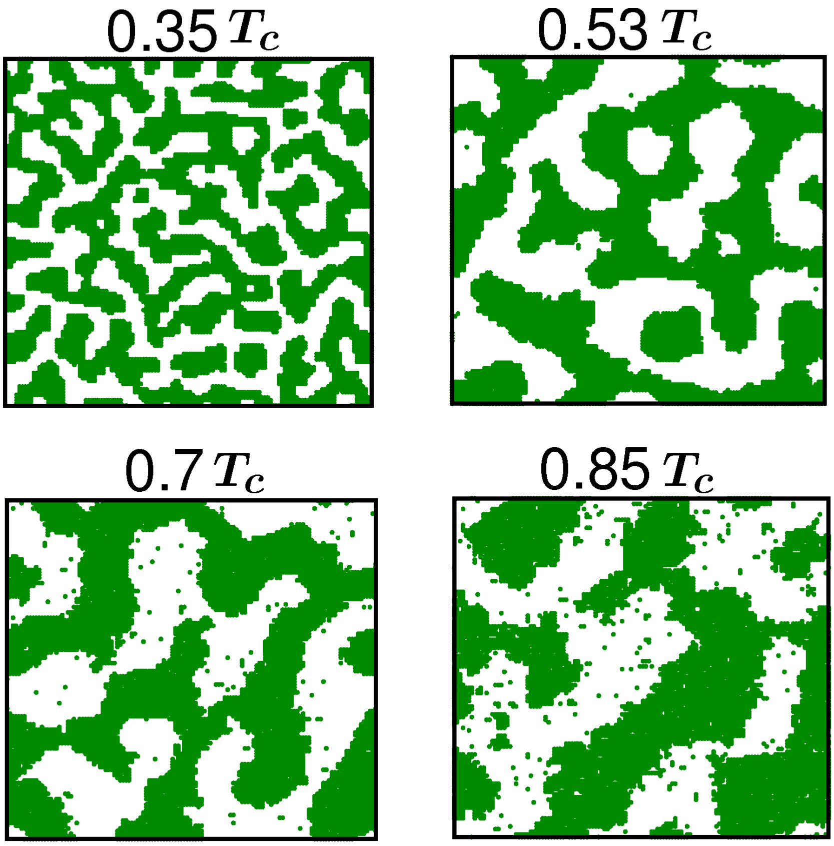

Figure 3.1: Snapshots during the evolution of Kawasaki exchange $2-d$ $50:50$ Ising model at $t = 10^5$ MCS from systems of linear dimension $L = 64$. Four different temperatures are included. Only A particles are shown.

3.2 Temperature Dependence

In this section we present results for the kinetics of phase separation in Ising model with critical composition for various depths of temperature quench.

In Fig. 3.1, we show the snapshots at $t = 10^5$ MCS , from the evolutions at four different temperatures, after quenching a homogeneously mixed $50 : 50$ Ising system to the mentioned temperatures below T_c, the critical temperature. Two observations are in order. First, the growth is faster for higher temperature. Second, the thermal noise, as expected, increases as one goes closer to T_c. The later poses difficulty in accurate estimation of domain length ℓ. To overcome this problem, we remove the noise, by employing the majority spin rule [13, 14] in the neighborhood of a lattice point, to obtain pure domain morphology.

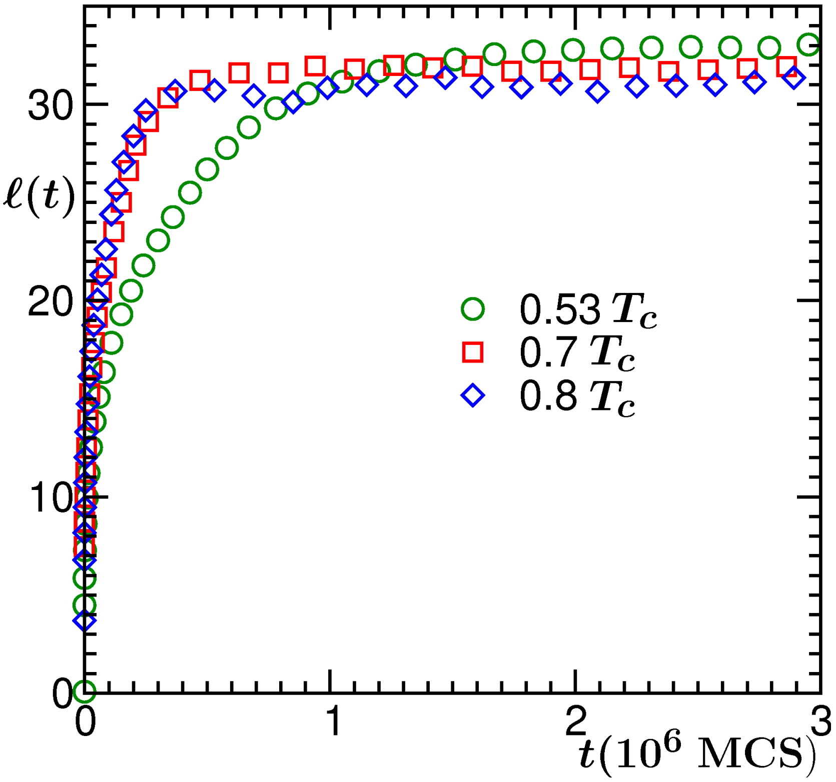

Figure 3.2: Plots of $\ell(t)$ vs t for three different temperatures, as indicated, for $L = 64$. Note that $\ell(t)$ was calculated from domain size distribution function.

Before presenting further results, we again mention that we have calculated $\ell(t)$ from three different methods: (a) From the decay of the correlation function $C(r,t) = \langle S_i S_j \rangle - \langle S_i \rangle \langle S_j \rangle$; $r = |\vec{i} - \vec{j}|$, more precisely from the distance when $C(r,t)$ crosses zero for the first time; (b) From the first moment of the structure factor $S(k,t)$ (k being the wave vector) which is the Fourier transform of $C(r,t)$; (c) Finally, from the first moment, $\int d\ell_d \; \ell_d P(\ell_d,t)$, of the normalized domain-size distribution function $P(\ell_d,t)$, where ℓ_d is the separation between two interfaces in $x-$ or $y-$ directions. Results from all three different methods are found to be consistent with each other for all temperatures and composition, differing only by a numerical factor. So, for the presentation purpose, we will use results from only one of them, viz., method (c).

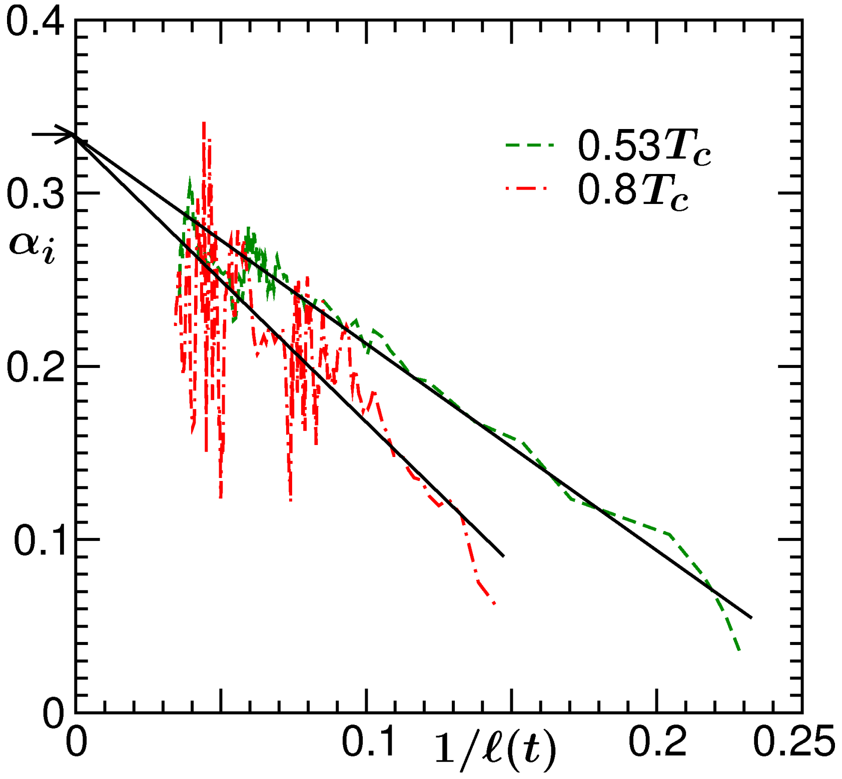

Figure 3.3: Plots of instantaneous exponents α_i vs $1/\ell(t)$, for two different temperatures, each with 50 : 50 composition. The solid lines are guides to the eye. The arrow on the ordinate marks the value of 1/3.

In Fig. 3.2, we show the plots of $\ell(t)$ vs t, for three different temperatures.

In all the cases same system size has been used. The results are presented after averaging over 50 independent initial configurations. As already mentioned, the equilibration occurs faster for higher temperature. This implies that, if the exponent is same, the amplitude of growth is larger for higher temperature. We will investigate it in detail in the following.

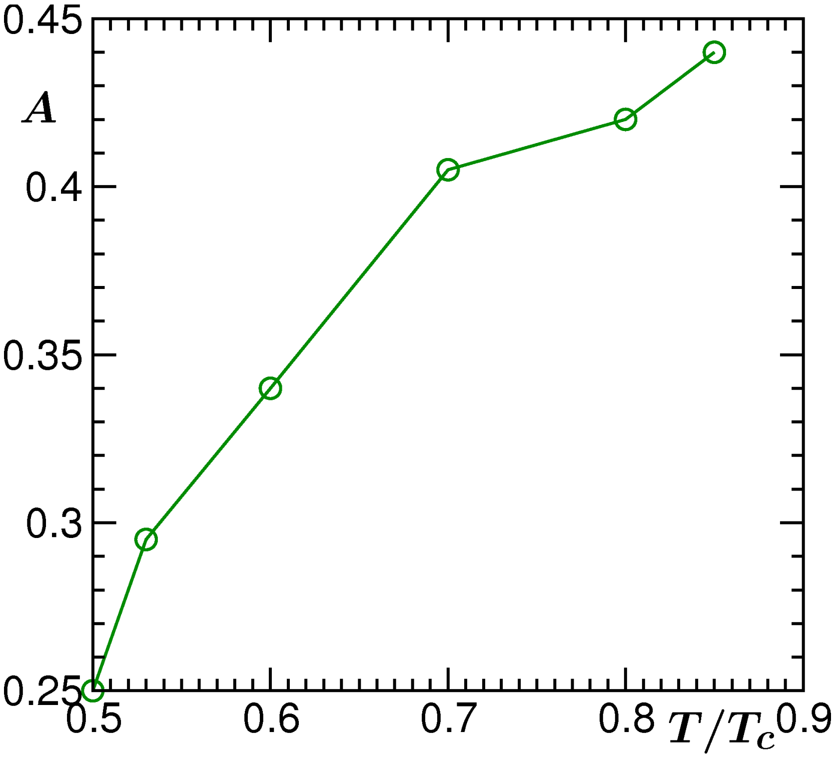

Figure 3.4: Plot of growth amplitude A vs temperature, for 50 : 50 composition.

In Fig. 3.3, we have shown the instantaneous exponent α_i $\left[= \frac{d\ln \ell}{d\ln t}\right]$ as a function of $1/\ell$, for two different temperatures. For both the cases, it can be appreciated that, in the limit $\ell \to \infty$, the exponent converges to the LS value $\alpha = 1/3$. From the temperature dependent slopes of these numerical results we can make a guess about the background length ℓ_0, discussed in the previous chapter in the context of finite-size scaling analysis. For the sake of brevity, we do not demonstrate the finite-size scaling analysis. In Fig. 3.4 we present a plot of amplitude A, extracted from the finite-size scaling, vs T. One observes that A monotonically increases with T. From the quality of data, however, it is difficult to figure out if there is any specific critical behavior of this quantity. Note that all these results correspond to reasonably high temperatures. Next we present results for low enough temperature to see if there is any signature of $\alpha = 1/4$, at early time.

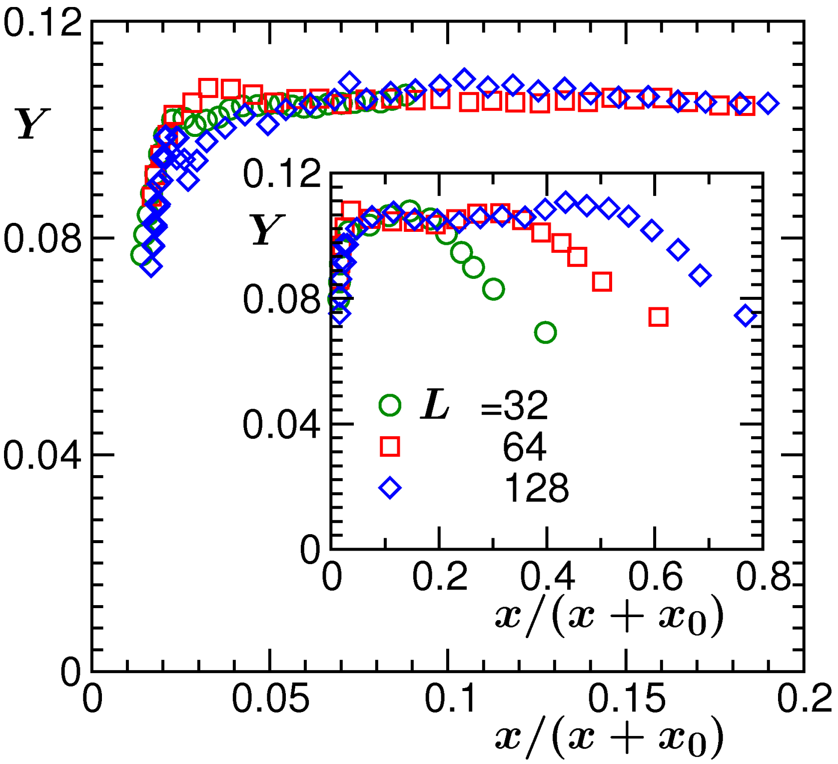

Figure 3.5: Finite-size scaling plot for 50 : 50 Ising model using $\ell(t)$ data from three different system sizes at $T = 0.35T_c$. The values of ℓ_0 and t_0 are 3.9 and 60 MCS respectively. The value of x_0 used is 5. Note that our counting of time starts from t_0 (time since quench) and ℓ_0 is the corresponding length.

From the nature of data at early time, for $T = 0.35T_c$, in Fig. 2.6, it appears that the interface diffusion mechanism at early time is perhaps giving rise to a smaller value of α. In fact we have struggled to obtain even a reasonable finite-size data collapse of data at early time, for this temperature, by fixing $\alpha = 1/3$, see Fig. 3.5. A good collapse of data is obtained only for $t > 10^5$ MCS. The nonscaling behavior of the data in the time range $[0, 10^5]$ and the trend of the early time data coming from the lower side (see inset) indicates that the exponent is lower at the beginning. This could, of course, be identified with the "expectation" of $\alpha = 1/4$ for lower temperature. However, some important discussion should be in order here.

It is argued that at lower temperature there should be crossover from $\alpha = 1/4$ to $1/3$. This means that bulk diffusion, which is negligible at early time becomes significant at late time. This is analogous to saying that the bulk order parameter is closer to saturation at early time which is contradictory to the actual fact. In view of that even though our finding is consistent with crossover in the exponent from 1/4 to 1/3, we feel that a better argument should be devised to understand this interesting fact.

We end this section by stating that the estimation of finite-size effects is consistent with the quantitative statement in the previous chapter, for all temperatures studied.

3.3 Composition Dependence

In this section, we present results for morphology and growth from the MC simulations of Ising model with various different compositions of up and down spins (A and B particles). Here all the results are obtained at

$T = 0.53T_c$.

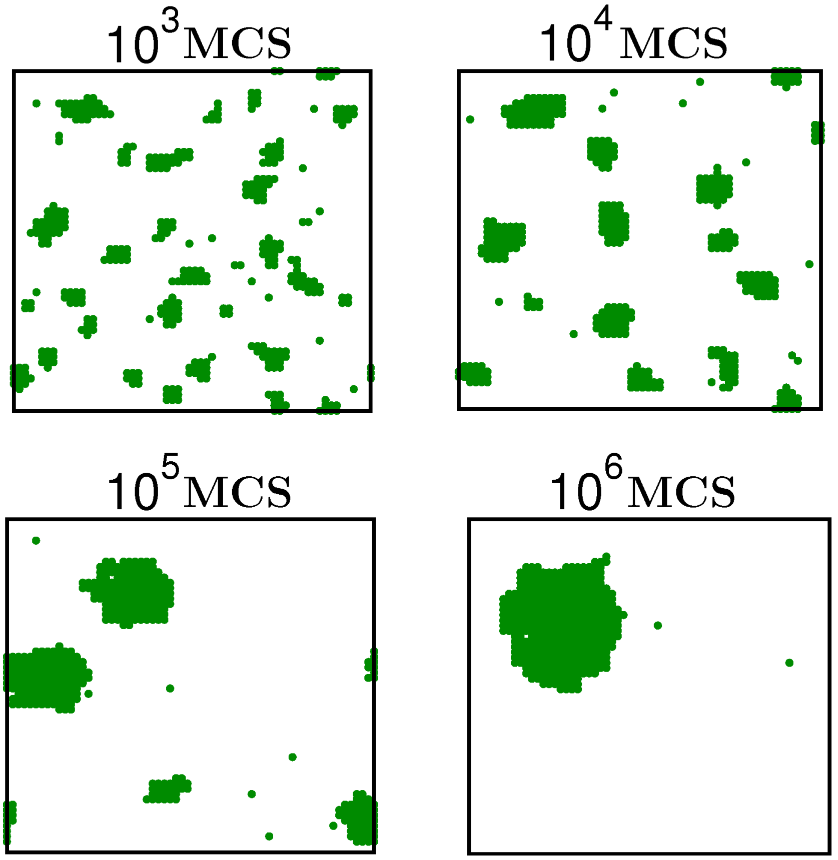

Figure 3.6: Snapshots obtained during the evolution of a 10 : 90 Ising model at $T = 0.53T_c$ in a square box of length $L = 64$. Only A particles are shown.

Fig. 3.6 shows the snapshots during the evolution of a 10 : 90 Ising system (10 % A and 90 % B) starting from a random initial configuration. Requirement of energy minimization and very off-critical composition restricts the domain geometry of the minority species to droplets. Since the hydrodynamics is unimportant in solid, growth of droplets, after their nucleation, takes place via diffusion mechanism. As already stated, our objective here is to find out correction to the LS growth law, if any, at early time, due to finite radius of curvature of droplets.

In Fig. 3.7, we show a comparative picture of snapshots from four different compositions at the same time. It is apparent that as one moves closer to the symmetric or critical composition, the growth is faster. This is easily understandable that with the decrease of overall concentration of A particles, they need to travel longer to get deposited on a domain.

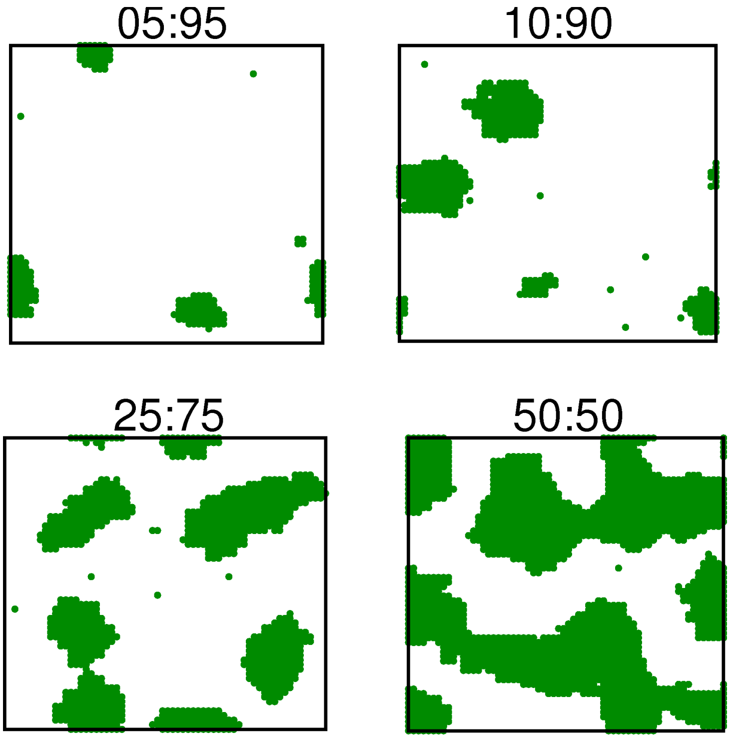

Figure 3.7: Snapshots from the evolution of Ising model at $T = 0.53T_c$, for four different compositions at $t = 10^5$ MCS, with $L = 64$.

In Fig. 3.8, we show scaling plots of the correlation function, for $10 : 90$ composition. Again, the length scale used here was obtained from the first moment of domain size distribution function. (Note here that in all the cases we have considered only the average size of A-domains). It is seen that one obtains good quality data collapse with the increase of time.

In Fig. 3.9, we show the plots for correlation functions from four different

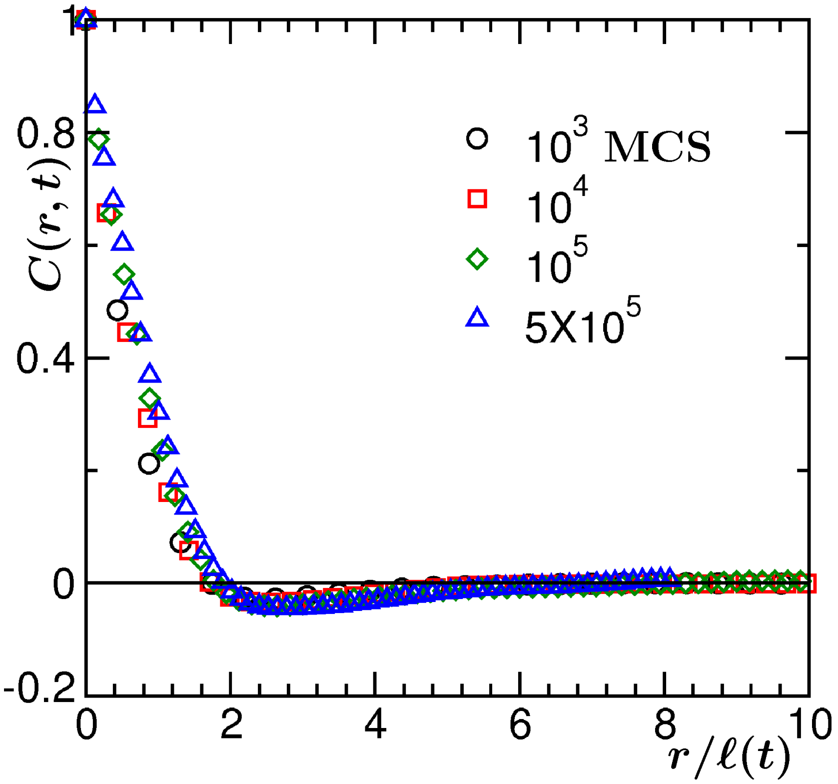

Figure 3.8: Scaling plots of the correlation functions for 10 : 90 composition at $T = 0.53T_c$. The results for all the times were obtained from a system of size $L = 64$, after averaging over 100 initial configurations.

compositions for the late time snapshots shown in Fig. 3.7. No scaling behavior is seen because of the method of calculation of $\ell(t)$. Recall, we have used only the A-domains. However, from the definition of $C(r,t)$, it is clear that the information of both A-rich and B-rich regions are incorporated in it. In the inset of this figure, however, we have obtained reasonable data collapse by using $\ell(t)$ from the decay of $C(r,t)$, except for the amplitude of damped oscillation. This discrepancy is due to the fact that integration of $C(r,t)$ with respect to r is proportional to the sum of the order parameter which is different for different compositions. Apart from that, reasonable collapse of data indicates that the basic structure is same in all the cases.

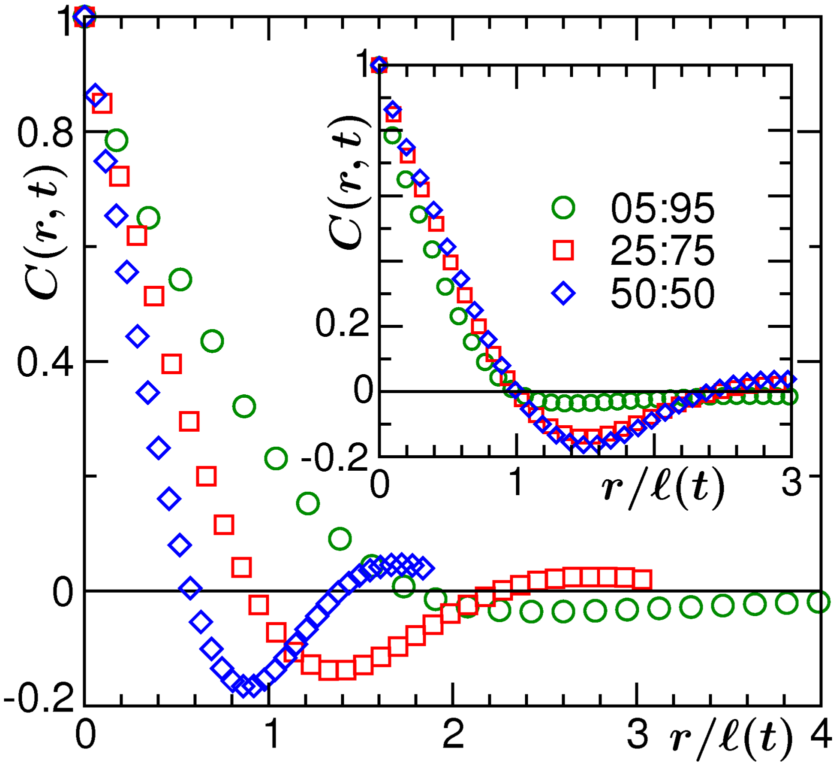

Figure 3.9: Scaling plots of $C(r,t)$ using data from three different compositions at $T = 0.53T_c$, for $L = 64$. Inset : Same as the main frame but here $\ell(t)$ was used from the first zero crossing of $C(r,t)$.

In Fig. 3.10, we show $\ell(t)$ as a function of time for three different compositions, as indicated. Interestingly it appears that the equilibration time t_{eq} is a non-monotonic function of composition. Another observation is that the amplitude of growth decreases with increasing asymmetry of composition. This fact explains the former considering that for extreme off-criticality smaller amount of A particles need to assemble to reach equilibrium. In Fig. 3.11, we show the instantaneous exponent obtained for the plots in Fig. 3.10. In all the cases it is seen that in the limit $\ell \to \infty$, there is a tendency of the data to converge to the LS value $\alpha = 1/3$.

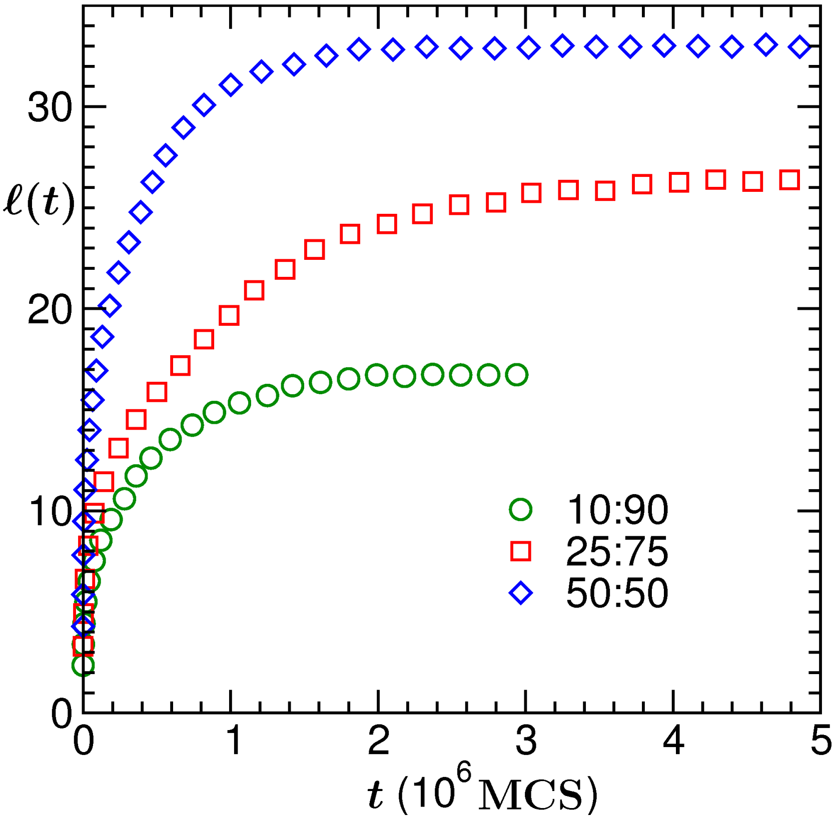

Figure 3.10: Plots of $\ell(t)$ vs t, at $T = 0.53T_c$, for three different compositions. The system size for all the cases is $L = 64$. Final results were obtained after averaging over 100 independent initial configurations.

In Fig. 3.12, we show the plots of $\ell(t)$ vs t from various different system sizes, for the composition 10 : 90. Corresponding finite-size scaling analysis is demonstrated in Fig. 3.13. Best data collapse, that is presented here, was obtained for $\ell_0 = 1.8$ and $t_0 = 80$ MCS. Note that here we have fixed α to the LS value 1/3 again. Reasonable flat nature of the data confirms that the correction is negligible and if at all present, it is buried in the statistical fluctuation of the simulation results. Again, from the ordinate of this flat region, we extract the amplitude of growth. This is plotted in Fig. 3.14. Further, we have extracted information on the finite-size effects from the

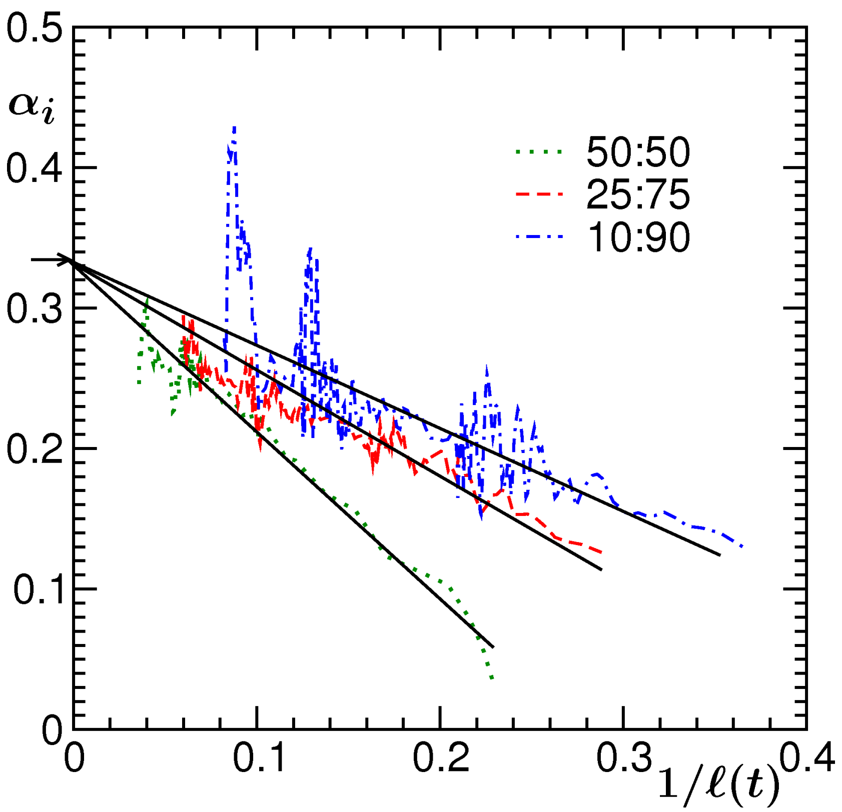

Figure 3.11: Plots of instantaneous exponent α_i vs $1/\ell(t)$ obtained from the plots in Fig. 3.10.

deviation of data from flat behavior in the scaling plots. In all the cases it appears rather weak and consistent with quantitative information provided in Chapter 2.

Coming back to the point of curvature dependent correction, we revert to a different analysis below. In our finite-size scaling analysis one may ask about the ambiguity in the choice of ℓ_0, however small it may be. To avoid such criticism, we search for a method where ℓ_0 can be gotten rid of in a different mathematical way. Writing

$$\ell(t) = \ell_0 + At^{\alpha}, \tag{3.2}$$

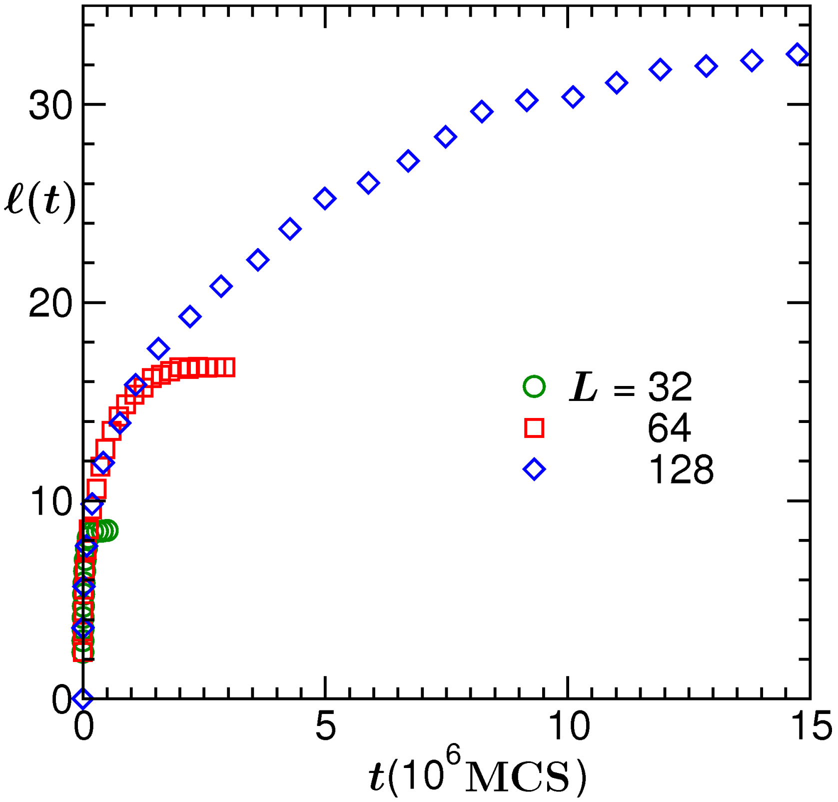

Figure 3.12: Average domain size, $\ell(t)$, is plotted vs t for 10 : 90 mixture. Results from three different system sizes at $T = 0.53T_c$ are shown.

one obtains

$$\frac{d\ell(t)}{dt} = \ell' = A\alpha t^{\alpha-1}. \tag{3.3}$$

By setting $\alpha = 1/3$, one has

$$\frac{1}{\ell'^{3/2}} = \left(\frac{3}{A}\right)^{3/2} t. \tag{3.4}$$

In Fig. 3.15, we plot $1/\ell'^{3/2}$ vs t for three different compositions, including the critical one. In all the cases, numerical results look consistent with linear

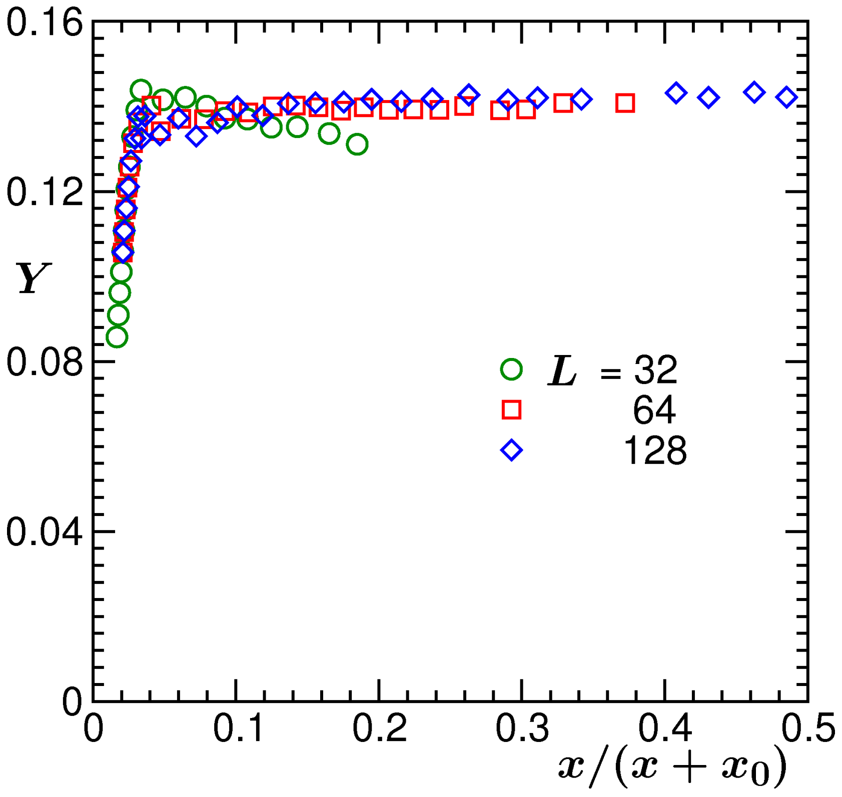

Figure 3.13: Finite-size scaling plot for data in Fig. 3.12. The values of ℓ_0 and t_0 are respectively 1.8 and 80 MCS. Note that the value of x_0 used is 5.

behavior from very early time. The solid lines there are guides to the eye for which we have used slopes $\left(\frac{3}{A}\right)^{3/2}$ by taking A from Fig. 3.14.

Despite all these findings, we do not discard the fact that a correction is present. Our analysis might have failed to capture this aspect because of statistical fluctuation in the data combined with the fact that the correction are of higher order in $1/\ell$ with very small value of prefactor. This argument stems for the curvature dependent interfacial tension

$$\sigma[\ell(t)] = \frac{\sigma(\infty)}{1 + 2\left(\ell_c/\ell(t)\right)^2}, \tag{3.5}$$

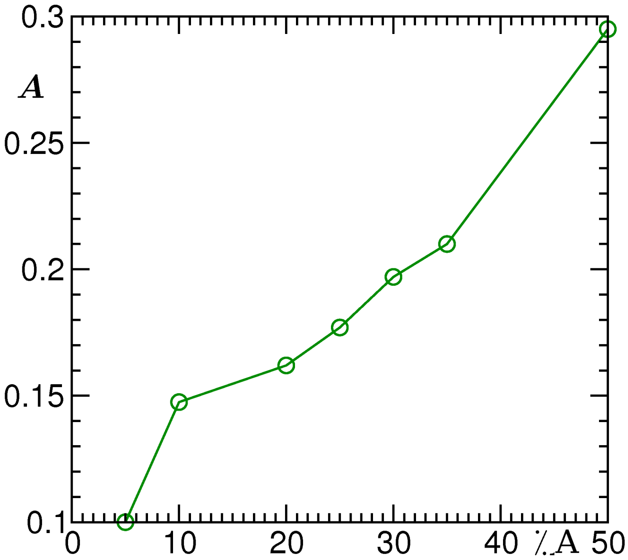

Figure 3.14: Plot of growth amplitude A vs % of A particles. All data points correspond to $T = 0.53T_c$.

for symmetric models like the Ising one with quadratic leading correction [19, 20]. From equilibrium studies of symmetric binary fluid that belongs to the Ising universality class of critical phenomena, it is observed that ℓ_c is very small at temperatures comparable to the present study. For temperatures significantly close to T_c, however, curvature dependent correction to the growth law may be significant. This statement can be justified from the finding that ℓ_c diverges at criticality [21]. But, closer to T_c, study of kinetics of phase separation is limited by lot of additional difficulties because of mixing of two diverging lengths, viz., the equilibrium correlation length ξ and domain size ℓ. So we leave it as a future task when we acquire better computational resources. We close this section, with the following comments. Irrespective of composition, at moderate temperatures, the correction to scaling appears very small and this contradicts and corrects our previous understandings

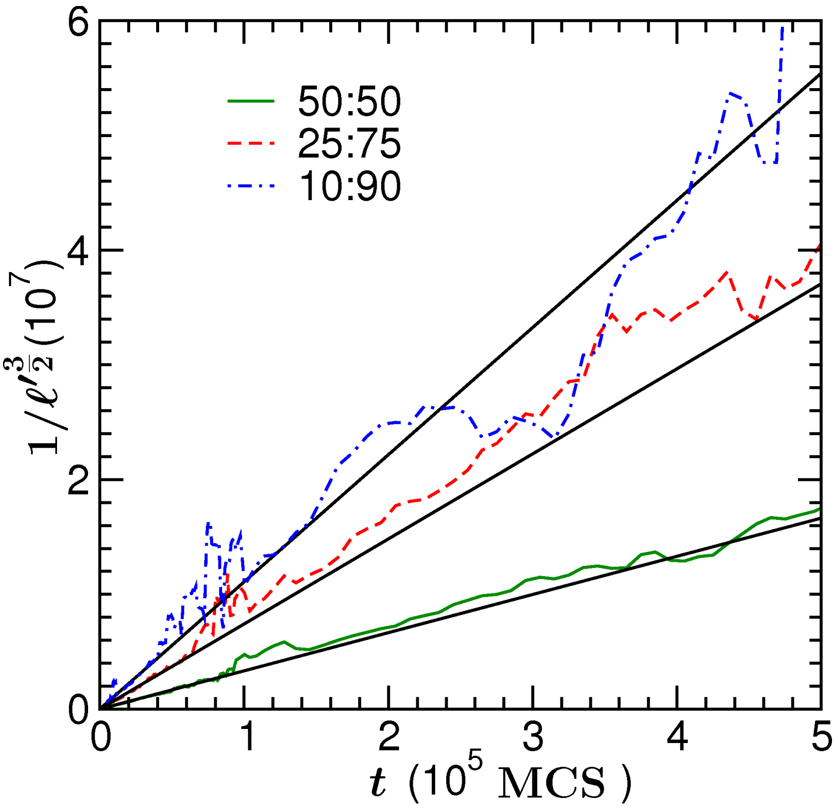

Figure 3.15: Plot of $1/\ell'^{3/2}$ vs t for three different compositions at $T = 0.53T_c$. The solid lines have slopes $\left(\frac{3}{A}\right)^{3/2}$.

about this phenomena of kinetics of phase separation. The finite-size effects in all the cases appears rather weak.

3.4 Conclusion

We have presented detailed results for the kinetics of phase separation in solid binary mixtures via Kawasaki exchange Monte Carlo simulation of Ising model. Results are understood via sophisticated finite-size scaling analysis and other methods. Important aspects related to the variation of quench depth and mixture composition are discussed.

A wide variation of temperatures was considered for the study related to the influence of quench depth. For temperatures above $0.5T_c$, it is observed that the growth laws are consistent with Lifshitz-Slyozov (LS) law ($\alpha = 1/3$) almost all along. For significantly low temperature, however, at early time, lower exponent of the growth was noticed which crosses over to the LS value only at much later time. In this case the early time behavior is consistent with the prediction for interface diffusion mechanism.

For the composition dependent case, our objective was to search for any significant correction to the scaling. The finding appears to be against it which again contradicts many existing studies in the literature. Our observation, however, is consistent with recent studies in the equilibrium context involving curvature dependent interfacial tension. Nevertheless, in line of these equilibrium studies, we expect noticeable corrections for temperatures close to the critical value. Because of scientific as well as technical reasons, we, however, leave it as a future problem.

In addition to results and analysis for the growth law, we have presented interesting results for the pattern formation as well. These patterns were characterized via calculation of correlation functions and related quantities. lastly, our observation about the weak finite-size effects appears to be generic at all temperatures and composition.

Bibliography

[1] I.M. Lifshitz and V.V. Slyozov, J. Phys. Chem. Solids **19**, 35 (1961).

[2] A.J. Bray, Adv. Phys. **51**, 481 (2002).

[3] J.S. Langer, M. Bar-on, and H.D. Miller, Phys. Rev. A **11**, 1417 (1975).

[4] H. Furukawa, Adv. Phys. **34**, 703 (1985).

[5] S. Puri, A.J. Bray and J.L. Lebowitz, Phys. Rev. E **56**, 758 (1997).

[6] S. van Gemmert, G.T. Barkema and S. Puri, Phys. Rev. E **72**, 046131 (2005).

[7] K. Binder and D. Stauffer, Phys. Rev. Lett. **33**, 1006 (1974).

[8] E.D. Siggia, Phys. Rev. A **20**, 595 (1979).

[9] H. Tanaka, J. Chem. Phys. **105**, 10099 (1996).

[10] S. Majumder and S.K. Das, Europhys. Lett. **95**, 46002 (2011).

[11] S. Roy and S.K. Das, Phys. Rev. E **85**, 050602 (2012).

[12] D.A. Huse, Phys. Rev. B **34**, 7845 (1986).

[13] S. Majumder and S.K. Das, Phys. Rev. E **81**, 050102 (R) (2010).

[14] S. Majumder and S.K. Das, Phys. Rev. E **84**, 021110 (2011).

[15] D.P. Landau and K. Binder, *A Guide to Monte Carlo Simulations in Statistical Physics*, (Cambridge University Press, Cambridge 2009).

[16] K. Kawasaki, in *Phase Transition and Critical Phenomena*, edited by C. Domd and M.S. Green (Academic, New York, 1972), Vol. 2, p.443.

[17] M.E. Fisher in *Critical Phenomena*, ed. M.S. Green (Academic, London, 1971), p1.

[18] *Finite Size Scaling and the Numerical Simulations of Statistical Systems* edited by V. Privman (World Scientific, Singapore, 1990).

[19] M.P.A. Fisher and M. Wortis, Phys. Rev. B **29**, 6252 (1984).

[20] B.J. Block, S.K. Das, M. Oettel, P. Virnau and K. Binder, J. Chem. Phys. **133**, 154702 (2010).

[21] S.K. Das and K.Binder, Phys. Rev. Lett. **107**, 235702 (2011).

Chapter 4

Phase Behavior and Dynamics of Vapor-Liquid Phase Transition

4.1 Introduction

Understanding nonequilibrium evolution during the phase separation in a system is of fundamental importance [1–4] and of much research interest, both theoretically and experimentally [5–22]. This phenomena has been introduced in length in the introduction chapter as well as in previous chapters related to solid-solid phase separation. For the sake of completeness, some of the issues we discuss here as well, before presenting the results. Note that, except for the phase behavior, all the results (including text) in this chapter are reproduced from References [23, 24].

Upon quenching from a high temperature homogeneous state to a temperature below the critical point, the system becomes unstable to fluctuations and starts phase separating with the formation and usually nonlinear growth of particle rich and particle depleted domains. Such coarsening is a scaling phenomenon [25], e.g., the shape functions characterizing the morphology obey the scaling relations [1–3, 20, 25]

$$\begin{aligned} C(r,t) &\equiv \tilde{C}(r/\ell(t)), && (4.1)\\ S(k,t) &\equiv \ell(t)^d \tilde{S}(k\ell(t)), && (4.2)\\ P(\ell_d,t) &\equiv \ell(t)^{-1}\tilde{P}[\ell_d/\ell(t)], && (4.3) \end{aligned}$$

where $C(r,t)$, $S(k,t)$ and $P(\ell_d,t)$ are respectively the two-point equal-time correlation function, structure factor and domain size distribution function. In Eqs. (4.1-4.3) $\tilde{C}(x)$, $\tilde{S}(y)$ and $\tilde{P}(z)$ are the master functions independent of time (t)-dependent average domain-size $\ell(t)$ that typically grows in a power law manner

$$\ell(t) \sim t^{\alpha}. \tag{4.4}$$

The growth exponent α, in Eq. (4.4), depends upon the transport mechanism driving the phase separation. For diffusive dynamics, associating the domain growth with the chemical potential gradient as

$$\frac{d\ell(t)}{dt} \sim |\vec{\nabla}\mu| \sim \frac{\gamma}{\ell(t)^2}, \tag{4.5}$$

γ being the inter-facial tension, one obtains $\alpha = 1/3$. This is referred to as the Lifshitz-Slyozov [26] (LS) law. While LS law is the only expected behavior for phase separating solid mixtures, one expects much faster growth, at large length scales, for fluids and polymers, where hydrodynamics is important. Compared to the kinetics in vapor-liquid phase separation, domain coarsening in binary fluids received much more attention [5–7, 11, 13, 14, 19, 27–30] where following consensus for the behavior of late stage growth [31–34] has been reached in $d = 3$. Considering a balance between the surface energy density ($\gamma/\ell(t)$) and the viscous stress ($6\pi\eta v_\ell/\ell(t)$, v_ℓ being the interface velocity and η the shear viscosity) for an interconnected domain structure, one can write

$$\frac{d\ell(t)}{dt} = v_\ell = \frac{\gamma}{\eta}. \tag{4.6}$$

Solution of Eq. (4.6) predicts a linear growth ($\alpha = 1$), a picture that holds for low Reynolds number. However, for $\ell(t) \gg \ell_{in} (= \eta^2/(\rho\gamma)$, ρ being the density), the inertial length, the surface energy density is balanced by kinetic energy density ρv_ℓ^2, so that

$$\frac{d\ell(t)}{dt} \sim \frac{1}{\ell(t)^{1/2}}, \tag{4.7}$$

giving $\alpha = 2/3$. Note that $\alpha = 1$ is referred to as the viscous hydrodynamic growth and $\alpha = 2/3$ as inertial hydrodynamic growth. While crossover from diffusive to viscous hydrodynamic regime was observed in molecular dynamics (MD) simulations [19, 30] and experiments [35–37], both viscous and inertial growths were observed in lattice-Boltzmann simulations [3].

While nonequilibrium universality for vapor-liquid phase separation is expected to be the same as the liquid-liquid, rare inconclusive MD simulations that exist [15, 38–41] for the vapor-liquid transition report an exponent $\alpha = 1/2$ for late time domain coarsening. Thus, even though our recent focus has turned to systems with realistic interactions and physical boundary conditions [5–11], our basic knowledge and understanding of segregation kinetics in bulk fluids still remains a challenge. In this chapter, we present results from large scale MD simulations for kinetics of vapor-liquid phase separation in a single-component Lennard-Jones (LJ) fluid. This work reports first observation of viscous hydrodynamic growth via MD simulation, thus computationally confirming that the nonequilibrium universality class of vapor-liquid and liquid-liquid phase separation is indeed the same as in the case of equilibrium critical phenomena for both static and dynamic properties. In addition to exploring the domain growth, in this chapter we have also investigated the extent of finite-size effects for this class of phase transition via the application of finite-size scaling analysis technique. An appropriate knowledge of the finite-size effects helps in the judicial choice of the system for the direct understanding of the asymptotic growth law so that any unexpected deviation is not inappropriately attributed to the deficiency in system size.

This chapter is divided into following sections. In Section 4.2 we will describe the model used in this study. Section 4.3 presents results for the phase diagram and estimation of critical point for the model. In Section 4.4 we present results from the nonequilibrium evolution during vapor-liquid phase transition. In Section 4.5 we estimate the finite size effects for such domain coarsening problem and finally we end the chapter in Section 4.6 with a summary and discussion.

4.2 Model and Method

We consider a model where particles interact via

$$V(r_{ij}) = U(r_{ij}) - U(r_c) - (r_{ij} - r_c)\left(\frac{dU(r_{ij})}{dr_{ij}}\right)_{r_{ij}=r_c}, \tag{4.8}$$

with

$$U(r_{ij}) = 4\epsilon\left[\left(\frac{\sigma}{r_{ij}}\right)^{12} - \left(\frac{\sigma}{r_{ij}}\right)^{6}\right] \tag{4.9}$$

being the standard LJ potential. In Eqs. (4.8) and (4.9), r_{ij} is the scalar distance between the ith and jth particles, σ is the particle diameter and ϵ is the interaction strength. The cut-off and shifting of the potential at r_c was used to facilitate faster computation. Further, introduction of the third term [42] on the right hand side ensures that both the effective potential and force are continuous at r_c which was set to 2.5σ. All particles were assigned equal mass m. For the sake of convenience, below we set m, σ, ϵ and k_B to unity. The MD runs were performed using the Verlet velocity algorithm [42, 43] with an integration time step of $\Delta t = 0.005\tau$, $\tau = (m\sigma^2/\epsilon)^{1/2} = 1$.

The phase-diagram of the model without the force-correction term is known [44], the critical temperature (T_c) and critical density (ρ_c) being 1.085 ± 0.005 and 0.317 ± 0.006 respectively. It is understood, of course, that the introduction of force-correction will somewhat change the value of T_c, which, from our experience [45–47] with a similar model that was used to study phase-separation in binary mixture, could be somewhat $(10\% - 20\%)$ lower. Nevertheless, to be sure and for completeness, we preferred to estimate the phase diagram for the corrected potential which is presented in the following section.

4.3 Estimation of the Phase Diagram

MD runs were performed at different temperatures in a rectangular box with dimensions L_x, L_y and L_z, where $L_x = L_y = L \ll L_z$. Periodic boundary conditions were applied in all directions. We have used NVT ensemble with fixed density of particles $\rho = 0.3$. The Nosé-Hoover thermostat was used to control the temperature. The choice of such a rectangular box is because of the fact that it will lead to configuration where the interface between the vapor and liquid domains will be perpendicular to the xy-plane which, in turn, will provide significant length in z-direction for both the vapor and liquid phases so that the co-existing densities can be calculated with better confidence.

In Fig. 4.1 (a) we have shown the $3-d$ snapshot of the equilibrium configuration obtained after MD simulation at $T = 0.6$ for a rectangular box with $L = 30$ and $L_z = 150$. It clearly shows the phase separation between the high density liquid phase and the low density vapor phase. The interface

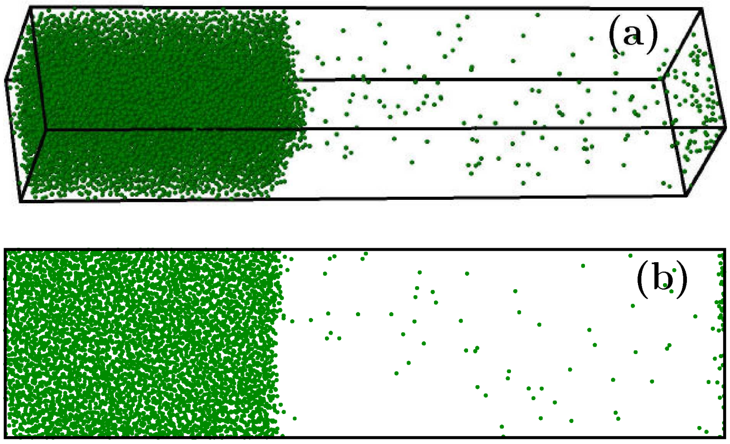

Figure 4.1: (a) $3-d$ snapshot of an equilibrium configuration obtained from MD simulation starting from random initial configuration with $L_x = L_y = 30$ and $L_z = 150$ and having density $\rho = 0.3$ at $T = 0.6$. (b) 2-dimensional cross-section of the same snapshot in an xz-plane. Further details are given in the text.

between the vapor and liquid domains is found to be perpendicular to the xy-plane, as expected. In Fig. 4.1 (b) we have shown a $2-d$ xz- cross-section of the same snapshot for $y = L/2$.

Our next task is to calculate the equilibrium densities for the liquid and vapor phases at different temperatures. We have extracted the equilibrium values of the densities from the density profile of the equilibrium configurations as function of the z-coordinates. The density profile was calculated by dividing the system into small rectangular boxes of width $\Delta z = 2$ and length L along the x and y- directions. In Fig. 4.2, we have shown the density profiles for three different temperatures as indicated. It is seen that the density has a reasonably constant high value for small of z and then suddenly drops at an intermediate value of z values (except at the beginning) and remains more or less constant almost till the end. The higher densities

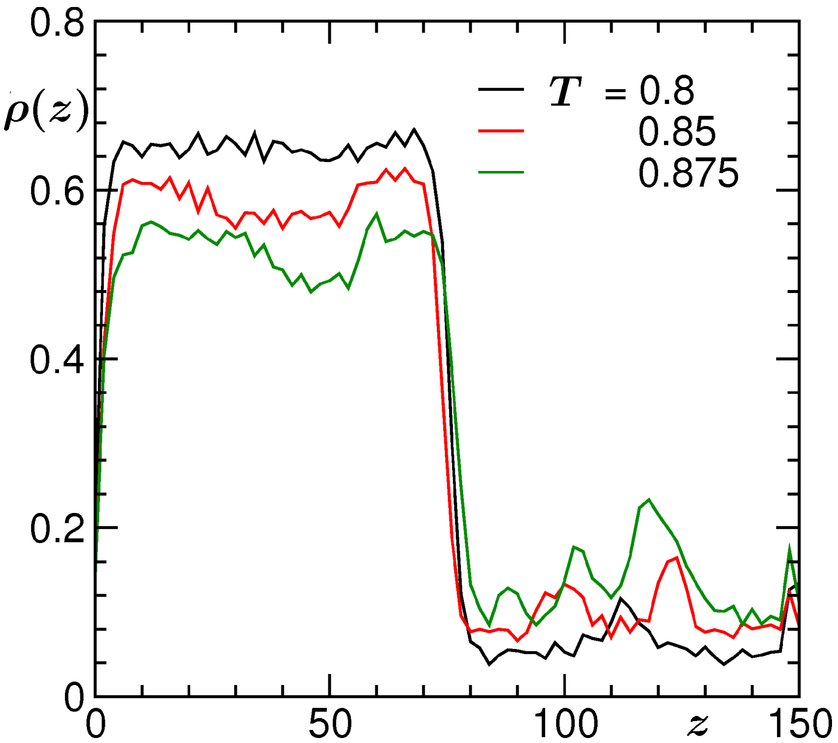

Figure 4.2: Density profiles at three different temperatures, as indicated, for the rectangular equilibrium configurations, obtained via MD simulations with $L_x = L_y = 30$ and $L_z = 150$, for overall density $\rho = 0.3$.

here correspond to the liquid phase and the lower ones for the vapor phase at respective temperatures. From the average of densities in the liquid range and vapor range, we extract the equilibrium values of the density for the vapor and liquid phases respectively. It should be noted that here that at very high temperature, due to strong thermal fluctuations, the estimations are less reliable.

In fig. 4.3 we show the phase diagram of the model in the temperature (T) vs density (ρ) plane. Here we have plotted the equilibrium densities of the liquid and vapor phases as function of the temperature. One can clearly see that the density difference between the two phases decreases with increase

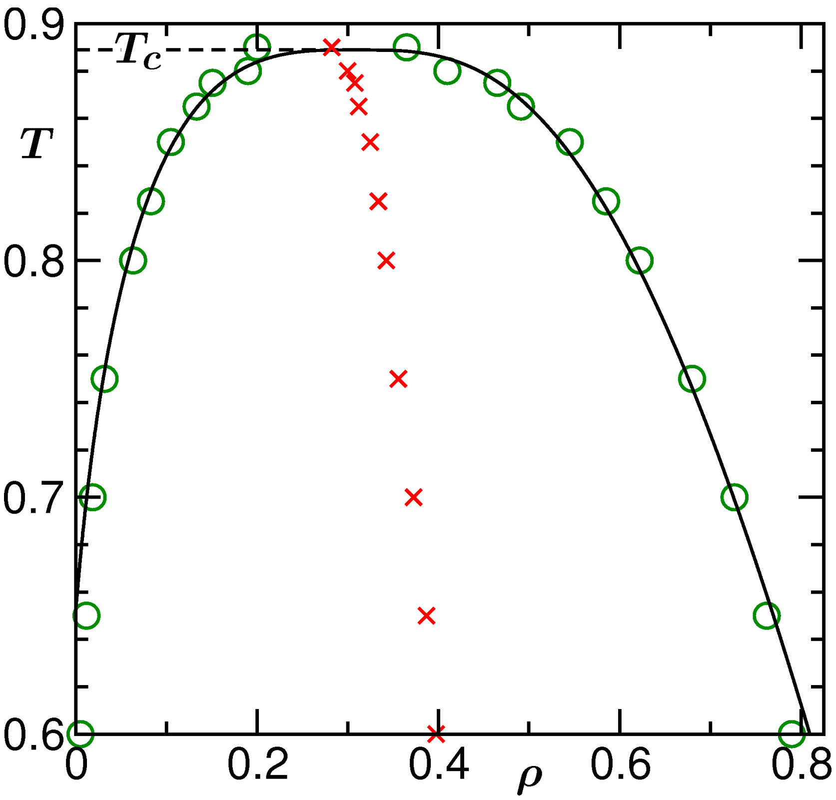

Figure 4.3: Phase behavior of the LJ model under study in the temperature vs density plane. The solid line corresponds to Eq. 4.11. For details about the estimation of parameters in this equation see text. The crosses represent the co-existence diameter.

of temperature. To estimate the critical point the data can be fitted to co-existence diameter (represented by the crosses in this figure) that behaves as

$$\frac{\rho_l + \rho_g}{2} = \rho_c + A(T_c - T), \tag{4.10}$$

where ρ_l and ρ_g are the densities of the liquid and gas phases respectively, ρ_c is the critical density, T_c is the critical temperature and A is a constant. In addition, the density difference between the two phases $(\rho_l - \rho_g)$ which is the order parameter for vapor liquid transition, is fitted to the form

$$(\rho_l - \rho_g) = B(T_c - T)^{\beta}, \tag{4.11}$$

where β is the critical exponent for the vanishing of the order parameter and B is a critical amplitude. During fitting we set $\beta = 0.325$ which is the value for Ising universality class [43]. In Fig. 4.4 we have shown the plot of $(\rho_l - \rho_g)^{1/\beta}$ vs T. The solid line there is a fit to the form (4.11), where we have used points towards the higher temperature excluding the last two points. The fitting gives $B = 1.22$ and $T_c = 0.895$. Further, from (4.10) we obtain $A = 0.375$ and $\rho_c = 0.305$. The continuous line in Fig. 4.4 corresponds to Eq. (4.11) with $B = 1.22$, $T_c = 0.895$ and $\beta = 0.325$. Nice consistence of the simulation data with continuous line confirms that this model indeed belongs to the Ising class. Again, we quote that, for this model

$$\begin{aligned} T_c &= 0.895 \pm 0.005, \qquad (4.12) \\ \rho_c &= 0.300 \pm 0.005 \qquad (4.13) \end{aligned}$$

4.4 Results for the Nonequilibrium Dynamics

In this section we discuss the main result of this chapter which is the kinetics of the vapor-liquid phase separation. For our study we have used

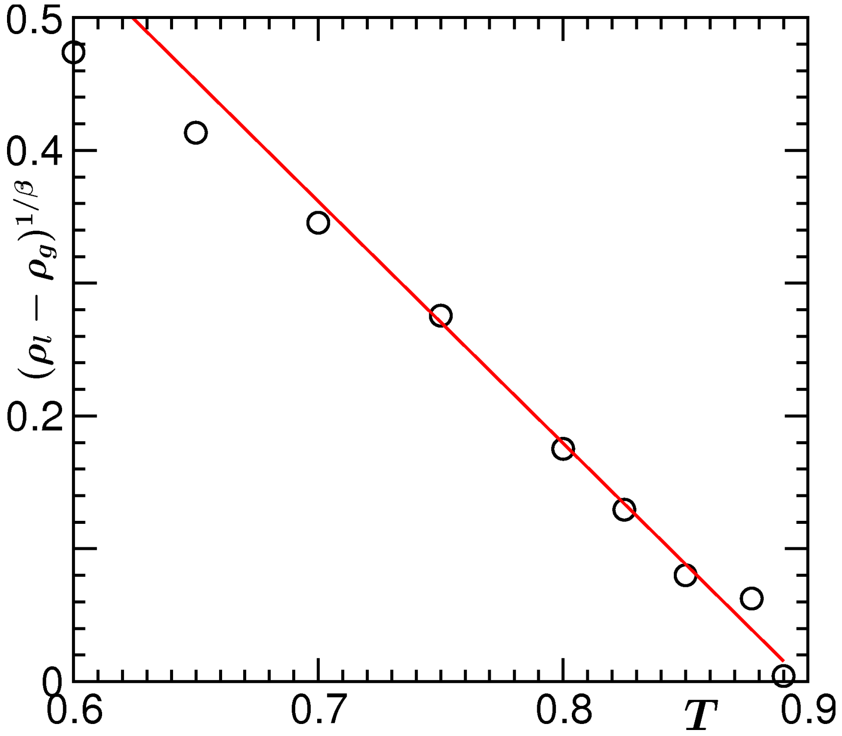

Figure 4.4: Plot of $(\rho_l - \rho_g)^{1/\beta}$ vs T with $\beta = 0.325$. The solid there is obtained from fitting to the form (4.11).

a total 265421 particles, confined in a periodic 3-dimensional cubic box of linear dimension $L = 96$, having a density $\rho = 0.3$. The temperature was controlled by using a Nosé-Hoover thermostat (NHT) [43], which is known to preserve hydrodynamics well. At $t = 0$ homogeneous initial configurations, prepared by equilibrating the system at $T = 5$, were quenched to $T < T_c$. All the results were obtained by averaging over 5 independent runs at a quench temperature $T = 0.7$.

The left frames of Fig. 4.5 are typical 3-dimensional evolution pictures from two different times where the dots represent particles. They demonstrate nice interconnected structure of segregating domains growing with time. The average density of liquid and vapor domains are respectively 0.72

and 0.02. A direct method to characterize the structure is to calculate the radial distribution function, $g(r)$, from these continuum configurations. However, we are interested in looking at $C(r,t)$, its Fourier transform $S(k,t)$ and $P(\ell_d,t)$ which have been more standard tools in the study of phase ordering dynamics. To facilitate the calculation of latter quantities, we map the continuum snapshots to a lattice one in such a way that a pure domain structure is obtained where all lattice sites inside a liquid domain have occupancy one while sites inside the vapor domain have occupancy zero. An appropriate renormalization procedure [12, 16, 19] is applied for this noise removal exercise. We further map this system into spin-1/2 Ising system where an occupied lattice site has spin value $S_i = 1$ and for a vacant site $S_i = -1$. The right frames in Fig. 4.5 show such mapped configurations. In Fig. 4.6 we demonstrate similar exercise by showing cross-sectional views at two other times. Which may be difficult to appreciate from the $3-d$ snapshots, these $2-d$ pictures clearly show that no significant structural change has occurred during this transformation that can hamper the analysis. Also during the entire duration of study, we find that the composition of up and down spins remains conserved within a tolerable limit of 5% fluctuations.

From the mapped configurations, the correlation function $C(r)$ is calculated as

$$C(r,t) = \langle S_i S_j \rangle \ - \ \langle S_i \rangle^2, \tag{4.14}$$

where the angular brackets stand for statistical averaging. The average domain size $\ell(t)$ from the decay of $C(r,t)$ was estimated as

$$C(r=\ell(t),t)=h, \tag{4.15}$$

where h was set to the first zero of $C(r,t)$. Other methods employed for the calculation of $\ell(t)$ are

$$\ell(t)=\frac{1}{\int dk\ kS(k)} \tag{4.16}$$

and

$$\ell(t)=\int d\ell_d\ell_d P(\ell_d,t). \tag{4.17}$$

In Eqs. (4.16) and (4.17), it is assumed that $S(k,t)$ and $P(\ell_d,t)$ are appropriately normalized. In Eq. (4.17), ℓ_d is obtained from the separation between two successive domain interfaces in $x-$, $y-$ or $z-$ directions.

In Fig. 4.7, we present the scaling plot of $C(r,t)$ vs. $r/\ell(t)$ for which four different times were chosen, as indicated on the figure. While collapse of data from the earliest time with the other ones is not good, excellent data collapse for three later times is indicative that a scaling regime is reached. In Fig. 4.8 we show the scaling behavior of $S(k,t)$ on a log-log plot. The parallel nature of the tail region to the continuous line confirms consistency with the Porod law [48, 49]. Fig. 4.9 shows the scaling plot of $P(\ell_d,t)$ on a semi-log plot where the linear behavior of the tail region is consistent with an exponential decay [16, 20]. Note that in all the cases, $\ell(t)$ used was obtained from Eq.

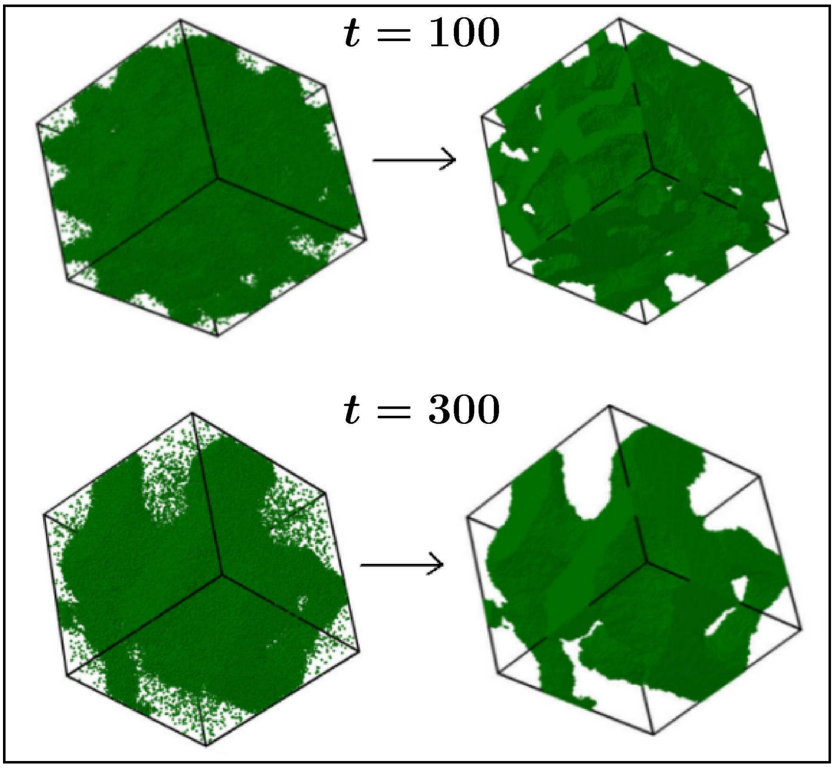

Figure 4.5: Left frames show the $3-d$ snapshots during evolution of the vapor-liquid phase separation in a simple Lennard-Jones system, at two different times, as indicated. The total density was set to 0.3 that gives interconnected domain morphology, as seen. The simulation was performed after quenching a homogeneous system prepared at a high temperature to a temperature $T = 0.7$. The right panel corresponds to the same snapshots, but after removing the noise (see text for details) to obtain a pure domain morphology.

(4.17). The nice data collapse obtained in all the quantities by using $\ell(t)$ from a single measure speaks about the consistency of different methods. Henceforth all the results for $\ell(t)$ will be presented after calculating via Eq. (4.17), unless otherwise mentioned.

Coming to the central objective of the chapter, viz., quantifying the dynamics, in Fig. 4.10 we present plot of $\ell(t)$ vs. t on a log scale. There

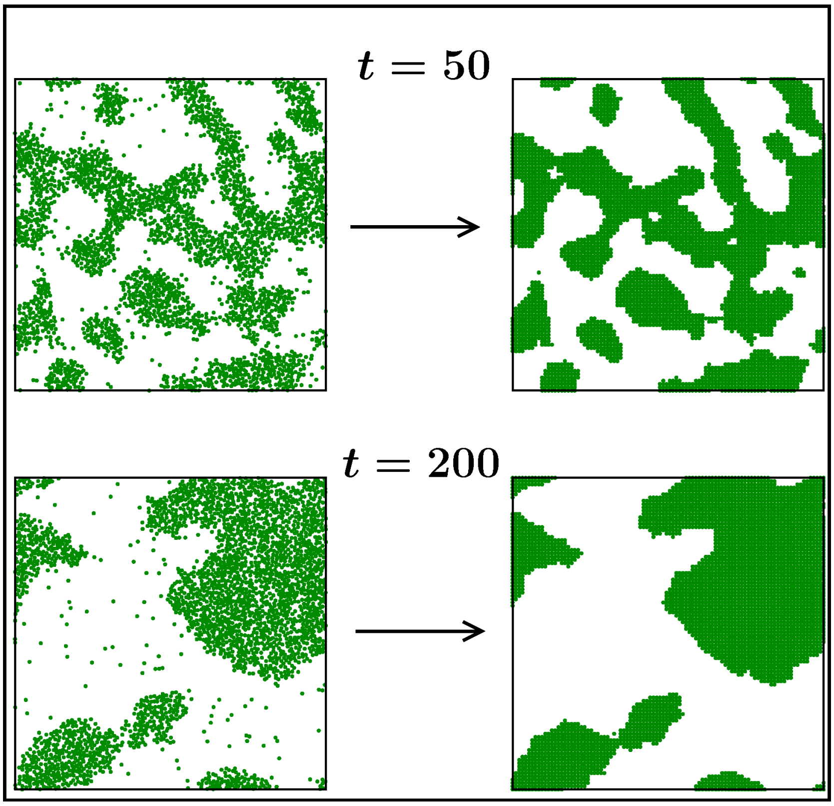

Figure 4.6: Cross-sectional view of the same system in xy plane at two other times. Here also the left frames show the original snapshots and the right ones show the same after removing noise.

various lines correspond to various growth laws in domain coarsening problem. While the early time data is more consistent with a diffusive growth ($\alpha = 1/3$), there appears a gradual crossover to a faster growth. The intermediate time data, of course, look consistent with $t^{1/2}$ as reported in previous works [15, 38–41] and at a later time there seems to be a further crossover. However, due to large offset at the crossover region(s), which will be clearer from further analysis and discussions, we warn the reader not to take this conclusion seriously. For similar reasons, an apparently $t^{1/3}$ looking behavior during early time should also not be taken seriously. In fact, due to this and

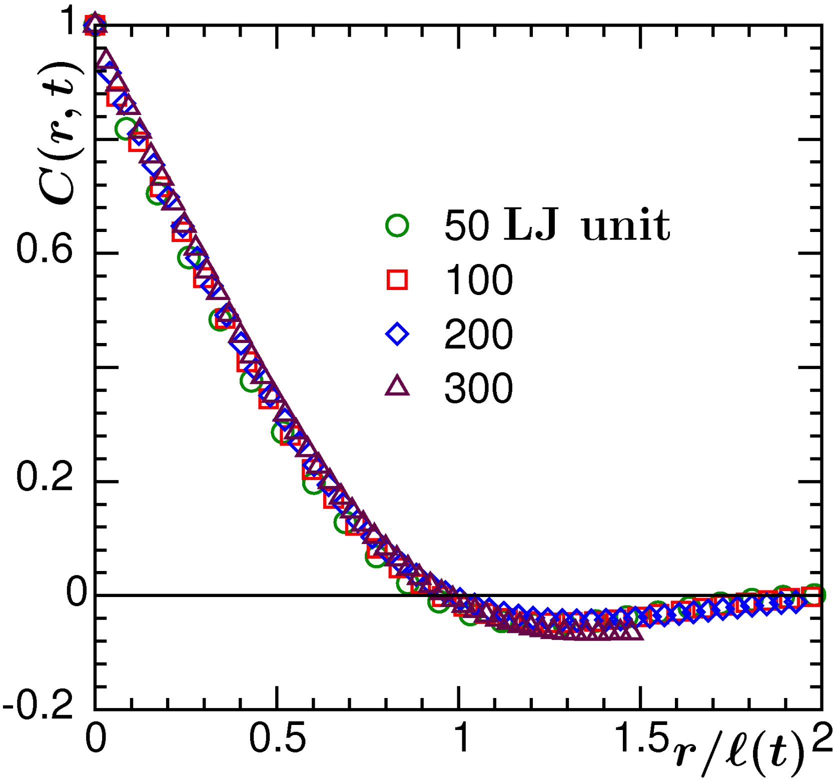

Figure 4.7: Scaling plot of (a) $C(r,t)$ vs $r/\ell(t)$ where data from four different times, as indicated, have been collapsed. All quantities were calculated from noise-free domain structures.

other practical difficulties, it is advisable not to reach a firm conclusion from looking at the behavior on a log-scale (which, of course, is a standard practice followed in the literature), unless one has results over several decades in time and length.

Fig. 4.11 shows a plot of $\ell(t)$ vs t on a linear scale where the data starting from $t \simeq 100$ look quite linear all the way till the end. The deviation from this linear behavior at early time ($t < 100$) could be attributed to slower diffusive growth, as discussed above. A fitting to the form,

$$\ell(t) = A + Bt^{\alpha}, \tag{4.18}$$

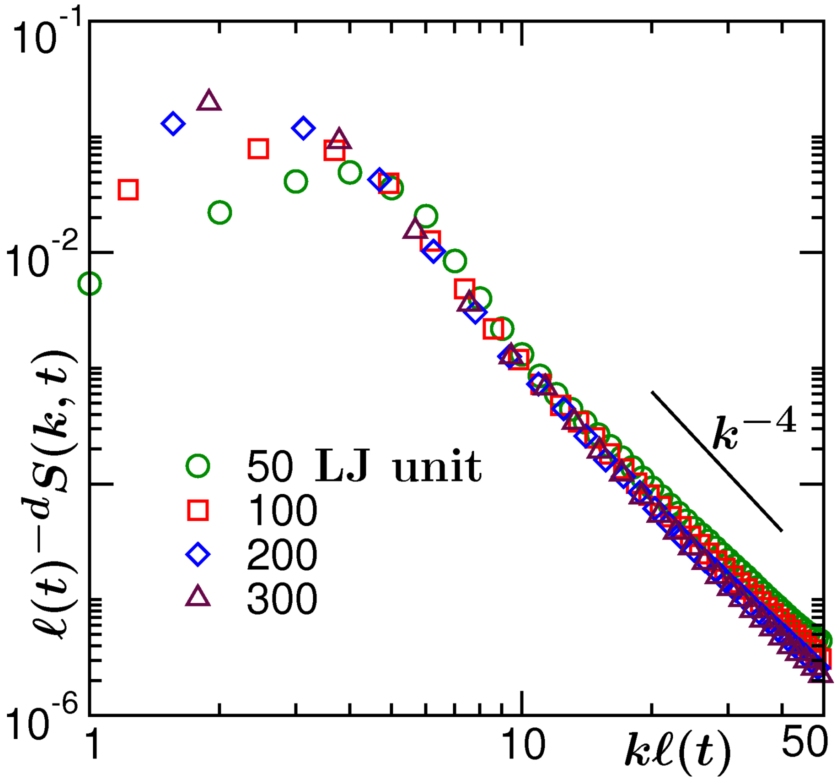

Figure 4.8: Scaling plot of $\ell(t)^{-d}S(k,t)$ vs $k\ell(t)$ from four different times, as indicated. The continuous line has a slope of -4 corresponding to the Porod law.

however, in the range $t \; \epsilon \; [0, 100]$ gives $\alpha = 0.66$. Since this diffusive regime is short lived and also accompanied by gradual crossover to a faster growth regime, it is in fact not practical to search for growth exponent $\alpha = 1/3$ in this region. On the other hand, a similar fitting to the range $t \; \epsilon \; [100, 350]$ gives $\alpha \simeq 0.9$, quite consistent with the predictions for viscous hydrodynamic growth. Note that for $t > 350$ one hits the finite-size effects for the system size used in this work. In Fig. 4.12 we present plot of the exponent α as a function of $1/t_0$ obtained by fitting the data to the form (4.18) in the range $[t_0,350]$. This exercise conclusively says that the exponent at late time

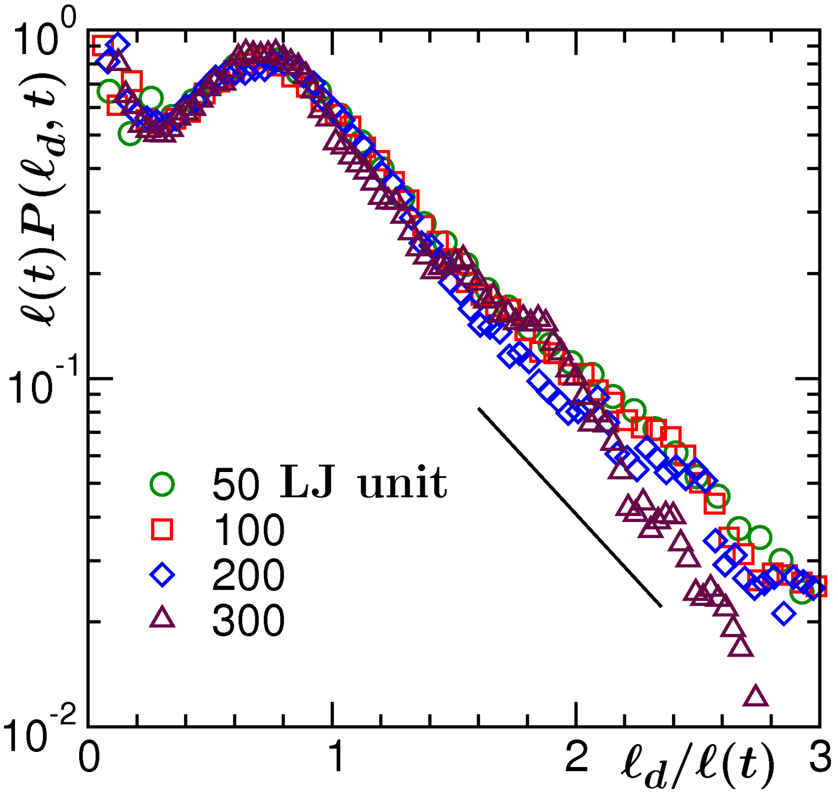

Figure 4.9: Scaling plot of $\ell(t)P(\ell_d,t)$ vs $\ell_d/\ell(t)$ from four different times, as indicated. The continuous line represents an exponential decay of the tail.

certainly is larger than 1/2 which was reported earlier.

Note that for $t > 350$ we expect to see the finite-size effects for this system size. In Fig. 4.13 we plot the system size L as a function of time t_s needed for the domain size to reach the saturation limit. The linear behavior of the data is again consistent with the viscous hydrodynamic growth. This should be compared with the corresponding result obtained from Kawasaki-exchange Monte Carlo simulation of Ising model [51] where, because of diffusive dynamics, L should scale as $t_s^{1/3}$ (dashed line) in accordance with the LS law. This analysis is analogous to the one presented in Chapter 2 [See Fig. 2.8]. Here instead of using $\ell_{\max}$ we have used L and t_s is the same as t_{eq} of Chapter

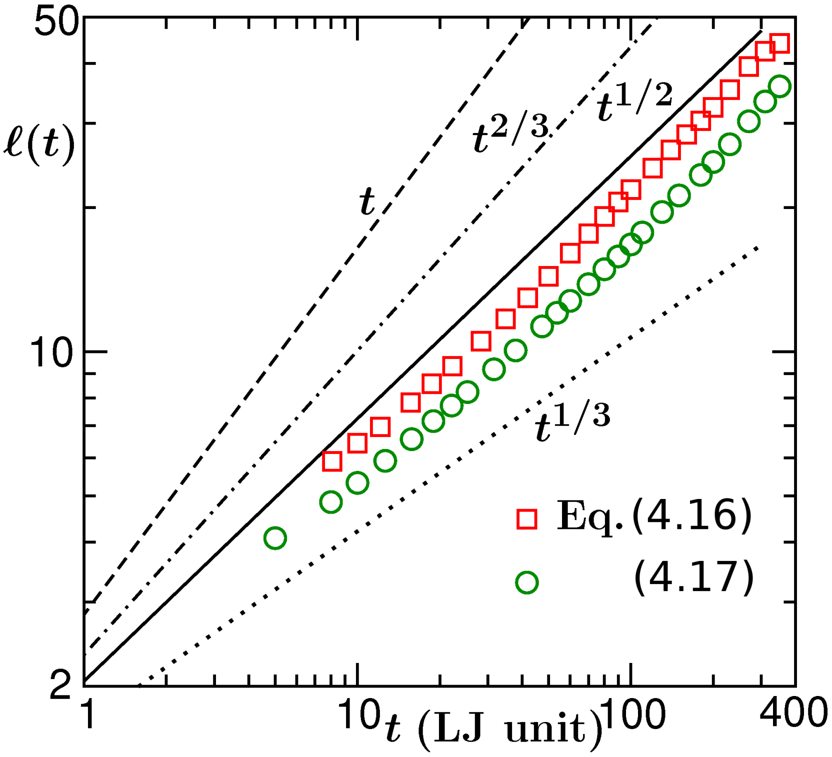

Figure 4.10: Plot of $\ell(t)$ vs t on a log-scale. All data were obtained after removing the noise as described in the text. Here different lines correspond to growth laws $\ell(t) \sim t^{1/3}$, $t^{1/2}$, $t^{2/3}$ and t, as indicated. Two different symbols correspond to calculation from $P(\ell_d, t)$ and $S(k, t)$.

2. While we already have enough evidence for a linear behavior of the time dependence of $\ell(t)$, for the sake of completeness and to further strengthen our claim we take the following route which, in addition to being a nice exercise, could be useful for other complex situations.

In Fig. 4.14 we present a plot of instantaneous exponent α_i calculated as [50]

$$\alpha_i = \frac{d[\ln \ell(t)]}{d[\ln t]}, \tag{4.19}$$

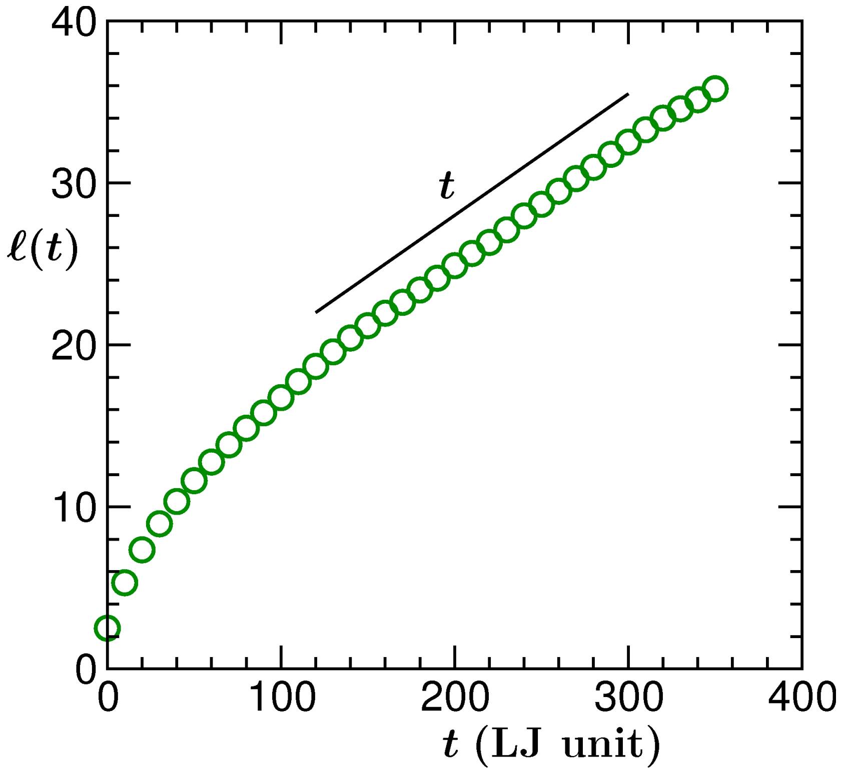

Figure 4.11: Plot of $\ell(t)$ vs t on a linear scale. All data were obtained after removing the noise as described in the text. The solid line corresponds to the expected linear growth in the viscous hydrodynamic regime.

vs $1/\ell(t)$. Due to the off-set (ℓ_0) at $t = 0$, as discussed in the context of Fig. 4.10, α_i is less than unity for the whole range. However it seems to be approaching unity in a non-linear fashion. The dashed line there with an arrow at the end serves as a guide to the eyes. The lower part in this figure represents the corresponding result obtained from MD simulation by using Andersen thermostat (AT) [43]. Due to the stochastic nature of this thermalization algorithm, it is expected that a diffusive growth will be seen for all time and length scales and indeed is seen. There the dashed line has

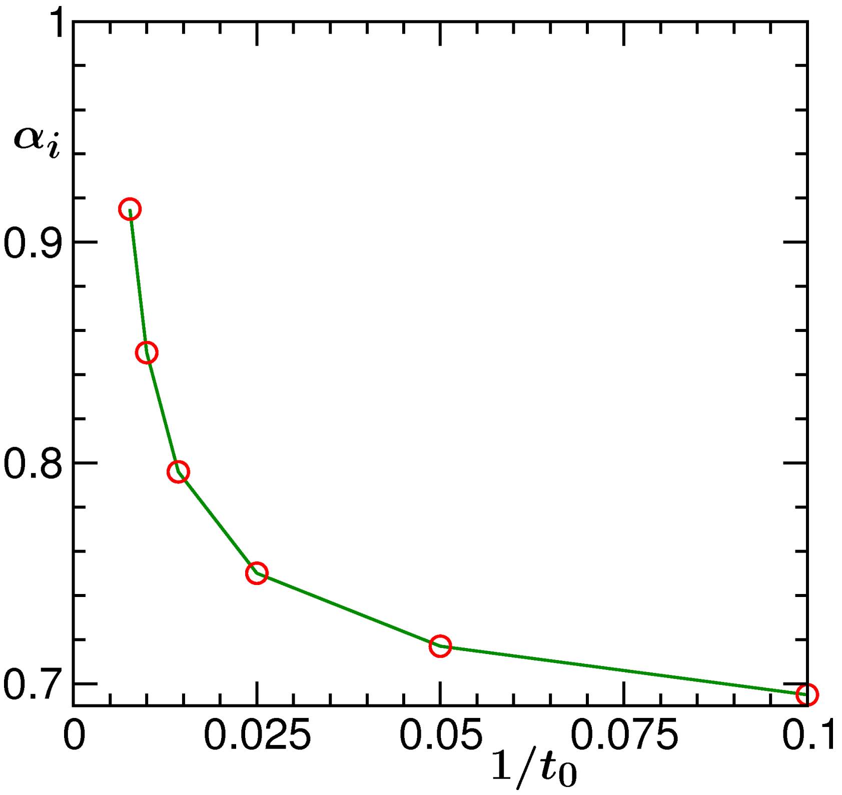

Figure 4.12: Plot of the growth exponent α, as a function of $1/t_0$, obtained by fitting the data in (a) to the form (4.18) in the range [t_0,350].

the form [12]

$$\alpha_i = \frac{1}{3}\left[1 - \frac{\ell_0}{\ell(t)}\right], \tag{4.20}$$

which says that the observation of $\alpha < 1/3$ for finite domain lengths is a mathematical artifact coming due to non-zero value of ℓ_0 and does not necessarily mean that the actual exponent is not $1/3$ at early time. Coming to the point of hydrodynamic preserving capability of NHT, of course, much better thermostats are available these days. However, from the difference seen for the results coming from NHT and AT, it is clear that NHT is preserving

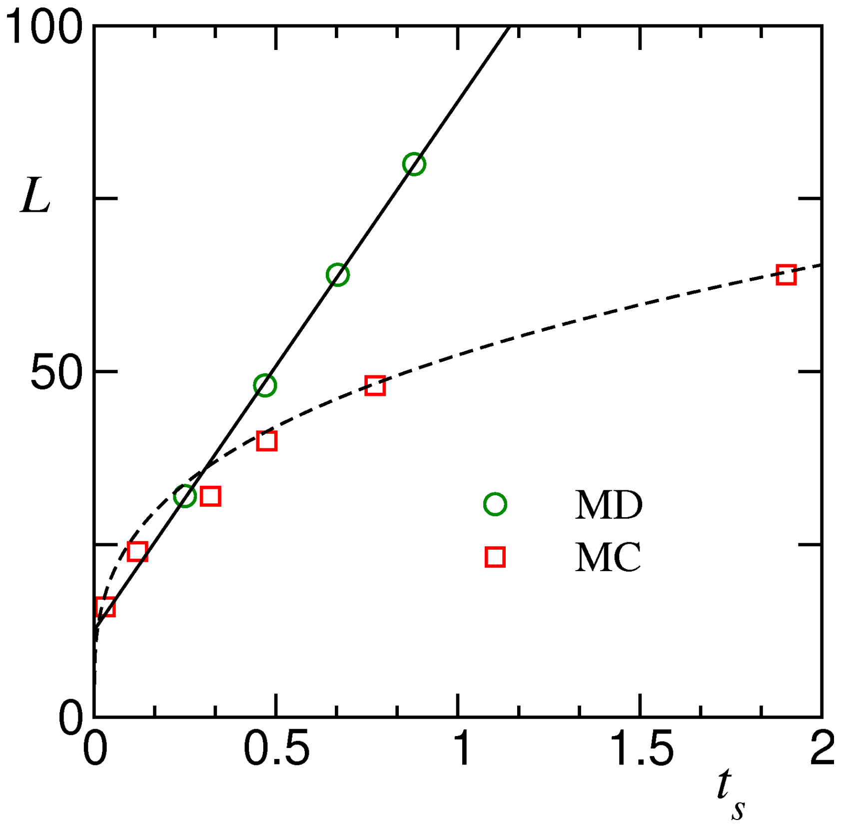

Figure 4.13: Plot of system size L vs saturation time t_s. For MD results, the time is in 10^3 LJ unit while for MC simulation it is in unit of 10^6 Monte Carlo steps.

it rather well. Thus the validity of the methodology adopted in this work is justified.

Note that in Eq. (4.20) ℓ_0 corresponds to the characteristic length scale at the beginning of a scaling regime and not necessarily the length at $t = 0$. In situations where one does not expect multiple scaling regimes (as is the case with AT) ℓ_0 can be nicely estimated from a data-collapse experiment in finite-size scaling analysis [12, 51]. But situation is more complex with NHT due to a crossover to hydrodynamic regime and non-availability of data for different system sizes. However, considering that the crossover, at time t_c,

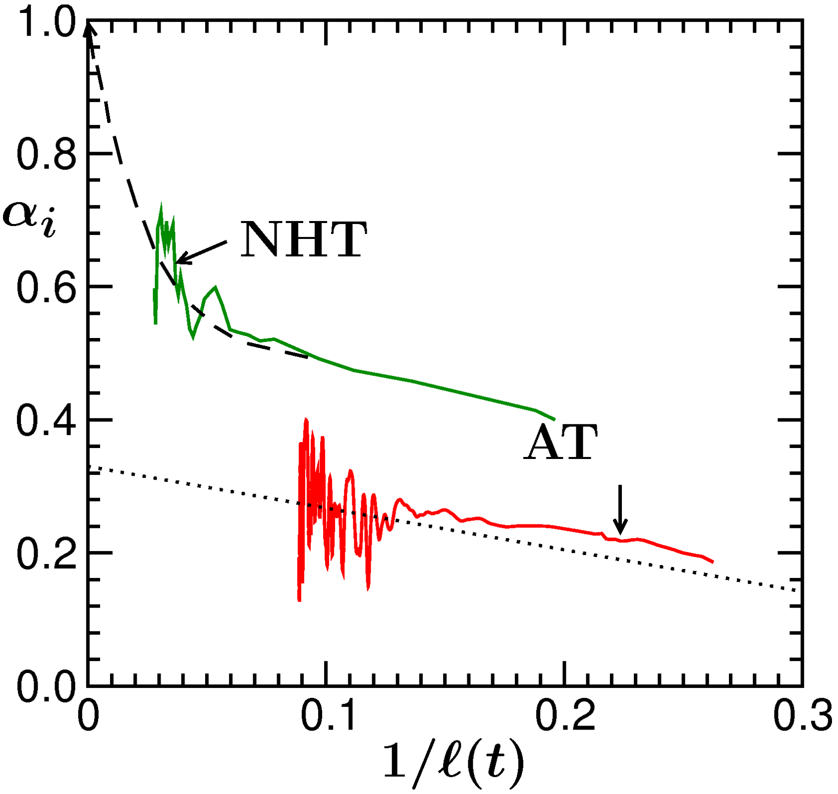

Figure 4.14: Plot of instantaneous exponent α_i vs $1/\ell(t)$. The dashed line is a guide to the eyes, while the dotted line corresponds to Eq. (4.20).

under discussion is to a linear regime, confirmation about it could be obtained by using the following simpler method. To start with, we assume that the growth obeys a power law behavior as a function of the shifted time $t' = t - t_c$ as

$$\ell'(t') = \ell(t) - \ell(t_c) = At'^{\alpha} \tag{4.21}$$

and calculate the instantaneous exponent

$$\alpha_i = \frac{d[\ln \ell'(t')]}{d[\ln t']}. \tag{4.22}$$

Eq. (4.21) is invariant under an arbitrary choice of t_c if we are in a linear

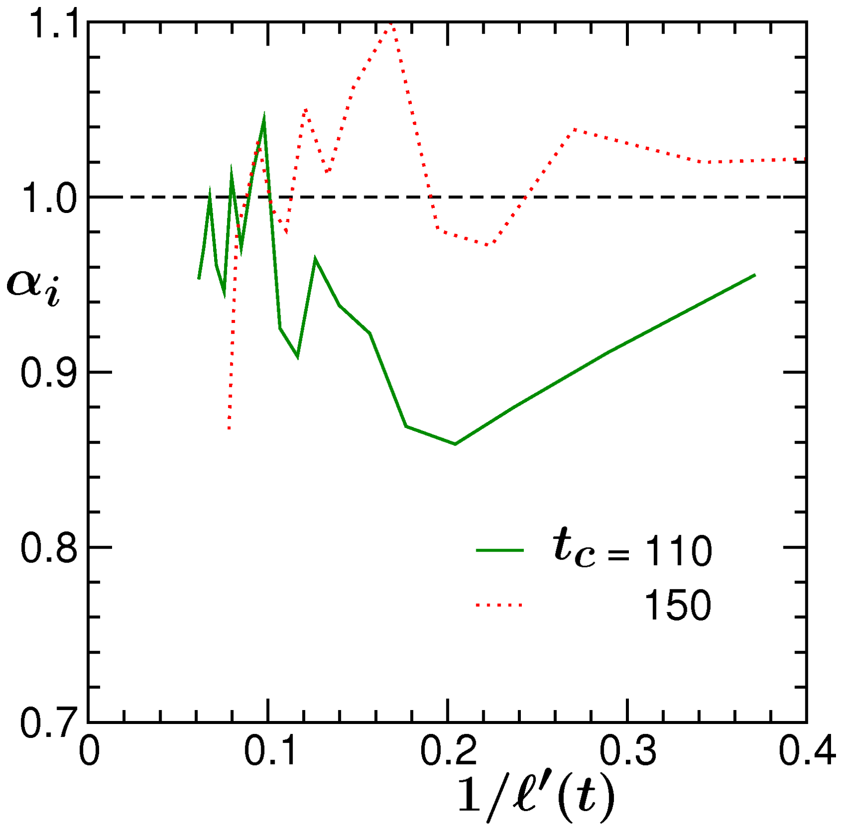

Figure 4.15: Plot of α_i vs $1/\ell'(t')$ for two different values of t_c, as indicated. There the horizontal line represents there the linear hydrodynamic growth.

growth regime and one should obtain a constant value $\alpha_i = 1$ for all choices of t_c in the post crossover regime. In Fig. 4.15, we present α_i for two different choices of t_c. For $t_c > 110$, α_i oscillates around the mean value 1 which is consistent with the viscous hydrodynamic regime. This oscillation of the data presented here, is also observed in other studies [12,27]. In a finite system, at later time only a few domains of comparable size exist which are separated from each other by large distances. Thus, as time increases, it takes longer time for them to merge which causes the exponent to come down. Finally merging of two huge domains after a long interval suddenly enhances the value of the exponent.

4.5 Finite Size Effects

After confirming the viscous hydrodynamic growth for the vapor liquid phase transition, the next task is to investigate the finite-size effect. The scaling analysis in this context will provide additional confirmation about the growth laws. We start the discussion about the finite size effect by showing the length scale plots for different finite system sizes for vapor-liquid phase separation in Fig. 4.16. From the plot it is clearly visible that the data for

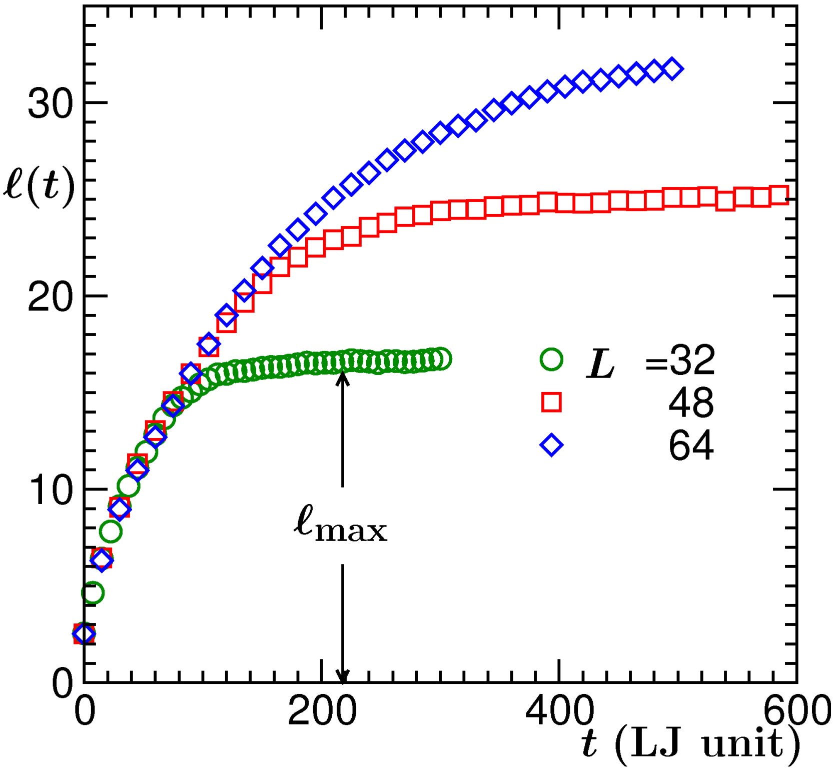

Figure 4.16: Plot of $\ell(t)$ as function of t for different system sizes as indicated. All the results correspond to temperature $T = 0.7$.

a smaller system size is following the data of larger system almost all the way until it attains the equilibrium value of the domain size. This itself is a signature of weak finite-size effect. But to quantify this effect we again called for the finite-size scaling analysis [52]. Let us first discuss it in the context of critical phenomena. Note that, even though the basic concept is same, here it is done in a way different from the one in Chapter 2.

In critical phenomena, the central quantity of interest is the equilibrium correlation length ξ which shows the following singularity at the critical point

$$\xi \approx \xi_0 \epsilon^{-\nu}, \tag{4.23}$$

where $\epsilon = |T - T_c|/T_c$, T_c being a critical temperature. Now let us consider a thermodynamic quantity X showing the singular behavior

$$X \approx X_0 \epsilon^{-x} \tag{4.24}$$

where the x is corresponding critical exponent. At the critical point, the singularity of X, as a function of the system size, is characterized as

$$X = A_0 L^{x/\nu}, \tag{4.25}$$

where $A_0 = X_0/(2\xi_0)^{x/\nu}$ and we have used the fact that $\xi = L/2$ at T_c. Away from T_c, one needs to introduce a scaling function $Y(y)$ to write

$$X = L^{x/\nu} Y(y), \tag{4.26}$$

where y is a function of the dimensionless variable L/ξ. While, $Y(y) = A_0$ at $T = T_c$, for the convenient choice $y = (L/\xi)^{1/\nu}$ ($\propto \epsilon L^{1/\nu}$) and $T \gg T_c$ ($L \gg \xi$), one must have

$$Y(y) \sim y^{-x}, \tag{4.27}$$

so that Eq.(4.24) is recovered. Thus, when $XL^{-x/\nu}$ is plotted vs y, in addition to collapse of data coming from different system sizes, one should obtain a power-law behavior with the exponent $-x$, for $y \gg 0$. A deviation from this power-law, for smaller y, signals the onset of finite-size effects.

In the nonequilibrium domain coarsening problem, a similar finite-size scaling tool could be constructed by making the obvious identification of $1/t$ with ϵ and $\ell(t)$ with ξ. Then the relation equivalent to Eq. (4.26) is

$$\ell(t) = LY(y); \quad y \;=\; (L/\ell)^{1/\alpha} \propto L^{1/\alpha}/t. \tag{4.28}$$

Thus, when $\ell(t)L^{-1}$ is plotted vs y, for large y, a power-law behavior with an exponent $-\alpha$ should be obtained. For the sake of convenience, we demonstrate this first for the $2-d$ Ising model, quenched to the temperature $T = 0.6T_c$.

In Fig. 4.17, we show a trial plot for the scaling behavior contained in Eq. (4.28) where, of course, we have correctly substituted L by the corresponding maximum domain length [see Fig. 4.16], $\ell_{\max}$, that represents the equilibrium limit. We have fixed $\alpha = 1/3$, as expected for diffusive domain growth in Kawasaki-exchange Ising model. Here, very poor quality of data collapse

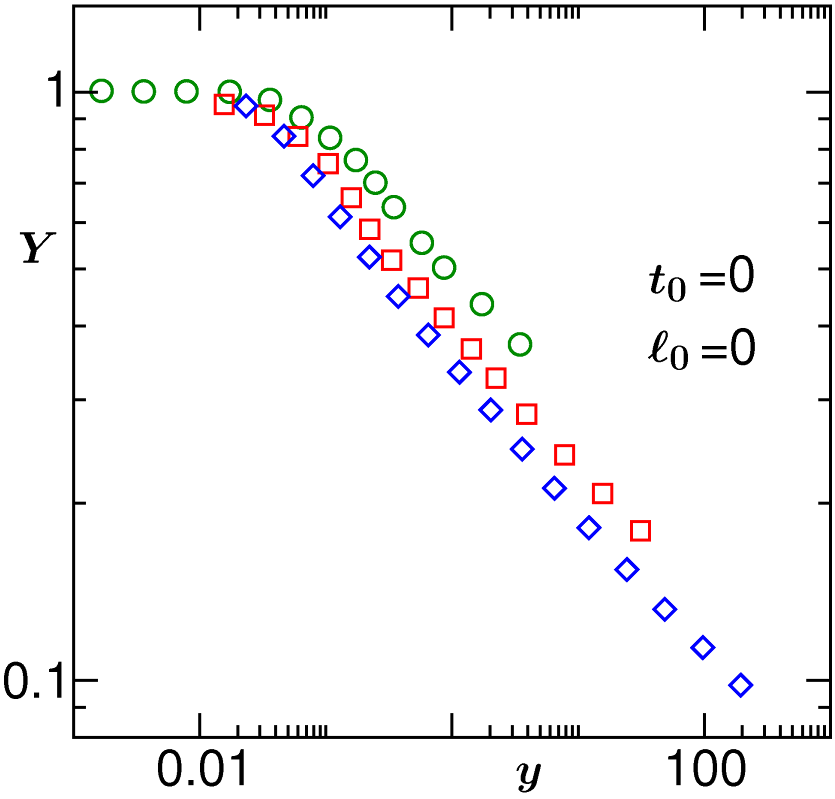

Figure 4.17: Finite-size scaling plot of $\ell(t)$, in accordance with Eq. (4.28) using 3 different system sizes with t_0 set to zero and $\ell_0 = 0$. The results correspond to conserved $2-d$ Ising model at $T = 0.6T_c$.

for large values of y is due to the fact that the systems do not enter the scaling regime immediately. In fact, after the quench the system requires a while to become unstable to fluctuations. Of course, this non-overlapping behavior will not be seen if one has data over many decades in time for a significantly large system. But this will be prominent for small systems. Thus, for a correct analysis, one needs to subtract a time t_0 from t (and corresponding length ℓ_0 from $\ell_{\max}$ as well as $\ell(t)$) to work with only the scaling part. Note that ℓ_0 is independent of time and is analogous to a weakly temperature dependent background contribution in critical phenomena. The

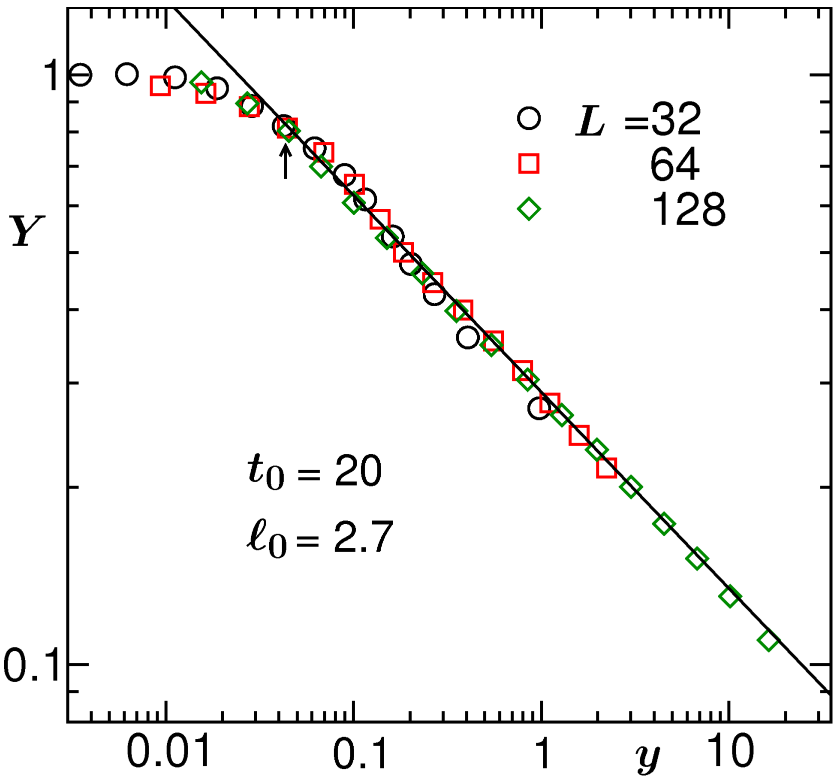

Figure 4.18: Same as Fig. 4.17 but t_0 (thus ℓ_0) was varied to obtain the optimum data collapse. The results correspond to conserved $2-d$ Ising model at $T = 0.6T_c$

correct value of t_0 (and so ℓ_0) must correspond to the optimum data collapse. This is illustrated in the Fig. 4.18 where excellent collapse is obtained for $t_0 = 20$. The solid line there has the form $y^{-\alpha}$ ($\alpha = 1/3$) with which, for $y \gg 0$, the simulation results are perfectly consistent. The point of deviation of the data from this solid line provides us with the information about the onset of finite-size effects at $\ell(t) \simeq 0.77\ell_{\max}$ which is informative of much weaker size effects compared to previous understanding. Now we use the same tool to investigate the size effect in vapor liquid domain coarsening.

In Fig. 4.19, we present the finite scaling plots for the single component

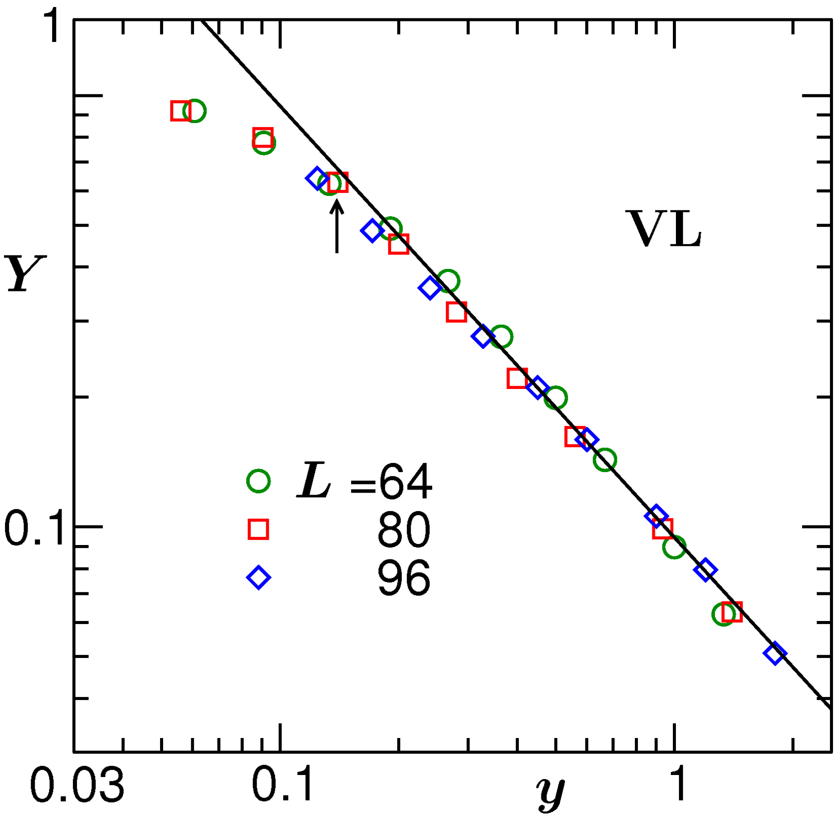

Figure 4.19: Finite-size scaling plots of length scale data for the single component LJ model showing vapor-liquid (VL) transition.

LJ fluid showing vapor liquid phase transition. As discussed, in fluid phase separation a diffusive domain growth is followed by a linear viscous growth and further by an inertial regime with an exponent $\alpha = 2/3$. Due to the obvious difficulty in dealing with significantly large system size for a long time, we are unable to observe the inertial growth. On the other hand, a gradual crossover to the linear regime from very early time does not allow us to observe a pure diffusive domain growth. Thus the focus in this exercise is to obtain a concrete answer for the linear behavior. On this occasion, a perfect data collapse could be obtained when the correct length (ℓ_c) and time (t_c), corresponding to crossover from diffusive to viscous regime, are subtracted. In Fig. 4.19, the best collapse is obtained (by fixing $\alpha = 1$) for $t_c = 50$ and $\ell_c = 12$. The consistency of the master curve with the solid line (y^{-1}) provides further confirmation about the linear behavior. We quantify the appearance of finite-size effects from the point of deviation of the data from the master curve and is appearing to be at $\ell(t) \simeq 0.78\ell_{\max}$. This speaks that the size effect is indeed very weak and is appearing at the same point where it appears for Ising model. Needless to say, the scaling would have failed if we were able to reach the inertial hydrodynamic regime by running a much bigger system for significantly longer period of time.

4.6 Conclusion

In conjunction with the phase behavior, we have presented results for the kinetics of vapor-liquid phase-separation from the molecular dynamics (MD) simulation of a simple Lennard-Jones fluid using both Andersen (AT) and Nosé-Hoover (NHT) thermostats. It is observed that NHT is reasonably useful for studying hydrodynamic effects in the fluid phase separation. A brief period of diffusive coarsening was followed by a linear viscous hydrodynamic growth. Our results are in contradiction with few previous MD studies which reported an exponent much less than unity, however, is consistent with the results of binary fluid phase separation. One requires much larger system size to observe the inertial hydrodynamic growth. This we leave out for a future exercise, in addition to the study of coarsening of liquid droplets for off-critical quench. For the latter problem one expects single asymptotic exponent 1/3 from droplet diffusion-coagulation mechanism [25,53]. Also, as discussed, MD with AT and a Monte Carlo simulation of the same system will provide a single diffusive 1/3 growth for all compositions. For off-critical composition the latter exercise should be able to provide information on the curvature dependent inter-facial tension which is expected to bring in early-time correction in the LS law. This will certainly be interesting to compare with the corresponding results obtained from equilibrium studies [54]. Lastly, we have quantified finite-size effects in kinetics of phase separation in solid binary mixtures as well as in vapor-liquid systems. It appears that the size effects are weak and universal.

Bibliography

[1] A.J. Bray, Adv. Phys. **51**, 481 (2002).

[2] K. Binder, in *Phase transformation of Materials*, Vol.**5**, p.405, R.W. Cahn, P. Haasen, E.J. Kramer (Eds.), (VCH, Weinheim) 1991.

[3] S. Puri, V. Wadhawan (Eds.), *Kinetics of Phase Transitions* (CRC Press, Boca Raton, 2009).

[4] R.A.L. Jones, *Soft Condensed Matter* (Oxford University Press, Oxford, 2008).

[5] S.K. Das, S. Puri, J. Horbach, K. Binder, Phys. Rev. E **72**, 061603 (2005).

[6] S.K. Das, S. Puri, J. Horbach, K. Binder, Phys. Rev. Lett. **96**, 016107 (2006).

[7] S.K. Das, S. Puri, J. Horbach, K. Binder, Phys. Rev. E **73**, 031604 (2006).

[8] S.J. Mitchell, D.P. Landau, Phys. Rev. Lett. **97**, 025701 (2006).

[9] K. Bucior, L. Yelash, K. Binder, Phys. Rev. E **77**, 051602 (2008).

[10] K. Bucior, L. Yelash, K. Binder, Phys. Rev. E **79**, 031604 (2009).

[11] M.J.A. Hore, M. Laradji, J. Chem. Phys. **132**, 024908 (2010).

[12] S. Majumder, S.K. Das, Phys. Rev. E **81**, 050102 (2010).

[13] V.M. Kendon, M.E. Cates, I. Pagonabaragga, J.C. Desplat, P. Blandon, J. Fluid Mech. **440**, 147 (2001).

[14] A.K. Thakre, W.K. den Otter, W.J. Briels, Phys. Rev. E **77**, 011503 (2008).

[15] H. Kabrede, R. Hentschke, Physica A. **361**, 485 (2006).

[16] S.K. Das, S. Puri, Phys. Rev. E **65**, 026141 (2002).

[17] N. Blondiaux, S. Morgenthaler, R. Pugin, N.D. Spencer, M. Liley, Appl. Surf. Sci. **254**, 6820 (2008).

[18] J. Liu, X. Wu, W.N. Lennard, D. Landheer, Phys. Rev. B **80**, R041403 (2009).

[19] S. Ahmad, S.K. Das, S. Puri, Phys. Rev. E **82**, 040107 (2010).

[20] A. Sicilia, Y. Sarrazin, J.J. Arenzon, A.J. Bray, L.F. Cugliandolo, Phys. Rev. E **80**, 031121 (2009).

[21] R. Khanna, N.K. Agnihotri, M. Vashisgtha, A. Sharma, P.K. Jaiswal, S. Puri, Phys. Rev. E. **82**, 011601 (2010).

[22] E. Lippilioe, A. Mukherjee, S. Puri, M. Zannetti, EPL **90**, 46006 (2010).

[23] S. Majumder and S.K. Das, Europhys. Lett. **95**, 46002 (2011).

[24] S.K.Das, S. Roy, S. Majumder and S. Ahmad Europhys. Lett. **97**, 66006 (2012).

[25] K. Binder, D. Stauffer, Phys. Rev. Lett. **33**, 1006 (1974).

[26] I.M. Lifshitz, V.V. Slyozov, J. Phys. Chem. Solids **19**, 35 (1961).

[27] A. Shinozaki, Y. Oono, Phys. Rev. E **48**, 2622 (1993).

[28] S. Puri, B. Dünweg, Phys. Rev. A **45**, R6977 (1991).

[29] W.J. Ma, A. Maritan, J.R. Banavar, J. Koplik, Phys. Rev. A **45**, R5347 (1992).

[30] M. Laradji, S. Toxvaerd, O.G. Mouritsen, Phys. Rev. Lett. **77**, 2253 (1996).

[31] E.D. Siggia, Phys. Rev. A **20**, 595 (1979).

[32] H. Furukawa, Phys. Rev. A **31**, 1103 (1985).

[33] H. Furukawa, Phys. Rev. A **36**, 2288 (1987).

[34] A. Onuki, *Phase Transition Dynamics* (Cambridge University Press, Cambridge, 2002).

[35] Y.C. Chou, W.I. Goldburg, Phys. Rev. A **20**, 2105 (1979).

[36] N.C. Wong, C.M. Knobler, Phys. Rev. A **24**, 3205 (1981).

[37] F.S. Bates, P. Wiltzius, J. Chem. Phys. **91**, 3258 (1989).

[38] F.F. Abraham, *Phys. Rep.* **53**, (1979) 93.

[39] M. Schöbinger, S.W. Koch, F.F. Abraham J. Stat. Phys. **42**, 1071 (1986).

[40] R. Yamamoto, K. Nakanishi, Phys. Rev. B **49**, 14958 (1994).

[41] R. Yamamoto, K. Nakanishi, Phys. Rev. B **51**, 2715 (1995).

[42] M.P. Allen, D.J. Tildesley, *Computer Simulations of Liquids* (Clarendon, Oxford, 1987).

[43] D. Frenkel, B. Smit, *Understanding Molecular Simulations:From Algorithm to Applications* (Academic Press, San Diego, 2002).

[44] B. Smit, J. Chem. Phys. **96**, 8639 (1992).

[45] S.K. Das, J. Horbach, K. Binder, J. Chem. Phys. **119**, 1547 (2003).

[46] S. Roy, S.K. Das, Europhys. Lett. 94, 36001 (2011).

[47] S.K. Das, M.E. Fisher, J.V. Sengers, J. Horbach, K. Binder, Phys. Rev. Lett. **97**, 025702 (2006).

[48] G. Porod, in *Small-Angle X-Ray Scattering*, O. Glatter, O. Kratky (Eds.), (Academic Press, New York 1982).

[49] Y. Oono, S. Puri, Mod. Phys. Lett. B **2**, 861 (1988).

[50] D.A. Huse, Phys. Rev. B **34**, 7845 (1986).

[51] S. Majumder, S.K. Das, Phys. Rev. E **84**, 061607 (2011).

[52] M.E. Fisher, in *Critical Phenomena*, edited by M.S. Green (Academic, London, 1971) p1.

[53] K. Binder, Phys. Rev. B **15**, 4425 (1977).

[54] B.J. Block, S.K. Das, M. Oettel, P. Virnau, K. Binder, J. Chem. Phys. **133**, 154702 (2010).

Chapter 5

Aging in Phase Ordering Systems: Conserved vs nonconserved order-parameter dynamics

5.1 Introduction

Study of aging phenomena is crucial to the understanding of dynamics in a variety of important physical situations [1] and are of much interest both theoretically and experimentally [2–9]. Glass transition dynamics, nonequilibrium dynamics related to phase transitions in systems of various types, e.g., phase separating binary mixtures, magnetic systems exhibiting para- to ferro-magnetic transition, etc., are some interesting candidates, among others. Aging processes are crucial to many applications that include biological systems [1, 4, 5]. Typically, to probe such aspect of dynamics [1, 10, 11], one uses the auto-correlation function

$$C(t, t_w) = \langle \psi(\vec{r}, t)\psi(\vec{r}, t_w)\rangle - \langle \psi(\vec{r}, t)\rangle\langle \psi(\vec{r}, t_w)\rangle, \tag{5.1}$$

where t and t_w are respectively the observation and waiting times and $\psi(\vec{r}, t)$ is the space ($\vec{r}$) and time dependent order parameter. In equilibrium phenomena there is time translational invariance of this two-time quantity with respect to the choice of t_w and this fact allows one to improve statistics by time averaging. In nonequilibrium systems, however, decay of such correlations becomes slower with the growing age of the system, i.e, with the increase of t_w, leading to nontrivial phenomena. There, an appropriate question to ask is the scaling form of $C(t, t_w)$ in terms of the time-dependent characteristic length scales, say, average domain size $\ell(t)$ of up and down spins in a ferromagnet, as the system tries to attain equilibrium following the phase transitions. Note that $\ell(t)$, a single time quantity, often grows in a power law manner [12–15],

$$\ell(t) \sim t^{\alpha}. \tag{5.2}$$

Kinetics involving single time quantities in both phase separating systems and systems exhibiting ferromagnetic ordering have been extensively studied. A primary difference between these two types is that the dynamics in the former respects the conservation of order parameter while the latter does not. Nevertheless, there are significant similarities in the nonequilibrium dynamics of the two cases even though they form two different universality classes [12, 14]. On the other hand, the situation with respect to the two-time quantities is unsatisfactory despite some preliminary understanding of the scaling behavior of $C(t, t_w)$ obtained analytically and computationally [1, 16, 17]. The results obtained there in various space dimensions (d) are seen to be in agreement with the prediction of power-law decay of $C(t, t_w)$, made in the context of spin glasses [11], despite disagreement in the value of the exponent. Furthermore, aging in conserved systems did not catch significant attention, perhaps because of the difficulty, with respect to the single time quantities, that had been faced relative to the non-conserved systems to understand the rich physics in the former.

Note that in case of a ferromagnet the growth of $\ell(t)$ is characterized by a single asymptotic exponent $\alpha = 1/2$, referred to as the Lifshitz-Cahn-Allen (LCA) law [12,14]. On the other hand, the situation is much complex for conserved systems. There the value of the exponent can be significantly modified by the presence or absence of hydrodynamic effects [12,14,18–23]. In solid binary mixtures, of course, one observes a single exponent $\alpha = 1/3$, due to the diffusive mechanism, referred to as the Lifshitz-Slyozov (LS) law [12–15, 24]. More interesting cases, however, are those when $\ell(t)$ exhibits crossover(s) from one power-law exponent (α) to another or to entirely different functional form. Phase separation in fluids is an ideal example of that. It needs to be seen if the prediction about the power-law decay of $C(t, t_w)$ holds even in conserved ordering dynamics, including fluids where one has rapid time fluctuation of density variable, as is well known from the hydrodynamics of simple liquids in equilibrium [25]. Indeed, hydrodynamics is expected to play crucial role at late stages of nonequilibrium growth as well and a crossover from the diffusive LS behavior to a regime with much larger value of the exponent ($\alpha = 1$), referred to as the viscous hydrodynamic regime [12], should be observed. It is, of course, more challenging and of much general interest to understand the effect of such crossovers on the two-time quantities such as the correlation function under discussion.

In this chapter, we report results related to the decay of $C(t, t_w)$ in conserved systems in $d = 3$, with particular emphasis on fluid phase transitions. Two systems in this category are studied, a solid binary mixture and a vapor-liquid system. The results obtained from these systems are also compared with the non-conserved case. We make crucial general observation that as a function of $x = \ell(t)/\ell(t_w)$, the behavior of $C(t, t_w)$ can be classified into two scaling forms. Namely, in absence of hydrodynamics

$$C(t, t_w) \sim x^{-\lambda}, \tag{5.3}$$

while in presence of hydrodynamics

$$C(t, t_w) \sim e^{-ax}. \tag{5.4}$$

Even though the value of the exponent λ obeys the bound $\frac{d}{2} \leq \lambda \leq d$, predicted by Fisher and Huse (FH) [11], they are different for conserved and non-conserved systems. Theoretical insight for the understanding of the exponential decay has been discussed.

5.2 Models and Methods

For our study in fluids, we adopted a model [21] where particles of equal mass (m), separated by distance r, in a periodic cubic box of linear dimension L (in units of particle diameter σ), interact via

$$u(r) = U(r) - U(r_c) - (r - r_c)\left(\frac{dU}{dr}\right)_{r=r_c}, \tag{5.5}$$

for $r \leq r_c$. In Eq. (5.5), $U(r)$ is the standard Lennard-Jones (LJ) pair potential with interaction strength ϵ. The cut-off distance $r_c(= 2.5\sigma)$ was introduced for faster computation. The last term in Eq. (5.5) removes the discontinuity in the force after shifting of the LJ potential to 0 at $r = r_c$ [26]. This model exhibits a vapor-liquid phase transition with a critical temperature $T_c \simeq 0.9\epsilon/k_B$ and a critical density $\rho_c(\equiv \frac{N\sigma^3}{L^3})\simeq 0.3$, N being the number of particles [23]. For the sake of convenience, in the rest of the chapter we set m, ϵ, σ and k_B to unity.

We have performed molecular dynamics (MD) [26,27] simulations to study aging in this model. To incorporate the hydrodynamic effects in the kinetics of phase transition, we have have used a Nosé-Hoover thermostat [27] to control the temperature. In the MD simulations, the Newton's equations of motion were solved by applying Verlet velocity algorithm with a time step $\Delta t = 0.005$ in units of $\tau = (\frac{m\sigma^2}{\epsilon})^{1/2}$. Systems with homogeneous density at the critical value were prepared at a very high temperature which was then quenched below T_c to study the far-from-equilibrium dynamics.

To make a comparison of our fluid results with those of solid binary mixture and ferromagnetic growth we have performed Monte Carlo (MC) simulations [28] of the Ising model

$$H = -J \sum_{<ij>} S_i S_j;\ \ S_i = \pm 1;\ \ J > 0. \tag{5.6}$$

In case of binary solid phase separation, to conserve the order parameter, we have implemented the standard Kawasaki exchange kinetics [28]. On the other hand, Glauber spin flip kinetics [28] was employed to study the nonequilibrium dynamics in ferromagnets. In both these cases time is presented in units of Monte Carlo steps (MCS). Note that, unless otherwise mentioned, results correspond to the MD simulations of vapor-liquid transition.

5.3 Results

In Fig. 5.1, we show the evolution snapshots from four different times after quenching a homogeneous fluid system of critical density to $T = 0.6$. Growth of the interconnected high (liquid) and low (vapor) density domains is quite clear from these snapshots. Note that in Ising systems spin is the variable analogous to density [14]. To quantify the growth of Fig. 5.1, in Fig. 5.2, we have plotted the average size, $\ell(t)$, of liquid and vapor domains, against t, on a linear scale, for two temperatures. Note that to facilitate the calculation of this and other observables in fluid systems, the snapshots were mapped onto Ising like lattice systems where a site containing a particle was assigned a spin or order-parameter value $+1$ and a vacant site was given a value -1 [21]. Then the values of $\ell(t)$ were obtained from the first moment

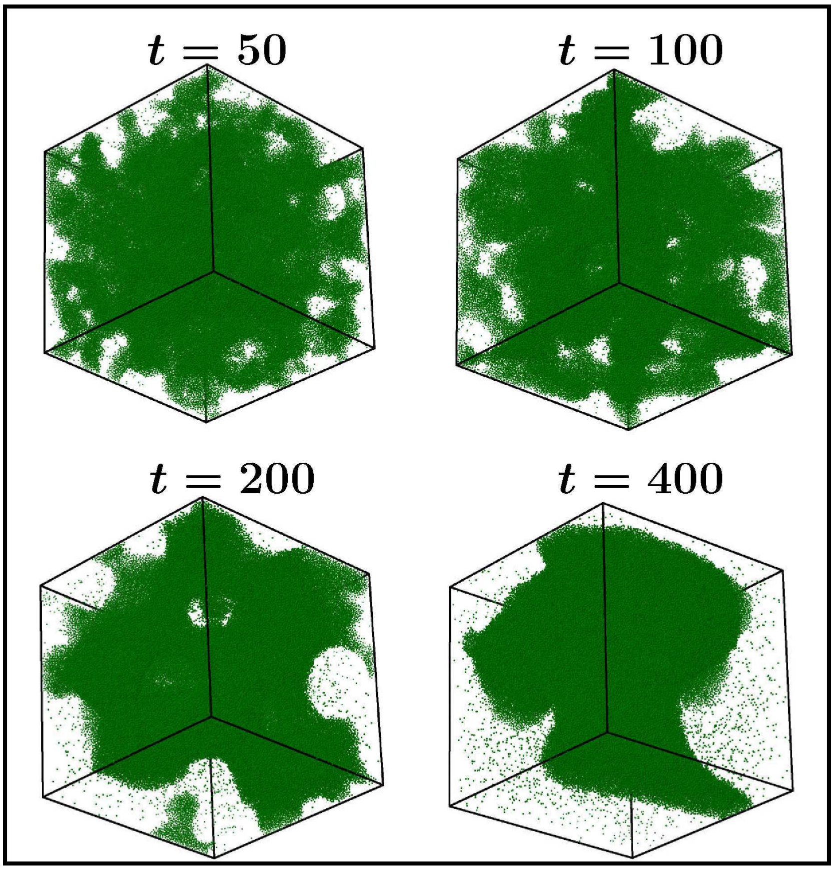

Figure 5.1: Snapshots from four different times during the evolution of a phase separating fluid system, starting from homogeneous initial configuration, for $L = 96$, upon quenching it to a temperature $T = 0.6 (\simeq 0.67T_c)$. The system has an overall density $\rho = 0.3 (\simeq \rho_c)$.

of the domain size distribution function $P(\ell_d, t)$ where ℓ_d is the distance between two successive domain boundaries in $x-$, $y-$, or $z-$ directions. The solid line in Fig. 5.2 acts as a guide to visualize the linear behavior of the late time data for $T = 0.7$. It should be appreciated that after an initial brief period of slow (diffusive) growth it crosses over to a linear regime consistent with the viscous hydrodynamic growth. However, at the higher temperature ($T = 0.8$), the diffusive regime extends over a relatively longer length of time.

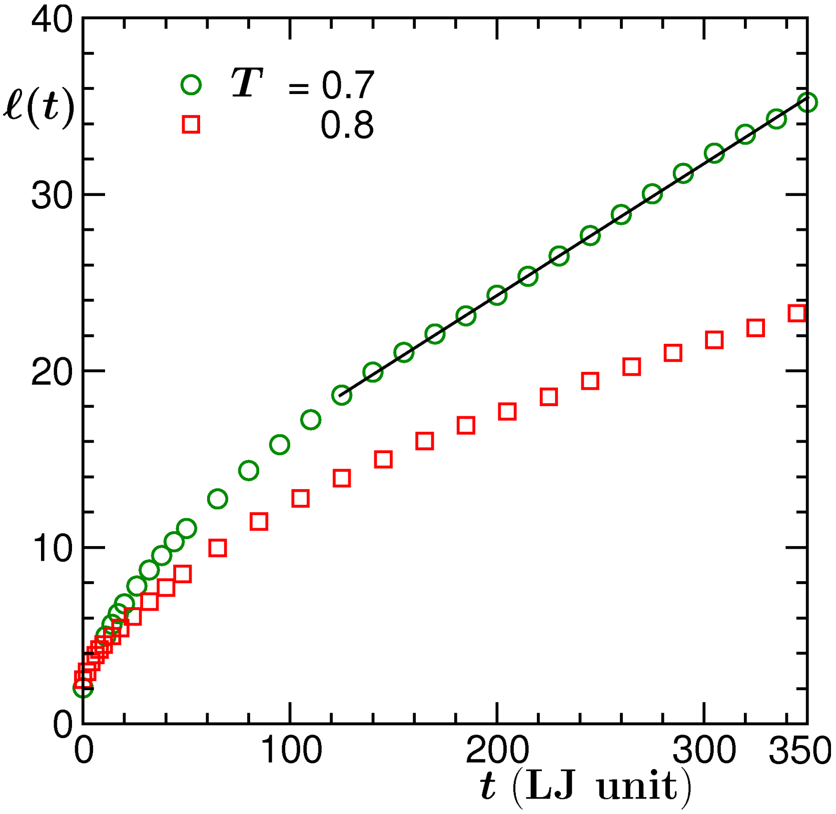

Figure 5.2: Plot of average domain size, $\ell(t)$, as a function of time for two different temperatures as indicated. The dashed straight line there is a guide to the eyes. All the results are with $L = 96$ for fluid systems. The method of estimation of $\ell(t)$ is described in the text.

Here we emphasize that the hydrodynamic effect is mixed with diffusive domain growth from very early time. Thus, to clearly confirm the LS value for the diffusive growth one needs to choose temperature very close to the critical value. However, because of mixing of the diverging correlation length with domain length it becomes challenging to analyze results in the neighborhood of criticality. On the other hand, while a fast growth due to hydrodynamics, at the presented temperatures, can be appreciated from these direct plots, for an unambiguous confirmation of viscous hydrodynamic growth ($\alpha = 1$), we refer the readers to Ref. [21]. Having presented the results on the characteristic lengths and discussion on the possible growth laws, we focus on the two-time quantity, viz., $C(t, t_w)$. As already pointed out, our primary objective in this chapter is to identify the scaling behavior of $C(t, t_w)$ in a rather general context and to learn how the crossover in single time quantity affects its behavior, in particular, the effect of fast hydrodynamic mechanism in the decay of $C(t, t_w)$.

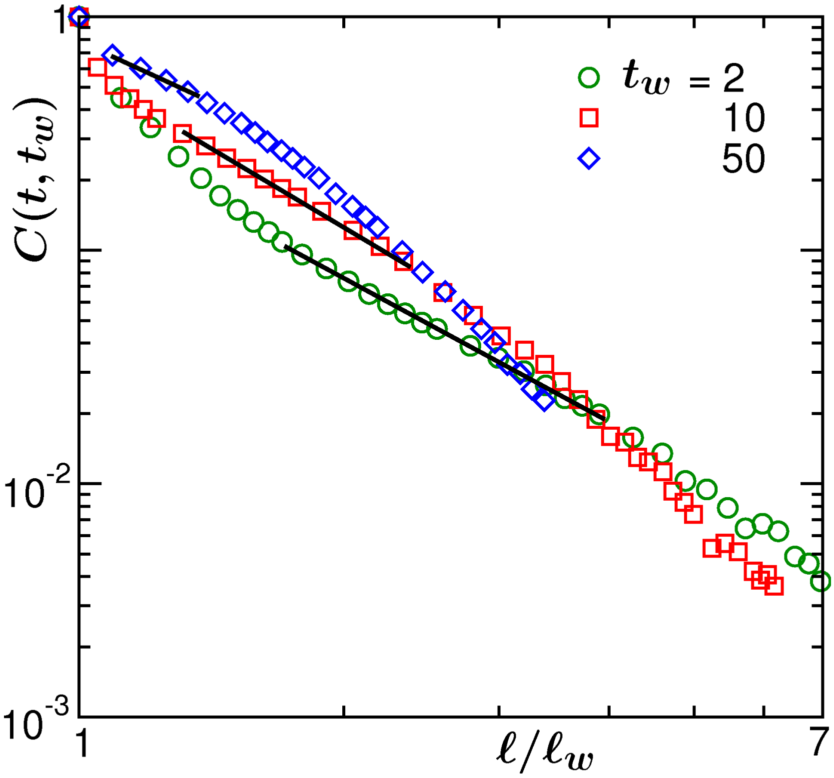

Figure 5.3: Log-log plots of $C(t, t_w)$, for the fluid case as a function of ℓ/ℓ_w for different values of the waiting time t_w, as indicated on the figure. The results are presented from systems of size $L = 96$ after averaging over 5 independent initial configurations at $T = 0.8$. The solid lines there are guides to eye to recognize the power-law decay.

In Fig. 5.3, we present $C(t, t_w)$ as a function of ℓ/ℓ_w on a log-log plot.

Results are shown for a number of different choices of t_w. All results for $C(t, t_w)$ are presented after normalizing its value at $t/t_w = 1$ to unity. Clearly, no collapse of data for different values of t_w is observed. This is due to the fact that for smaller values of t_w the domain magnetization did not reach its equilibrium value yet. But presentation of results for only larger values of t_w is uncalled for because of the fact that the early time diffusive regime will then be invisible. Important observations from these plots are the following. There is a power-law behavior at early time and the range of this power-law behavior (identified by the straight lines passing through the relevant data points) gets shorter with the increase of t_w. This latter fact, as already pointed out, is

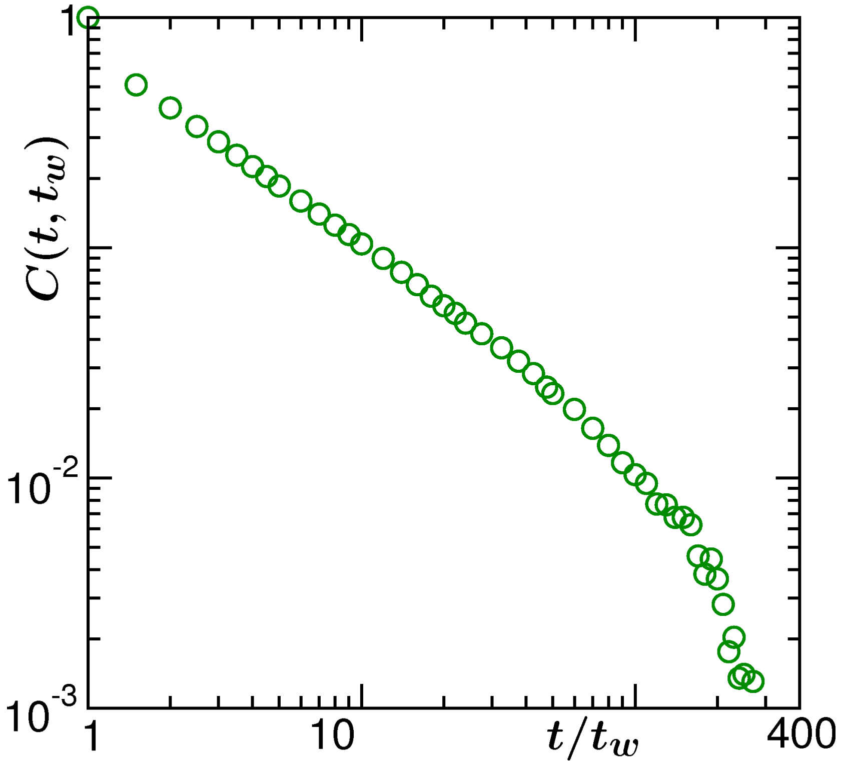

Figure 5.4: Plot of $C(t, t_w)$ vs t/t_w for the same system as in Fig. 5.3, only for $t_w = 2$, on a double-log scale.

because, with the increase of t_w, one gets closer to the strong hydrodynamic regime. While this power-law decay is consistent with the prediction of FH, the apparent crossover to a much faster decay is very interesting. Fig. 5.4 shows the plot of $C(t, t_w)$ for the same system as in Fig. 5.3, for $t_w = 2$, as a function of t/t_w. There also it is quite evident that a faster non-algebraic growth is in place at late time. The objective of this work is to obtain a deeper understanding of this whole phenomena.

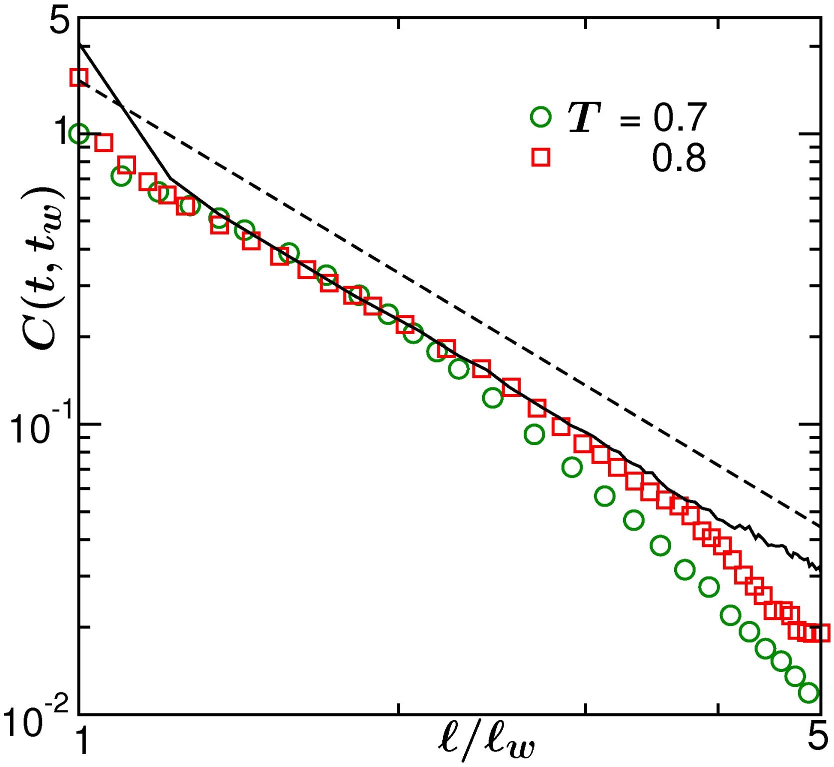

Figure 5.5: Log-log plots of $C(t, t_w)$ vs ℓ/ℓ_w for fluid, from two different temperatures, as indicated, for $t_w = 10$. The continuous curve there is a corresponding plot for conserved Ising model at $T = 0.6T_c$, for $L = 64$ and $t_w = 10$. The dashed line has a power-law exponent -2.2. Results from different temperatures are multiplied by numerical factors to obtain collapse in the power-law regime.

In Fig. 5.5, we show $C(t, t_w)$ as a function of ℓ/ℓ_w, again on a log-log plot. This time, instead of different values of ℓ_w at the same temperature, we present results for different temperatures. The qualitative behavior of the numerical results is the same as that in Fig. 5.3, viz., for smaller values of ℓ/ℓ_w there is power law behavior which deviates with the increase of ℓ/ℓ_w. The deviation occurs earlier for lower temperature and is consistent with the fact of Fig. 5.2 that a crossover to the hydrodynamic regime gets delayed with the increase of temperature. Here, the results from different temperatures were multiplied by numerical factors to obtain data collapse in the power-law regime. The apparent mismatch, without these numerical factors, is due to different equilibrium order-parameter values at different temperatures. Considering this fact, these numbers should scale as [14] m^{-2} or $(T_c - T)^{-2\beta}$, $\beta(= 0.325$ for Ising universality class) being the equilibrium critical exponent for magnetization (m). This is demonstrated in Fig. 5.6.

In Fig. 5.5, in addition to the fluid results, we have also presented result from the conserved Ising model. The fluid auto-correlation is nicely consistent with the latter at early time. At late time, while the Ising one continues to decay in the power law fashion, the fluid correlations deviate, as already pointed out, towards an exponential behavior. This is interesting that even in fluids, though at early time, these two time quantities follow power-law, particularly with the same exponent as the solid binary mixture. This, of course, confirms the dominance of simple diffusion over hydrodynamics in this regime. The dashed line in this figure has an exponent -2.2 which is consistent with FH bound [11]. Here some discussion about the theoretical prediction of λ should be in place.

The bounds were obtained via the following arguments [11,16]. A domain

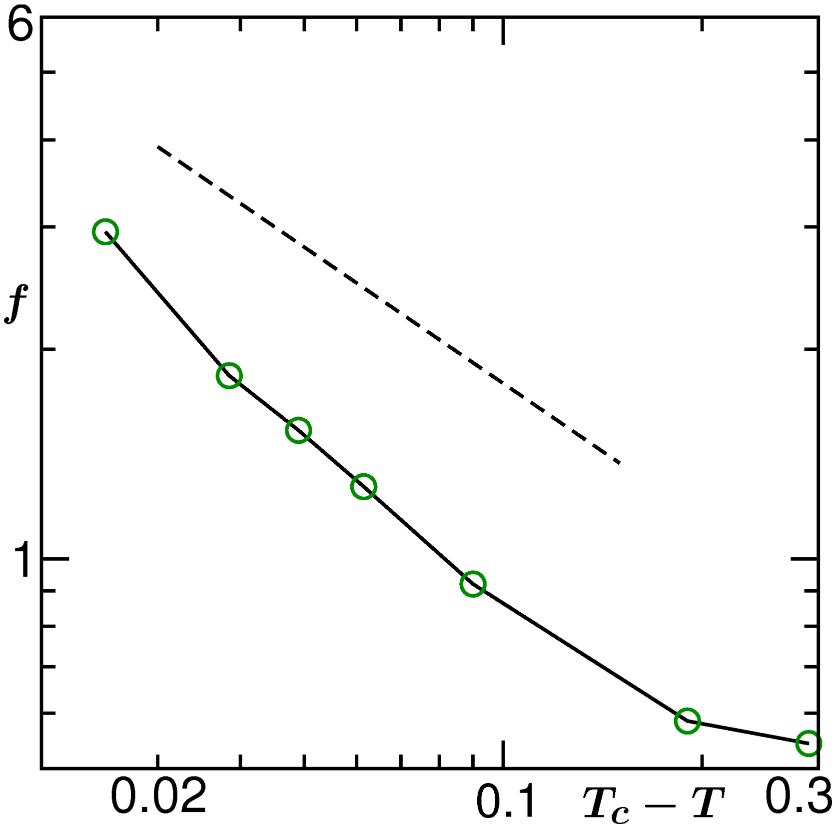

Figure 5.6: Plot of the numerical factors needed to obtain data collapse in the power-law regime of data from different temperatures, as a function of $(T_c - T)$, on double log scale. The dashed line there, has a slope of $-\beta$, with $\beta = 0.325$.

of size ℓ consisting of only one type of spin has grown to this pure domain starting from a situation at early time when only random values of spins did exist. Applying the central limit theorem to the early time scenario, one obtains the magnetization per unit volume to be $\sim \ell^{-d/2}$, multiplication of which with the value unity at the later time will provide the lower bound $d/2$. On the other hand, consideration of the fact that the bias, that gave rise to the magnetization $\ell^{-d/2}$, does not completely go away at late time, provides the upper bound. Further, Liu and Mazenko used dynamical equations for

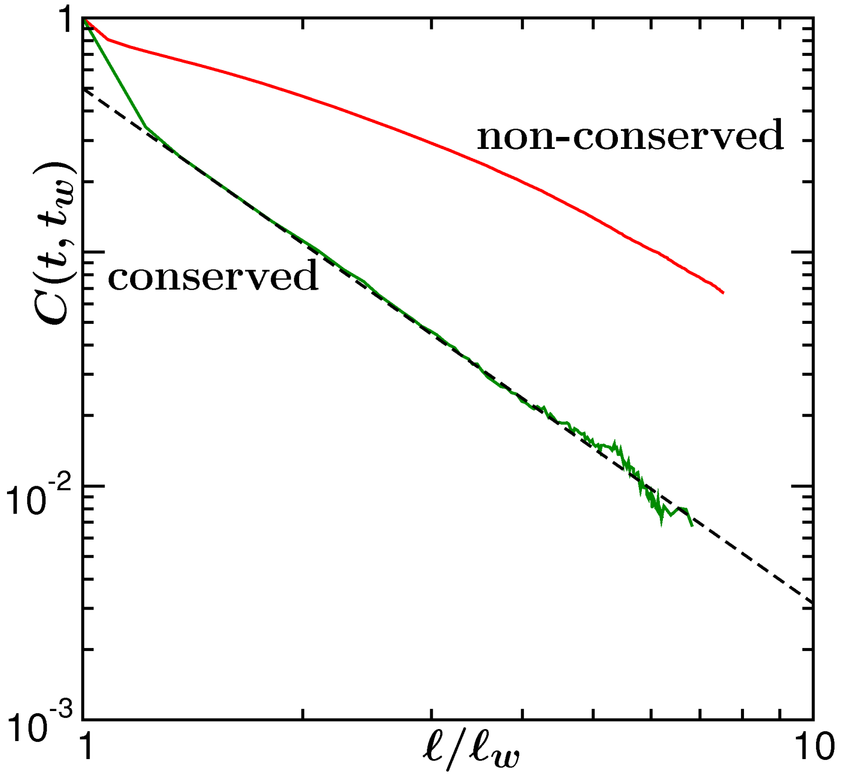

Figure 5.7: Log-log plots of $C(t, t_w)$ vs ℓ/ℓ_w for conserved and non-conserved 3-d Ising model at $T = 0.6T_c$. For the conserved case result was obtained from systems with linear dimension $L = 64$ while for the nonconserved case the dimension is $L = 150$. In both the cases the value of t_w was set to be 10. The dashed line there has a slope of -2.2.

correlation functions, via Gaussian auxiliary field ansatz, to calculate the value of λ. In $d = 3$, their calculation predicted $\lambda = 1.675$. This and the existing reliable computer simulations [16, 29] are involving non-conserved order parameter (to the best of our knowledge) in Ising or Cell Dynamical System (CDS) models [30]. It will be then interesting to make a comparison between the conserved and non-conserved dynamics.

In Fig. 5.7, we compare the results from the MC simulations of conserved and non-conserved Ising model dynamics. For the conserved case, from the

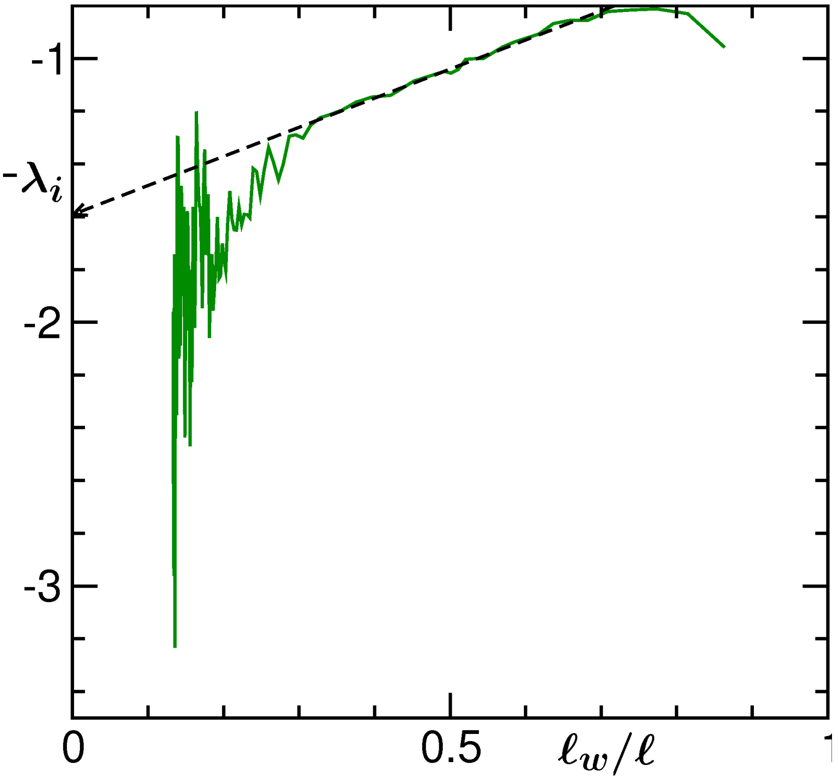

Figure 5.8: Plot of instantaneous exponent λ_i vs ℓ_w/ℓ, for the decay of non-conserved autocorrelation function.

double-log plot, as already seen, it is quite clear that $C(t,t_w)$ decays in a power-law manner from the very beginning till the extended time regime with $\lambda = 2.2$. In contrary, there is continuous change of slope in the non-conserved case which is consistent with the $2-d$ results [1]. Liu and Mazenko [16] quoted the asymptotic ($t \to \infty$) value of the exponent from the CDS model to be 1.835. In Fig. 5.8, we have presented the instantaneous exponent, λ_i, as a function of ℓ_w/ℓ, for the non-conserved case. For an early period of time, the results show convergence (as depicted by the dashed line with an arrow head) to the value 1.6 which is consistent with the theoretical prediction of Liu and Mazenko but differs from the value obtained by them from the CDS model simulation. On the other hand, for length beyond $\ell \simeq 30$, the data show a different trend. Note that the system size chosen here is large enough ($L = 150$). From our experience of finite-size effects with conserved systems [22], we do not think that this is due to any such artificial effect. If, however, we consider data at late time for an extrapolation, there is consistency of the asymptotic exponent with the conserved Ising model. In future we will clarify this point in greater detail. Having pointed out these important differences between the conserved and non-conserved dynamics, we move back to the fluid dynamics.

Considering the fact that at early time the decay of the auto-correlation in fluid is very similar to the conserved Ising case because of the diffusive dynamics in both the cases, a plot of the fluid data as a function of t/t_w should give an exponent, in the power-law regime, that will be consistent with $\alpha = 1/3$. In fact the exponent extracted from Fig. 5.4 is 0.8 which when compared with 2.2 from the plot vs. ℓ/ℓ_w, gives $\simeq 0.36$. However, we caution the reader that the actual effective growth exponent in this regime should be a little higher due to the mixing of hydrodynamics, whatever little its influence may be. But the value, strikingly close to $\alpha = 1/3$, as quoted above is due to the fact that the initial length in the form

$$\ell(t) = \ell_0 + At^\alpha \tag{5.7}$$

is not subtracted in this analysis [31].

Next we look at the post crossover regime to learn and understand the effect of hydrodynamics. In Fig. 5.9, we show the auto-correlations as a function of ℓ/ℓ_w on a semi-log plot. Two reasonably lower values of temperatures are considered so that the exhibited behavior can be seen over an extended window. Very linear looks of both the data sets confirm an exponential behavior. In the following we try to understand this important observation from simple hydrodynamic equations for fluid phase transitions.

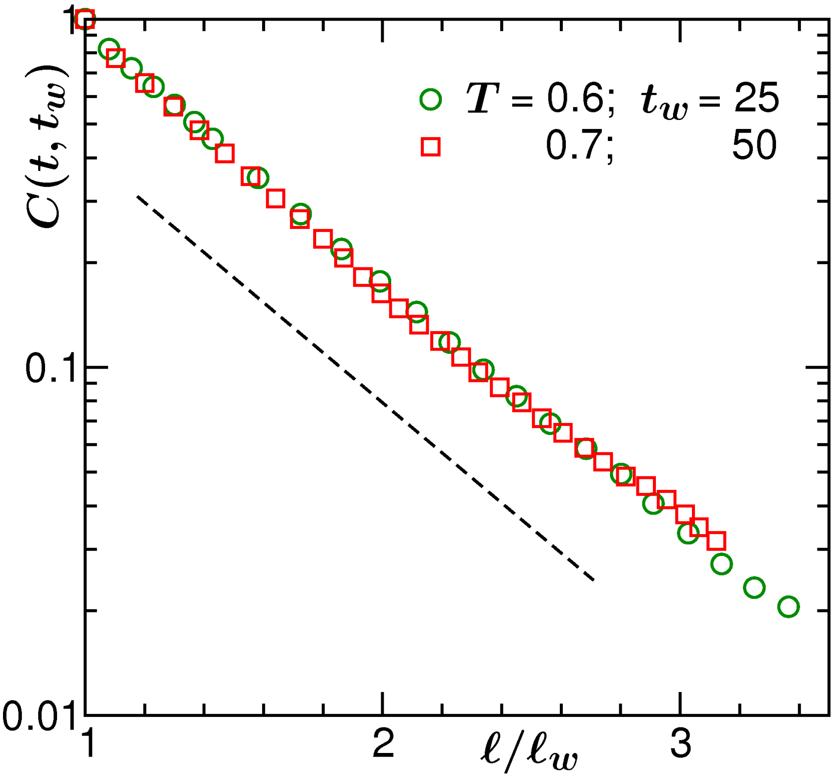

Figure 5.9: Semi-log plots of $C(t, t_w)$ vs ℓ/ℓ_w for fluids at two temperatures. The straight line there corresponds to an exponential decay.

According to the definition of the auto-correlation function, it is quite evident that to get an exponential decay of it, the density fluctuation should decay exponentially in time. This can be obtained from the order parameter evolution equation of model H [12, 32]

$$\frac{\partial \psi}{\partial t} + \vec{v}.\nabla\psi = D\nabla^2\mu, \tag{5.8}$$

where $\vec{v}$ is the advection field, D is a diffusion constant and μ is the chemical potential. At late time when diffusive mechanism is negligible compared to hydrodynamics, one can ignore the right hand side of Eq. (5.8). Further, via the substitutions $v = \ell/t = C =$ constant and $\nabla\psi = \frac{2\psi}{w}$, w being the interfacial width, one obtains

$$\frac{\partial \psi}{\partial t} \simeq -\psi. \tag{5.9}$$

Using the fact that $\ell = \frac{\eta}{\sigma}t$, η and σ being respectively the shear viscosity of the background fluid and interfacial tension, one obtains $\psi \sim \exp(-\frac{2\psi}{w}\ell)$. Very close to the critical point, one, however, needs to take into account the complexity due to diverging correlation length.

5.4 Conclusion

In summary, we have presented results for aging dynamics during nonequilibrium growth in solid binary mixture, ferromagnet and phase separating fluid. While the results for the first two cases were obtained from Monte Carlo simulations, molecular dynamics was used for the latter, to incorporate hydrodynamics. We have pointed out that in absence of hydrodynamics, the decay of the auto-correlation function, $C(t, t_w)$, in conserved systems follow power-law behavior, the exponent of which falls in the bound predicted by Fisher and Huse. The difference of this case with the aging dynamics in non-conserved systems have been discussed including the possible disagreement in the value of power-law exponent. In the conserved case, the effect of hydrodynamics is demonstrated. It is shown that there is a crossover from power-law to exponential decay of $C(t, t_w)$. Discussion is provided for the theoretical understanding of the latter. Our results are very general. Similarity of the results for vapor-liquid transition is also observed for liquid-liquid transition [32]. We expect these to be confirmed via experiments.

Bibliography

[1] M. Zannetti in *Kinetics of Phase Transitions*, edited by S. Puri and V. Wadhawan (CRC, Boca Raton, FL, 2009).

[2] R. Mathieu, P. Norblad, D.N.H. Nam, N.X. Phue and N.V. Khiem, Phys. Rev. B **63**, 174405 (2001).

[3] B. Abou and F. Gallet, Phys. Rev. Lett. **93**, 160603 (2004).

[4] M. Costa, A.L. Goldberger and C.-K. Peng, Phys. Rev. Lett. **95**, 198102 (2005).

[5] G.G. Kenning, G.F. Rodriguez and R. Orbach, Phys. Rev. Lett. **97**, 057201 (2006).

[6] L. Berthier, Phys. Rev. Lett. **98**, 220601 (2007).

[7] D.E. Masri, L. Berthier and L. Cipelletti, Phys. Rev. E **82**, 031503 (2007).

[8] E. Bouchbinder and J.S. Langer, Phys. Rev. E **83**, 061503 (2011).

[9] J. Bergli and Y.M. Galperin, Phys. Rev. B **85**, 214202 (2012).

[10] D.A. Huse, Phys. Rev. B, **40**, 304 (1989).

[11] D.S. Fisher and D.A. Huse, Phys. Rev. B, **38**, 373 (1989).

[12] A.J. Bray, Adv. Phys. **51**, 481 (2002).

[13] K. Binder, in *Phase Transformation of Materials*, Vol 5, p.405 edited by R.W. Cahn, P. Haasen and E.J. Kramer (VCH, Weinheim, 1991).

[14] A. Onuki, *Phase Transition Dynamics* (Cambridge University Press, Cambridge, 2002).

[15] R.A.L. Jones, *Soft Condensed Matter* (Oxford University Press, Oxford, 2008).

[16] F. Liu and G.F. Mazenko, Phys. Rev. B **44**, 9185 (1991).

[17] G.F. Mazenko, Phys. Rev. E **58**, 1543 (1998).

[18] E.D. Siggia, Phys. Rev. A **20**, 595 (1979).

[19] H. Furukawa, Phys. Rev. A **31**, 1103 (1985); ibid **36**, 2288 (1987).

[20] S. Ahmad, S.K. Das and S. Puri, Phys. Rev. E **82**, 040107 (2010).

[21] S. Majumder and S.K. Das, Europhys. Lett. **95**, 46002 (2011).

[22] S.K. Das, Sutapa Roy, S. Majumder and S. Ahmad, Europhys. Lett. **97**, 66006 (2012).

[23] S. Roy and S.K. Das, Phys. Rev. E **85**, 050602 (2012).

[24] I.M. Lifshitz and V.V. Slyozov, J. Phys. Chem. Solids **19**, 35 (1961).

[25] J.-P.Hansen and I.R. McDonald, *Theory of Simple Liquids*, (Academic Press, London, 3rd Edition 2009).

[26] M.P. Allen and D.J. Tildesley, *Computer Simulations of Liquids* (Clarendon, Oxford, 1987).

[27] D. Frenkel and B. Smit, *Understanding Molecular Simulations: From Algorithm to Applications* (Academic Press, San Diego, 2002).

[28] D.P. Landau and K. Binder, *A Guide to Monte Carlo Simulations in Statistical Physics*, (Cambridge University Press, 3rd Edition 2009).

[29] K. Humayun and A.J. Bray, J. Phys. A **24**, 1915 (1991).

[30] Y. oono and S. Puri, Phys. Rev. Lett. **58**, 836 (1987).

[31] S. Majumder and S.K. Das, Phys. Rev. E **81**, 050102 (2010).

[32] S. Ahmad, F. Corberi, S.K. Das, E. Lippiello, S. Puri and M. Zannetti, to be published.

Chapter 6

Kinetics of Phase Separation in Thin Films: Atomistic studies

6.1 Introduction

In the previous chapters we have dealt with phase separation in bulk [1], both for solids and fluids. It is important to mention that recently there is growing interest to study the kinetics of phase separation in restricted geometries to understand surface effects [2–6]. In this regard, a particular problem of interest is to study the kinetics of phase separation in thin films [2–6]. From technological point of view thin films have a wide range of applications [7–10] as lubricants, protecting layers, in micro-electronics, nanotechnology, etc. From scientific point of view, it is challenging due to the simultaneous presence of surface effects and finite-size effects. Many phenomena differ significantly from bulk behavior when a reduced geometry is considered. In case of phase separation in thin films, there is interesting interplay between the surface effects and bulk phase separation which gives rise to many complex situations such as wetting, dewetting, layering transition [11–14], etc., each of which is of longstanding research interest. Such spinodal decomposition in presence of surface effects goes by the name of *Surface Directed Spinodal Decomposition* (SDSD) [15–17].

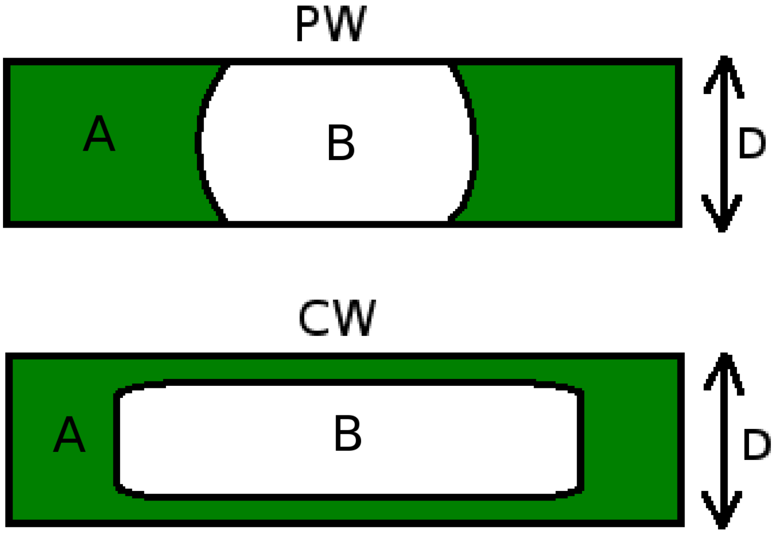

Figure 6.1: Schematic representation of binary mixture phase separation in a film with symmetric surface fields attracting the A-particles, marked in green. The B particles are unmarked. The diagram is shown in a plane, perpendicular to the walls S_1 and S_2. The lateral dimension of the system is L and the film thickness is D ($D \ll L$). The upper part shows the partially wet (PW) morphology with non-zero contact angle. The lower part corresponds to the completely wet (CW) scenario.

Let us consider a 50 : 50 binary mixture (A+B), confined between two surfaces S_1 and S_2, quenched to a temperature below the critical point. Fig. 6.1 shows schematics to describe situations where there are symmetric fields applied on the surfaces of a thin film of thickness D. By symmetric field

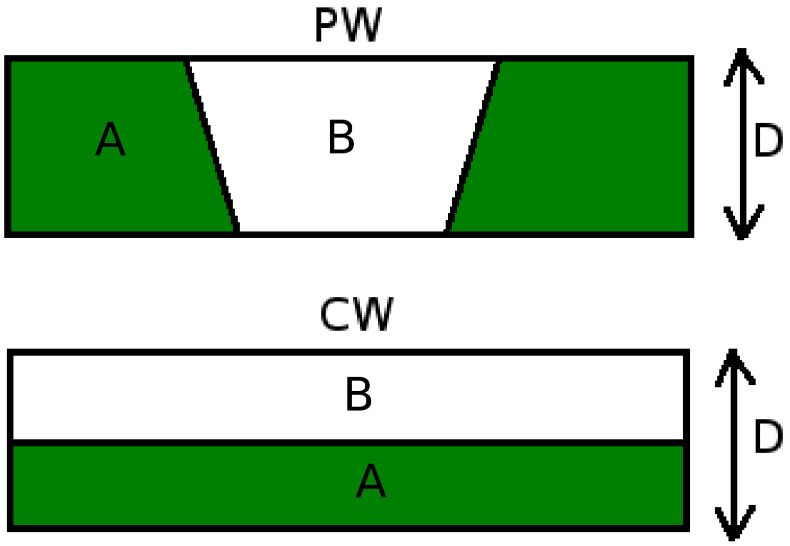

Figure 6.2: Schematic representation of phase separation in a binary mixture in a thinfilm geometry under antisymmetric fields at the two surfaces. The color code and dimensions are same as in Fig. 6.1. Here the upper picture corresponds to partially wet (PW) situation. The lower picture represents the completely wet (CW) morphology.

we mean that both the surfaces will attract the same particle (say A), with equal strength to simplify the problem. Under this condition there could be two possible pictures. First one is shown in the upper part of Fig. 6.1 which describes a partially wet (PW) situation. Here the A-B interface touches the surfaces S_1 and S_2 at a non-zero contact angle, θ_c [18]. On the other hand, the lower part describes the other possible scenario which is the completely wet (CW) morphology. It shows the presence of A-rich layering at the surfaces. In this case the A-B interface never touches the surfaces. These two scenarios can arise for a given thin film depending on the wetting transition dictated by temperature and the applied fields on the surfaces.

The other interesting case is when the field applied on the surfaces are anti-symmetric in nature, i.e., one surface attracts A particles and the other one attracts the B particles, say with equal strengths. The upper picture in Fig. 6.2 shows the equilibrium morphology for the PW situation in this case. In the lower part we show the schematic for the CW morphology for the antisymmetric film. This latter situation shows the presence of a single interface at the center of the film, parallel to the walls, corresponding to a contact angle $\theta_c = 0$, with formation of A-rich and B rich layer at the two surfaces.

Kinetics of phase separation in thin films have been studied for binary solid mixtures using coarse-grained dynamical models [15, 16, 19–22]. In this work we intend to study SDSD via atomistic models. We consider solid binary mixtures as well as fluids under confinement. While for solid binary mixture we have considered both symmetric and asymmetric compositions, for the fluid case (with vapor-liquid transition) we have used only asymmetric density. The asymmetric case in this context is of relevance for the study of heterogeneous nucleation [23]. We have studied the binary solid via Monte Carlo (MC) [24] simulations of the appropriate atomistic Ising model and for fluid we have used molecular dynamics (MD) [25] simulations to the single component Lennard Jones (LJ) fluid.

This chapter is organized as follows. We discuss the models and methods in Sec 6.2. In Sec 6.3 we present the results. Finally, Sec 6.4 concludes the Chapter with a summary and discussion on future possibilities.

6.2 Models and Methods

We consider our systems of interest in confined thin film geometry, having lateral dimensions $L_x = L_y = L$ and thickness D ($D \ll L$), the separation between two walls S_1 and S_2 located at $z = 0$ and $z = D$ respectively. For solid binary mixtures, δ- function fields H_1 and H_2 are applied on the two surfaces. The interaction between the particles, in this case, is given by the simple spin 1/2 Ising model. The full Hamiltonian is written as

$$H = -J \sum_{<ij>} S_i S_j - J_S \sum_{<ij>} S_i S_j - H_1 \sum_{i \epsilon S_1} S_i - H_2 \sum_{i \epsilon S_2} S_i; \; S_i = \pm 1, \quad (6.1)$$

where J, $J_S (> 0)$ are the interaction strengths in the bulk and at the surfaces, respectively. If $H_1 = H_2$, the thin film is a symmetric one and for $H_1 = -H_2$, it is antisymmetric. To simplify the problem, we have considered $J = J_S$. We have performed MC simulations of this model via the Kawasaki exchange [26] mechanism which mimics the diffusive transport of materials in solids. In Kawasaki exchange one picks up a spin randomly and exchanges it with one of its randomly chosen nearest neighbors. The moves are accepted according to the standard Metropolis algorithm [24]. During our simulation we have applied periodic boundary conditions in the x- and y- directions but not in z-direction (which is the direction perpendicular to the surfaces), in order to incorporate the surface effects. We start with initial conditions containing random distributions of A and B particles, which correspond to the high temperature situation. Then we quench the system to a temperature $T = 0.6T_c$, well below the bulk critical temperature ($T_c = 4.51J/k_B$).

Here we note that, in addition to studying the physical processes, an objective of this work is to verify the popular coarse-grained model, due to Puri and Binder (PB) [15, 16], presented in the introduction, where writing the boundary conditions is rather nontrivial. Note that at the critical vicinity such models are extremely useful due to the divergence of equilibrium correlation length. On the other hand, these models have drawbacks for deep temperature quenches [2]. So, we demonstrate that with present day computer powers, it is possible to use microscopic models to gain accurate information at low temperature.

For the vapor-liquid case we have performed MD simulations [25] of the following model. The particles interact with each other via the pairwise potential given as

$$V(r_{ij}) = U(r_{ij}) - U(r_c) - (r_{ij} - r_c)\left(\frac{dU(r_{ij})}{dr_{ij}}\right)_{r_{ij}=r_c}, \tag{6.2}$$

with

$$U(r_{ij}) = 4\epsilon\left[\left(\frac{\sigma}{r_{ij}}\right)^{12} - \left(\frac{\sigma}{r_{ij}}\right)^{6}\right], \tag{6.3}$$

being the standard LJ potential. This model and the corresponding bulk phase diagram are well described [27] in Chapter 4. Here also we have used the same values for different model parameters. In the present study, to introduce the surface effect, we considered a situation where only the surface at $z = 0$ attracts the particles via the following wall potential [28, 29]

$$u(z) = \frac{2\pi\rho}{3}\left\{\epsilon_r\left[\left(\frac{\sigma}{z+\delta}\right)^9 + \left(\frac{\sigma}{D+\delta-z}\right)^9\right] - \epsilon_a\left(\frac{\sigma}{z+\delta}\right)^3\right\}, \quad (6.4)$$

where $0 \leq z \leq D$ and $\delta = \sigma/2$, introduced to avoid the singularity at the walls, ϵ_r is the repulsion by the walls and ϵ_a is the strength of attraction by the wall at $z = 0$. We have considered that both the walls are exerting the same repulsive force ($\epsilon_r = \epsilon/15$). This surface potential could be thought of an integrated LJ potential. As in the previous Chapters, we have set J, ϵ, m, k_B, etc., to unity. Nosé-Hoover thermostat was used to control the temperature in this case.

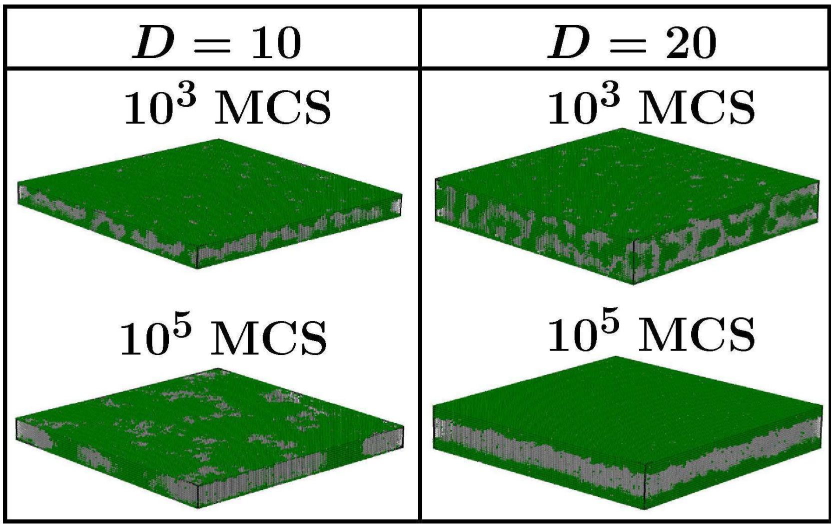

Figure 6.3: $3-d$ evolution snapshots in thin films with symmetric fields at the surfaces with the film thicknesses $D = 10$ and 20, and lateral dimension $L = 128$. The snapshots are obtained via MC simulations after quenching the 50 : 50 solid binary mixtures from the high temperature homogeneous phase to a temperature deep inside the bulk co-existence curve. The A particles are marked green and the B-particles are marked in grey. Here $H_1 = H_2 = H = 1.0$.

6.3 Results

6.3.1 Bulk Critical Composition for Solid mixtures

(a) Symmetric Fields

First we present results for symmetric fields, i.e., both the surfaces attract one of the species (say A), with equal strength ($H_1 = H_2 = H = 1$). Here we will present results for two different film thicknesses $D = 10$ and 20. In Fig. 6.3, we show the $3-d$ snapshots for both $D = 10$ and 20 with $L = 128$. While these $3-d$ pictures do not provide a clear view, in Fig. 6.4 we take a look at the cross-section of the film in the xz plane $y = L/2$. Let us discuss the case for $D = 10$. At an intermediate time, say, $t = 10^4$ MCS, one sees surface enrichment of A-particles. Then at late time it is quite clear that the layered structures break up to form domains in direction parallel to the surfaces. Essentially, the time scale of the surface enrichment is faster than the bulk phase separation leading to a CW morphology at intermediate time,

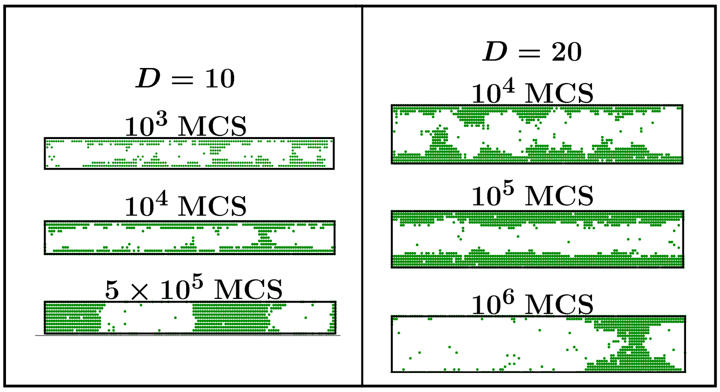

Figure 6.4: $2-d$ xz cross sections of the snapshots for the same systems in Fig. 6.3, for $y = L/2$. Note that A particles are marked green and B is left unmarked. From each D values, pictures from three times are shown.

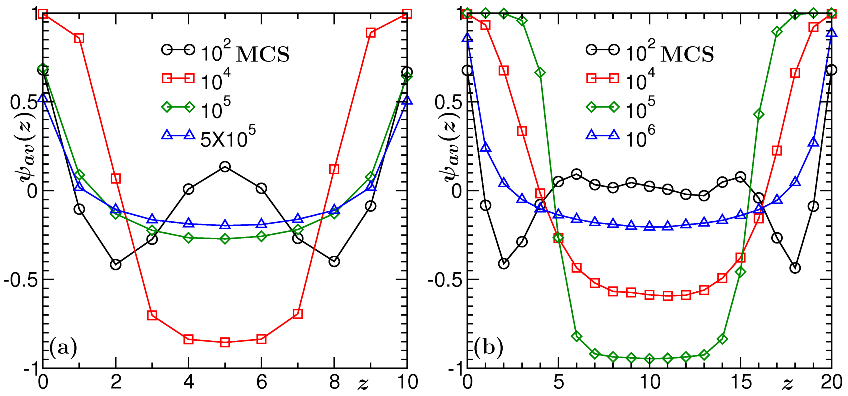

Figure 6.5: Laterally averaged order parameter, $\psi_{av}(z)$, vs z (coordinates perpendicular to the direction of the walls) from four different times for the same systems presented in Fig. 6.3.

even though this may not be the equilibrium structure. At later time, for the value of H used here, the wetting layers break up and finally the morphology becomes PW as shown in the last snapshot of Fig. 6.4, for $D = 10$. This general picture applies for $D = 20$ as well. Similar sequence of events were also observed in studies with PB coarse-grained model [15, 16, 21, 22]. Thus, our studies confirm the usefulness of such model in this context. Here we again stress that the PB model is advantageous to use in close vicinity of criticality where the equilibrium correlation length, ξ, diverges.

Next we calculate the laterally averaged order parameter profile which is obtained by taking average of the spins along the xy direction for all the layers parallel to the surfaces. In Fig. 6.5, we have presented these profiles from four different times for the systems presented in Fig. 6.3. The profiles at early time ($t = 100$ MCS) shows the formation of two symmetric waves which propagates to the center of the film. At little later time ($t = 10^4$ MCS) the high value at the surfaces represents the layered structures. At

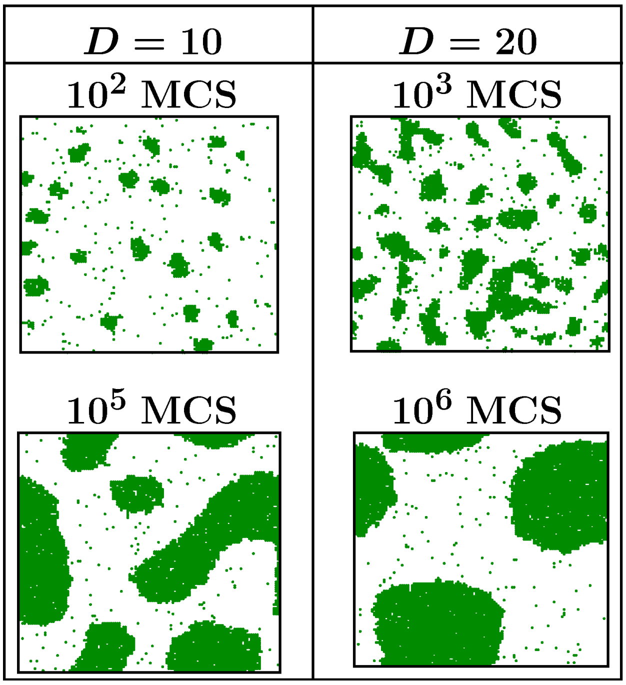

Figure 6.6: Cross-sections of the same systems presented in Fig. 6.3, in the xy plane for $z = D/2$. The A particles are marked green and the B particles are left unmarked.

much later time, since the layer structures break up, the profiles show small values at the surfaces and in the intermediate layers they are very close to zero. The symmetric nature of the profiles around the center

$$\psi_{av}(z) = \psi_{av}(D - z). \tag{6.5}$$

is due to the symmetric fields at the surfaces of the film.

It will also be interesting to study the cross-sections of the systems parallel to the surfaces, i.e., in the xy-planes. In Fig. 6.6, we present the cross-sections of the systems in Fig. 6.3, for $z = D/2$. The snapshot at early time shows the formation of A-rich droplets due to depletion of A particles

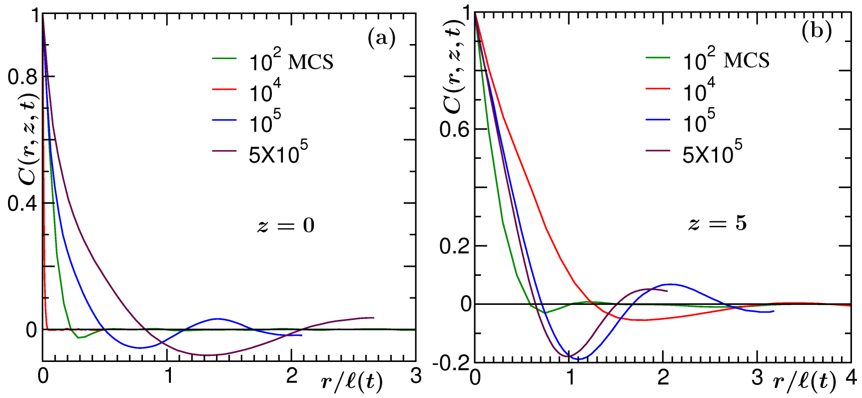

Figure 6.7: Layer-wise scaled correlation functions for different times from two different layers $z = 0$ and $z = 5$ for the film with $D = 10$.

in this layer. Recall that at early time there is fast surface enrichment. At later time, when such metastable wetting layers break-up, share of A-species increases in the center, leading to more elongated domain morphology.

Next we look at the scaling properties of the layer wise correlation functions and growth laws in such composition fluctuating environment. The layer wise correlation functions are calculated as

$$C(r, z, t) = \langle S(\vec{\sigma}, z, t)S(\vec{\sigma} + \vec{r}, z, t)\rangle - \langle S(\vec{\sigma}, z, t)\rangle\langle S(\vec{\sigma} + \vec{r}, z, t)\rangle, \tag{6.6}$$

where instead of using i or j as site index we have specified the coordinates of the spin location inside the bracket. As already mentioned, $\vec{\sigma}$ is the coordinate in direction parallel to the surfaces. One can define the layer-wise average domain size from the decay of the $C(r, z, t)$ as

$$C(r = \ell, z, t) = \frac{1}{2}C(0, z, t). \tag{6.7}$$

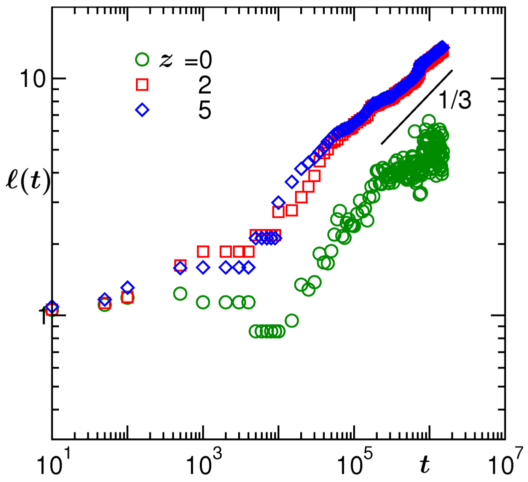

Figure 6.8: Layer-wise average domain size vs time plot for three different layers $z = 0, 2$ and 5 for $D = 10$ of Fig. 6.3. The solid line has a slope of 1/3.

In Fig. 6.7, we have shown the plots of scaled correlation functions at different times for $z = 0$ and $z = 5$ for $D = 10$. In bulk phase separation these correlation functions obey a scaling relation $C(\vec{r}, t) \equiv g(r/\ell)$. From these plots, however, one can see that such scaling is absent because in this case the morphology obtained at different times are not self-similar in nature. The comparisons of the plots from different times is analogous to the comparison of $C(r, t)$ from different compositions in Chapter 3. However, at very late time reasonable quality of scaling is obtained. In Fig. 6.8 we take a look at the plots of layer-wise average domain size, $\ell(t)$, vs time, for three different layers. The initial non monotonic behavior of the length scale is due to the formation and breakup of structures at the surfaces. But at late time limit the growth is found to be consistent with the Lifshitz-Slyozov (LS) [1, 30] growth law ($\ell(t) \sim t^{1/3}$), which is the scaling law for the diffusive bulk phase separation. Note that the time beyond which the LS behavior is observed,

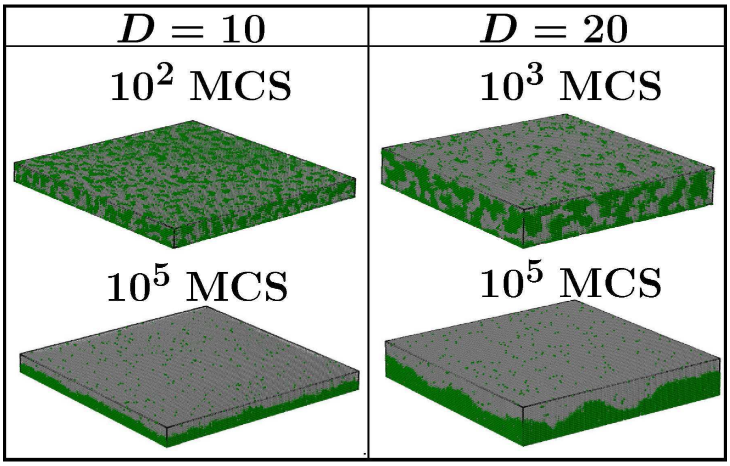

Figure 6.9: $3-d$ evolution snapshots of antisymmetric films for a binary solid mixture with bulk critical composition after quenching far below the bulk critical temperature. The left frame represent a film with $L = 128$ and $D = 10$ and the right one corresponds to a film with $L = 128$ and $D = 20$. The color coding is same as in Fig. 6.3. Strengths of the fields are $H_1 = 1.0$ and $H_2 = -1.0$.

the change in layer magnetization is rather small in time as is also reflected in the scaling plot of the correlation functions in Fig. 6.7.

(b) Anti-symmetric Fields

Here we discuss the results from the binary solid phase separation in an anti-symmetric thin film. In this case $H_{S_1} = -H_{S_2}$ which means that the surface S_1 at $z = 0$ attracts the A particles and the surface at $z = D$ attracts the B-particles. Here also we have started with homogeneous initial mixtures of A and B particles with 50 : 50 composition and quenched it well below the bulk critical temperature.

In Fig. 6.9, we show the $3-d$ snapshots for the evolution of anti-symmetric thin film with $D = 10$ and 20, as indicated. In Fig. 6.10, we present the $2-d$ cross-section in xz plane for the snapshots shown in Fig.

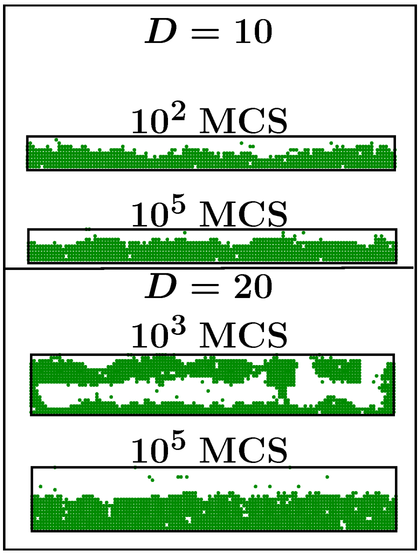

Figure 6.10: $2-d$ cross-sectional (in xz- plane) view of the evolution snapshots for the systems in Fig. 6.9. Here the A particles are marked green and the B particles are left unmarked.

6.9. In both the cases, completely wet morphology forms at the end.

Next we take a look at the layer wise order parameter profile for the above mentioned thin films. In Fig. 6.11, we have shown the plots of the laterally averaged order parameter for antisymmetric thin films with $D = 10$ [part (a)] and $D = 20$ [part (b)]. As pointed out for symmetric thin films, here also it is important to look at the cross-sections of films in xy planes since the domains can grow indefinitely in direction parallel to the surfaces. Fig. 6.12 shows the cross-section of the system in xy- plane for the central layer of the film. The left part shows the snapshot for $D = 10$ and the right one for $D = 20$. For both of them since the composition is critical at the center of the film the snapshots in the xy-plane show presence of nearly interconnected bicontinuous structure as seen during the bulk phase separation. Here we note that there is a higher level of noise in the thinner

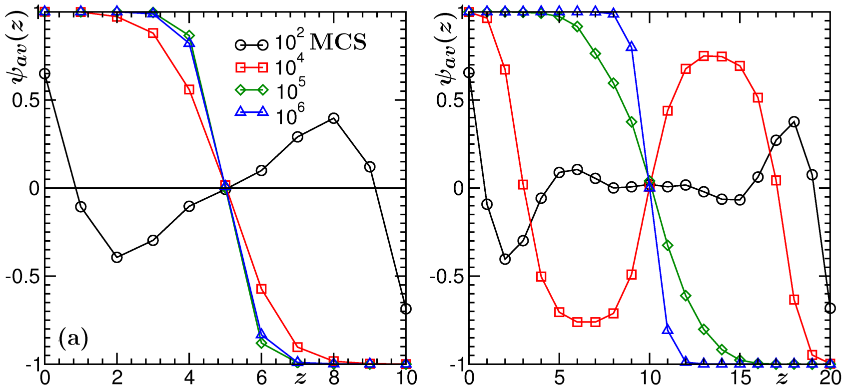

Figure 6.11: Layer-wise averaged order parameter profiles from four different times for (a) $D = 10$ and (b) $D = 20$ for the antisymmetric thin films presented in Fig. 6.9.

film. This is due to the following fact. In thin film, critical temperature is suppressed. Thus, considering the fact that simulations were performed at the same temperature for both values of D, the thinner one is closer to the corresponding thin film critical temperature.

Finally, in Fig. 6.13 we show the plot of $\ell(t)$ vs t, from the central layer for $D = 20$. The results at late time is consistent with the LS behavior.

6.3.2 Off-critical Compositions or Densities

Because of the preliminary nature of the studies here we stick to present only the snapshots of evolution here. In Fig. 6.14, we show the evolution snapshots for the solid off-critical binary mixture with antisymmetric fields. It is nicely seen that droplets are formed on the preferred surface and they are growing with time. Similar picture for the vapor-liquid system is shown in Fig. 6.15. As already stated, these systems correspond to heterogeneous nucleation in presence of surface. Our next objective would be to understand

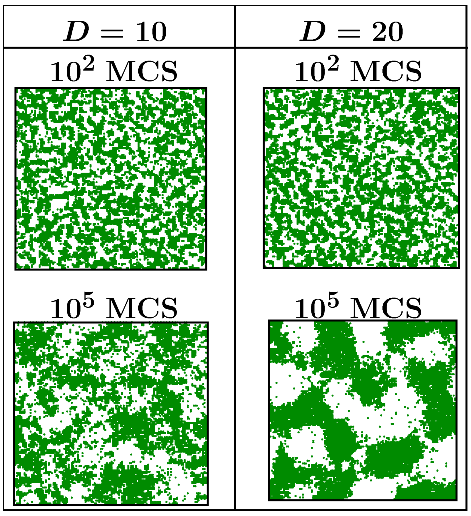

Figure 6.12: $2-d$ snapshots in the xy-plane for the central layer of the thin films presented in Fig .6.9. Here the color coding is same as in Fig .6.10.

the growth dynamics in both the situations and compare them with the bulk homogeneous nucleation and growth processes (results presented in Chapter 3). It is expected that the time scale of nucleation in presence of surface would be shorter.

6.4 Conclusion

In conclusion, in this chapter, we have presented results for the kinetics of phase separation in thin films. Primary results are presented for the binary solid mixtures. We have observed interesting interplay between the surface effects and the bulk phase separation. For both symmetric and antisymmetric fields, at late time when there is scaling in the structural property, it is observed that the domains grow following the LS law in layers parallel to the surfaces. In future, we would like to do finite-size scaling analysis to

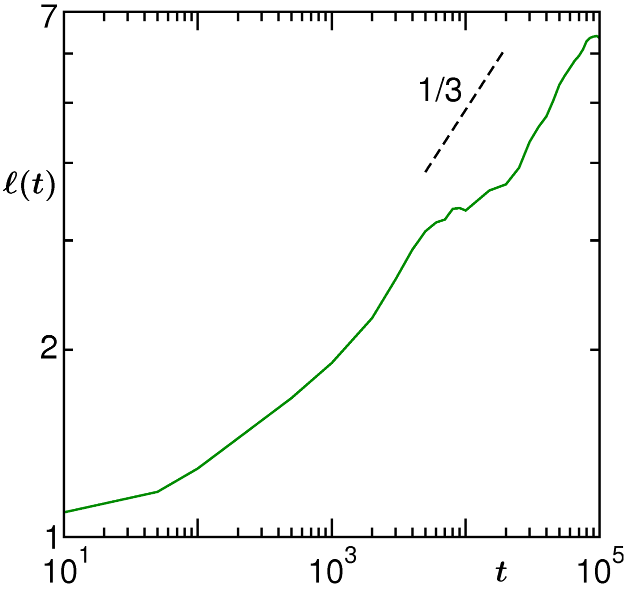

Figure 6.13: Layer wise (in xy plane) average domain size, $\ell(t)$, as a function of time for $D = 20$ antisymmetric film. We have considered only the central layer.

accurately quantify the growth law.

An objective of this study was to show the plausibility of Monte Carlo simulation in this case and justify the validity of the PB model. The sequence of events that we observed in these studies is qualitatively consistent with the coarse-grained PB model. The later, of course, is more useful close to the critical point.

Finally, we have presented some preliminary results for droplet nucleation and growth on surfaces, for both solid-solid and vapor-liquid systems. In future, we will elaborate on this. In thin film geometry, many further interesting studies can be done. Kinetics of phase separation under temperature gradient is one such good candidate.

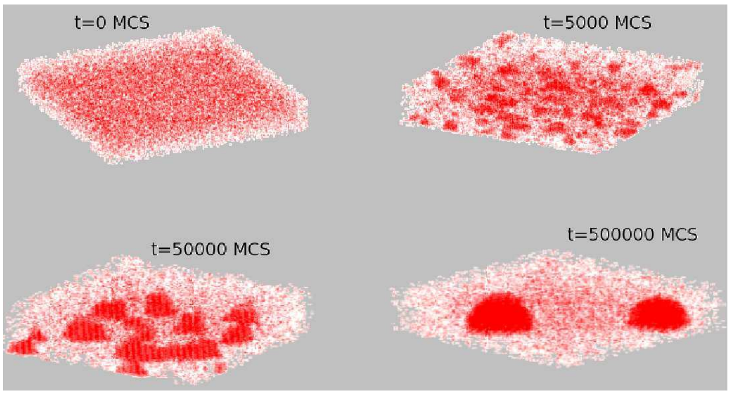

Figure 6.14: Formation and growth of droplets of A-particles (minority species) on the preferred surface, in solid binary mixture phase separation with asymmetric composition.

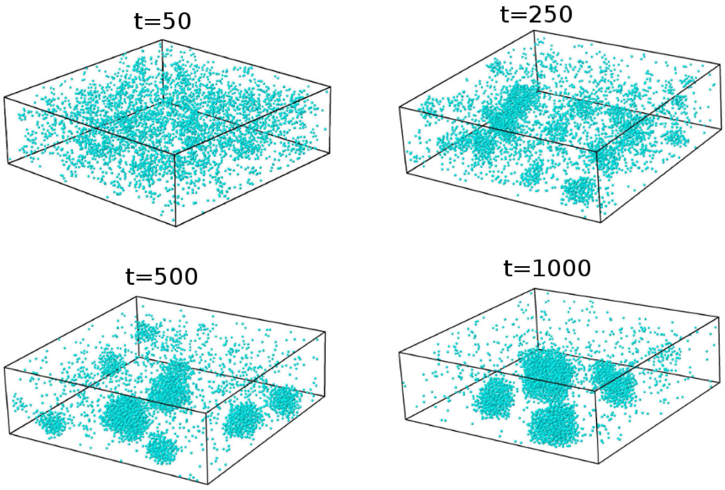

Figure 6.15: Nucleation and growth of liquid droplets on a surface that attracts the particles. This is related to vapor-liquid phase separation in confined geometry with asymmetric densities.

Bibliography

[1] A.J. Bray, Adv. Phys. **51**, 481 (2002).

[2] S.K.Das, J. Horbach and K.Binder, Phys. Rev. E. **79**, 021602 (2009).

[3] M.J.A. Hore and M. Laradji J. Chem. Phys. **132**, 024908 (2010).

[4] R. Siquieri and H. Emmerich, J. Phys: Condens. Matter **21**, 464105 (2009).

[5] N. Blondiaux, S. Morgenthaler, R. Pugin, N.D. Sepncer amd M. Liley, Appl. Surf. Sci. **254**, 6820 (2008).

[6] J. Liu, X. Wu, W.N. Lennard and D. Landheer, Phys. Rev. B **80**, 041403 (R) (2009).

[7] L.D. Gelb, K.E. Gubbins, R. Radhakrishnan and M. Sliwinska-Bartkoviak, Rep. Prog. Phys. **62**, 1573 (1999).

[8] T. Thorsen, S.J. Maerkl and S.R. Quake, Science **298**, 580 (2002).

[9] A. Meller, J. Phys: Condens. Matter **15**, R581 (2003).

[10] E.L. Wolf, *Nanophysics and Nanotechnology* (Wiley, VCH, Weinheim, 2004).

[11] J.S. Rowlinson and B. Widom, *Molecular Theory of Capillarity* (Oxford University Press, Oxford, 1982).

[12] P.G. Gennes, Rev. Mod. Phys. **57**, 827 (1985).

[13] D. Bonn and D. Ross, Rep. Prog. Phys. **64**, 1085 (2001).

[14] M.E. Fisher and H. Wen, Phys. Rev. Lett. **68**, 3654 (1992).

[15] S. Puri and K.Binder, Phys. Rev. A **46**, R4487 (1992).

[16] S. Puri and K.Binder, Phys. Rev. E **49**, 5359 (1994).

[17] R.A.L. Jones, *Soft Condensed Matter* (Oxford University Press, Oxford, 2008).

[18] T. Young, Philos. Trans.R. Soc. London **95**, 65 (1805).

[19] A. Bhattacharya, M. Rao and A. Chakrabarti, Phys. Rev. E **49**, 524 (1994).

[20] G. Brown and A. Chakrabarti, Phys. Rev. A **46**, 4829 (1992).

[21] S.K. Das, S. Puri, J. Horbach and K. Binder, Phys. Rev. Lett. **96**, 016107 (2006).

[22] S.K. Das, S. Puri, J. Horbach and K. Binder, Phys. Rev. E **72**, 61603 (2005).

[23] K. Binder, Rep. Prog. Phys. **50**, 783 (1987).

[24] D.P. Landau and K. Binder, *A Guide to Monte Carlo Simulations in Statistical Physics* (Cambridge University Press, Cambridge, 2009).

[25] D. Frenkel and B. Smit, *Understanding Molecular Simulations: From Algorithms to Applications* (Academic Press, San Diego, 2002).

[26] K. Kawasaki, in *Phase Transition and Critical Phenomena*, edited by C. Domd and M.S. Green (Academic, New York, 1972), Vol. 2, p.443.

[27] S. Majumder and S.K. Das Europhys. Lett. **95**, 46002 (2011).

[28] S.K. Das and K. Binder, Europhys. Lett. **92**, 26006 (2010).

[29] S.K. Das and K. Binder, Mol. Phys. **109**, 1043 (2011).

[30] I.M. Lifshitz and V.V. Slyozov, J. Phys. Chem. Solids **19**, 35 (1961).

APS Journals
About the Journals
Browse the Journals
Search the Journals
APS Home
Join APS
PACS Scheme
Annual Index
BAPS

Authors
General Information
Submit a Manuscript
Publication Rights
Open Access
Policies & Practices
Tips for Authors
Professional Conduct

Referees
General Information
Submit a Report
Update Your Information
Policies & Practices
Referee FAQ
Advice to Referees
Outstanding Referees

Librarians
General Information
Subscriptions
Online License Agreement
Usage Statistics
Your Account

Students
Physics
PhysicsCentral
Student Membership

APS Members
Subscriptions
Article Packs
Membership
FAQ
APS News
Meetings and Events

APS Copyright Policies and Frequently Asked Questions

What is copyright? http://www.copyright.gov/
Copyright is a form of legal protection for original works of authorship. Copyright covers both published and unpublished works.

What does copyright protect?
Copyright, a form of intellectual property law, protects original works of authorship including literary, dramatic, musical, and artistic works, such as poetry, novels, movies, songs, computer software, and architecture. Copyright does not protect facts, ideas, systems, or methods of operation, although it may protect the way these things are expressed. See Circular 1, Copyright Basics, section "What Works Are Protected", see http://www.copyright.gov/circs/circ1.html#wwp

How is a copyright different from a patent or a trademark?
Copyright protects original works of authorship, while a patent protects inventions or discoveries. Ideas and discoveries are not protected by the copyright law, although the way in which they are expressed may be. A trademark protects words, phrases, symbols, or designs identifying the source of the goods or services of one party and distinguishing them from those of others.

What is the difference between copyright infringement and plagiarism?
Copyright infringement occurs when an author's work is reused or republished without the permission of the copyright owner, whether or not author attribution accompanied the reuse.

Plagiarism occurs when an author's work has been reused or republished in such a manner as to make it appear as someone else's work, e.g., without quotation marks and citation of the original work.

Why should I transfer copyright to APS?
Like many other scientific publishers, the American Physical Society (APS) requires authors or their employers to provide transfer of copyright prior to publication. This permits APS to publish the article and to defend against improper use (or even theft) of the article. It also permits APS to mount the article online and to use the article in other forms or media, such as PROLA. By the APS transfer agreement, authors and their employers retain substantial rights in the work, as specified in the agreement (http://forms.aps.org/author/copytrnsfr.pdf) and discussed in this document.

Why should I transfer copyright to APS before the article is accepted for publication by an APS journal?
Transferring copyright early in the process avoids the possibility of delaying publication if the transfer has to be obtained later in the process. By

the terms of the copyright transfer agreement itself, it has no effect until the paper is accepted by an APS journal. The author retains the copyright until acceptance, and has the full freedom, for example, to withdraw the paper from consideration by an APS journal and submit it elsewhere.

Does transferring copyright affect my patent rights?
No. Copyright is separate from any patent rights, and the APS transfer agreement specifically states that patent rights are not affected. However, you should be aware that submitting a manuscript to a journal without first taking steps to protect your patent rights (e.g., filing for a patent) could endanger those rights. Consult your patent attorney.

As the author of an APS-published article, may I post my article or a portion of my article on my own website?
Yes, the author or the author's employer may use all or part of the APS published article, including the APS-prepared version (e.g., the PDF from the online journal) without revision or modification, on the author's or employer's website as long as a fee is not charged. If a fee is charged, then APS permission must be sought. In all cases, the appropriate bibliographic citation and notice of the APS copyright must be included.

What happens if the author has posted an APS-published article on a free access e-print server or on the authors' or institutions' web page and subsequently a fee is imposed for access to those sites?
When a fee is imposed, the author must either obtain permission from APS or withdraw the article from the e-print server or Institutional Repository.

As the author of an APS-published article, may I post my article or a portion of my article on an e-print server?
The author has the right to post and update the article on a free-access e-print server using files prepared and formatted by the author. Any such posting made or updated after acceptance of the article for publication by APS shall include a link to the online abstract in the APS journal or to the entry page of the journal. In all cases, the appropriate bibliographic citation and notice of the APS copyright must be included. If the author wishes to use the APS-prepared version (e.g., the PDF from the online journal) on an e-print server other than authors' or employer's website, then APS permission must be sought. Similarly, if the author wishes to post the article (any version) on an e-print server that charges a fee for use, APS permission must be sought.

As the author of an APS-published article, can I post my article or a portion of my article on a web resource like wikipedia or quantiki?
Sites like wikipedia and quantiki are strict about permissions and require that authors hold copyright to articles that they post there. In order to allow authors to comply with this requirement, APS permits authors to hold copyright to a "derived work" based on an article published in an APS journal as long as the work contains at least 10% new material not covered by APS's copyright and does not contain more than 50% of the text (including equations) of the original article.

As the author of an APS-published article, will I hold copyright to a "derived work", as described above, even if the original article was published prior to 1 October 2008?
Yes. The APS will extend this author right to all papers published in APS journals.

As the author (or the author's employer) of an APS-published article, may I use copies of part or all of my article in the classroom?
Yes, the author or his/her employer may use all or part of the APS-prepared version for educational purposes without requesting permission from the APS as long as the appropriate bibliographic citation is included.

As the author of an APS-published article, may I use figures, tables, graphs, etc. in future publications?
Yes, as the author you have the right to use figures, tables, graphs, etc. in subsequent publications using files prepared and formatted by you or the APS-prepared versions. The appropriate bibliographic citation must be included.

As the author of an APS-published article, may I include my article or a portion of my article in my thesis or dissertation?
Yes, the author has the right to use the article or a portion of the article in a thesis or dissertation without requesting permission from APS, provided the bibliographic citation and the APS copyright credit line are given on the appropriate pages.

As the author of an APS-published article, may I give permission to a colleague or third party to republish all or part of the article in a print publication?
Yes, as the author you can grant permission to third parties to republish print versions of the article provided the APS-prepared version (e.g., the PDF from the online journal, or a copy of the article from the print journal) is not used for this purpose, the article is not published in another journal, and the third party does not charge a fee. The appropriate bibliographic citation and notice of the APS copyright must be included.

As the author of an APS-published article, may I give permission to a colleague or third party to republish all or part of the article in an online journal, book, database compilation, etc.?
Authors should direct the third party request to APS.

As the author of an APS-published article, may I provide a PDF of my paper to a colleague or third party?
The author is permitted to provide, for research purposes and as long as a fee is not charged, a PDF copy of his/her article using either the APS-prepared version or the author prepared version.

As a third party (not an author), may I republish an article or portion of an article published by APS?
Yes, APS will grant permission to republish articles or portions of articles (e.g., tables, graphs, excerpts) published by APS. Depending on the reuse and medium APS has the right to grant permission subject to APS terms and conditions and a fee may be assessed.

As a third party, may I use articles published by APS for lecture and classroom purposes?
Yes, you may use photocopied articles published by APS for lecture and classroom purposes for a single semester without asking permission from APS. However, if the article becomes part of your course material beyond one semester, you must obtain permission from APS. Also, there is no limitation on the use of APS articles using links to the material accessible through institutional subscriptions.

How do I request permission to republish APS-copyrighted material?
To request permission to republish APS-copyrighted material, please provide the following information:

1. Title of journal
2. Title of article
3. Name of author
4. Volume number, page number (or article identifier), year
5. Indicate if you are requesting to republish in print, online, CD-ROM, and/or other format

6. Indicate if you wish to republish all or portion of article; if a portion describe the specific material, e.g., figure numbers, excerpt
7. Indicate how the material will be used, e.g., in a book, journal, proceeding, thesis, etc.
8. Indicate the title of the article/thesis/chapter etc., and the name of the publication in which your work will appear
9. Indicate the name of the publisher
10. Indicate whether or not a fee will be charged for the publication

*To prevent clerical error, please include all requests in a single email or letter.

All permission requests must be in writing (email is acceptable). Blanket permissions are not granted. Please note all requests are subject to APS terms and conditions and a fee may be assessed.

Please allow 5-7 business days for us to respond to a permission request provided all the above information is provided at the time of the request.

Send all permission requests to:

Associate Publisher
American Physical Society
One Physics Ellipse
College Park, MD 20740
Email: assocpub@aps.org

If your questions have not been addressed and you need further assistance, please call: 301-209-3283.

How do I provide a proper bibliographic citation and notice of the APS copyright?
Provide the following information in this order:

Authors names, journal title, volume number, page number (or article identifier), year of publication. "Copyright (year) by the American Physical Society."

Further information
For further information about copyright in general, please refer to the Library of Congress FAQ at: http://www.copyright.gov/help/faq/

Journals published by the American Physical Society can be found at http://publish.aps.org/

FAQ Version: October 1, 2008

Re: Permission for Copyright

From : suman@jncasr.ac.in Mon, Dec 17, 2012 06:43 PM
Subject : Re: Permission for Copyright
To : editorial <editorial.office@epletters.net>

Dear Caroline Orbann,

Thank you for your reply.

Regards,
Suman Majumder
Theoretical Sciences Unit
Jawaharlal Nehru Centre for Advanced Scientific Research

From: "editorial" <editorial.office@epletters.net>
To: suman@jncasr.ac.in
Sent: Monday, December 17, 2012 6:27:38 PM
Subject: Re: Permission for Copyright

Dear Dr. Majumder,

In answer to your request, we are pleased to inform you that you are allowed to use material from
the papers entitled :
Universality in Fluid Domain Coarsening: The case of vapor-liquid transition
by Suman Majumder and Subir K. Das
EPL 95, 46002 (2011)

and

Finite-size effects in dynamics: Critical vs coarsening phenomena
by S. K. Das, S. Roy, S. Majumder and S. Ahmad
EPL 97, 66006 (2012).

The references of the sources must be given (title, year, issue).

Sincerely yours,

--
Caroline Orbann
Editorial assistant

EPL - European Physical Society
6, rue des Freres Lumiere
68200 Mulhouse

+33 389 32 94 40
+33 389 32 94 49

On vendredi 14 décembre 2012 6:46, suman@jncasr.ac.in wrote:
>p { margin: 0; }
>
>To,
>
>
> EPL Editorial Office
>
>
>Subject : Permission for copyright
>
>
>Dear Sir,
>
>
> I am Suman Majumder , a final year Ph.D student under the
>supervision of Dr. Subir K. Das,
>
>in the Theoretical Sciences Unit of Jawaharlal Nehru Centre for
>Advance Scientific Research,
>
>Bangalore, India. I have two publications in Europhysics
>Letters. Currently I am writting my
>
>thesis and would like to include the results (including text)
>presented in those two papers.
>
> Following are the details of the mentioned publications:
>

>
>
>
> 1. âœfont face="Liberation Serif, sans-serif">Universality in
>Fluid Domain Coarsening: The case of vapor-liquid transitionâ�/font>
>   Europhysics Letters, Vol-95, Page-46002, 2011.
>
>   Authors: Suman Majumder and Subir K. Das
>
>   Affiliation: Theoretical Sciences Unit of Jawaharlal
>Nehru Centre for Advance Scientific Research, Bangalore, India
>
>
> 2.âœinite-size effects in dynamics: Critical vs coarsening phenomenaâ�/font>
>   Europhysics Letters, Vol-97, Page-66006, 2012.
>
>   Authors: Subir K. Das, Sutapa Roy, Suman Majumder and Shaista Ahmad
>   Affiliation: Theoretical Sciences Unit of Jawaharlal Nehru
>Centre for Advance Scientific Reserch, Bangalore, India
>
>
>
> I will be highly obliged if you permit me to use those results
>in thesis. Looking forward to your reply.
>
>
> Yours Sincerely,
>
> Suman Majumder
>Theoretical Sciences Unit
>Jawaharlal Nehru Centre for Advanced Scientific Research
>Phone-+91-080-22082962
>